
Characterization of the Atmospheres of Terrestrial Exoplanets

A thesis submitted for the degree of

Doctor of Philosophy

in

The Department of Physics,
Pondicherry University,
Puducherry - 605 014, India



by

Manika Singla

Indian Institute of Astrophysics
Bengaluru - 560034



April, 2023

Characterization of the Atmospheres of Terrestrial Exoplanets

Manika Singla
Indian Institute of Astrophysics



Indian Institute of Astrophysics
Bengaluru - 560034, India

Title of the thesis : **Characterization of the Atmospheres of Terrestrial Exoplanets**

Name of the author : **Manika Singla**

Address : Indian Institute of Astrophysics
II Block, Koramangala
Bengaluru - 560034, India

Email : manika.singla@iiap.res.in,
manikasingla07@gmail.com

Name of the supervisor : **Prof. Sujan Sengupta**

Address : Indian Institute of Astrophysics
II Block, Koramangala
Bengaluru - 560034, India

Email : sujan@iiap.res.in

Declaration of Authorship

I hereby declare that the matter contained in this thesis is the result of the investigations carried out by me at Indian Institute of Astrophysics, Bengaluru, under the supervision of Prof. Sujan Sengupta.

This work has not been submitted for the award of any other degree, diploma, associateship, fellowship etc. of any other university or institute.

Signed:

A handwritten signature in blue ink that reads "Manika". The signature is written in a cursive style with a small circle above the 'i' and a double underline under the 'a'. There is a period at the end of the signature.

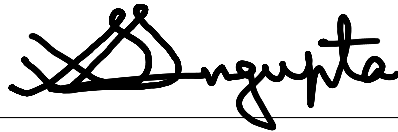
Date:

April 20, 2023

Certificate

This is to certify that the thesis entitled '**Characterization of the Atmospheres of Terrestrial Exoplanets**' submitted to Pondicherry University by Ms. Manika Singla for the award of the degree of Doctor of Philosophy, is based on the results of the investigation carried out by her under my supervision and guidance, at Indian Institute of Astrophysics. This thesis has not been submitted for the award of any other degree, diploma, associateship, fellowship, etc. of any other university or institute.

Signed:



Date:

April 20, 2023

List of Publications

1. **Effect of multiple scattering on the Transmission spectra and the Polarization phase curves for Earth-like Exoplanets**

Manika Singla, Aritra Chakrabarty & Sujan Sengupta, 2023, Astrophysical Journal (ApJ), 944 155

DOI: 10.3847/1538-4357/acb495

2. **New models of reflection spectra for terrestrial exoplanets: Present and prebiotic Earth orbiting around stars of different spectral types**

Manika Singla & Sujan Sengupta, 2023, New Astronomy (NewA), Volume 102, August 2023, 102024

DOI: <https://doi.org/10.1016/j.newast.2023.102024>

Conference Participation

1. National Conference:

- (a) *Meeting:* 40th Annual Meeting of the Astronomical Society of India (ASI), March 25 - 29, 2022, IIT, Roorkee,
Nature of Participation: **Poster Presentation**
Title: **Habitability in exoplanets: Reflection spectra of Earths and super-Earths**
Author: Manika Singla
- (b) *Meeting:* 38th Annual Meeting of the Astronomical Society of India (ASI), February 13 - 17, 2020, IISER, Tirupati,
Nature of Participation: **Contributory Talk**
Title: **Characterization of the atmospheres of the Terrestrial exoplanets**
Author: Manika Singla
- (c) *Meeting:* Young Science Conference (YSC) at India International Science Festival (IISF), November 5 - 8, 2019, Kolkata,
Nature of Participation: **Poster Presentation**
Title: **Characterization of the atmospheres of the terrestrial exoplanets**
Author: Manika Singla
- (d) *Meeting:* Modern Engineering Trends in Astronomy META-2022; META-2019, Indian Institute of Astrophysics, Bengaluru,
Nature of Participation: **Participant**
- (e) *Meeting:* 150 years of Periodic Table, December 16-19, 2019, Indian Institute of Astrophysics, Bengaluru,
Nature of Participation: **Participant**

2. International Conference:

- (a) *Meeting:* Indo-French CEFIPRA meeting in Astronomy (IFCAM)-3, January 9-13, 2023, Indian Institute of Astrophysics, Bengaluru, India

Nature of Participation: **Poster Presentation**

Title: **Effect of multiple scattering on the transmission spectra and the polarization phase curves for Earth-like Exoplanets**

Author: Manika Singla

- (b) *Workshop:* 2021 Sagan Exoplanet Summer Virtual Workshop Circumstellar Disks and Young Planets, July 19-23, 2021, NASA Exoplanet Science Institute, California Institute of Technology, PASADENA, CA

Nature of Participation: **Poster Presentation**

Title: **Reflection and Transmission spectra of Terrestrial exoplanets around F, G, K and M spectral types of stars**

Author: Manika Singla

- (c) *School:* Red' 21 - ASTROBIOLOGY INTRODUCTORY COURSE 2021 (virtual), June 21-25, 2021,

Nature of Participation: **Participant**

- (d) *Meeting:* The 6th UK Exoplanet community Meeting, April 22, 2021, Birmingham (in Virtual mode)

Nature of Participation: **Participant**

- (e) *Meeting:* International Symposium on Extra-Solar Planets, 7 – 9 January, 2019, IIA, India

Nature of Participation: **Participant**

3. Organizer

(a) *Meeting:* Young Astronomers' Meeting (YAM), November 9 -13, 2022, ARIES, Nainital, Uttarakhand,

Nature of Participation: **Scientific Organizing Committee (SOC)**

(b) *School cum Workshop:* Frontiers in 21 cm Cosmology, December 10 - 18, 2018, Kodaikanal, Tamil Nadu,

Nature of Participation: **Local Organizing Committee (LOC)**

Dedicated to

My Parents,
Mr. Krishan Singla & Ms. Kanta Singla

My Brother, Naman Singla

My Sister, Late Ishu Singla

My Grandparents,
Late Ishwar Chand Singla & Late Bimla
Singla

Acknowledgements

Firstly, I would like to thank Indian Institute of Astrophysics and my supervisor Prof. Sujan Sengupta for giving me the opportunity to do research in exoplanets. I am grateful to him for his invaluable guidance in the right direction, time, effort, knowledge and experience throughout the journey. I sincerely acknowledge my senior and collaborator Dr. Aritra Chakrabarty for his help and contributions in my work. I also thank my Doctoral Committee members Prof. Gajendra Pandey and Dr. Muthukumar B. for fruitful discussions and suggestions during my Ph.D. tenure.

I deeply thank my friend Soumya Sengupta for his continuous support, research discussions and making the journey more enjoyable. I am also thankful to my friends Sharmila Rani, Dr. Priya Goyal, Dr. Satabdwa Majumdar, Suman Saha, Vishnu Madhu, Saritha, Dr. Bhumika Rajput and Dr. Sandeep Kataria for keeping me motivated throughout the journey. I would like to express my heartfelt gratitude to my old friends Monika Kajla, Anmol Bhambri, Dr. Bhaskar Ghawri, Dr. Anjali, Vaibhav Thareja, Shikha, Dr. Prashant Singh, Soumyadip Basak and Neha Gupta. I also acknowledge Shivani Gupta, Maya Prabhakar, Dr. Aditya Komanduri, Prateek Gupta, Basavraj, Koena Majhi and Vikranth for making the time more enjoyable towards the end of my journey. I also thank my colleagues for always being there whenever I needed to continue in my hard days.

I also express my deep gratitude to the actress Kalki Koechlin and actor Milind Soman because of whom I learnt freedom, perseverance and to give more importance to the journey rather than the destination. I acknowledge all the books that I read during my PhD which changed the inner me towards the best. I am also grateful to Shihan Suresh Kenichira, Sen-

sei Dwrshwn Narzary, Sensei Loyd Pinto, Sensei Chandu Naidu and Sensei Karthik for teaching me not just Karate but hardwork, perseverance, discipline, tolerance, endurance, joy and fulfilment which led to the betterment of my research and my life.

Finally, I would like to thank my family, my parents and my brother for their love, care, support and understanding especially during the COVID time. Last but not the least, I want to thank myself that I worked hard and reached one step closer to my dreams.

Bengaluru,
April, 2023

Manika Singla

Abstract

Context: Over 5,000 exoplanets have been discovered to date, yet our knowledge of their atmospheres is still quite limited, and we have not yet identified any truly habitable exoplanets. It is the high time to characterize the atmospheres of Earth-like planets, especially as we enter an era of ambitious, big missions such as the Roman Space Telescope, the Thirty Meter Telescope, HabEx, the Extremely Large Telescope, and the Habitable Worlds Observatory (HWO). These groundbreaking missions are poised to significantly enhance our understanding and bring us closer to discovering potentially habitable worlds.

Aim: Our goal is to characterize the atmospheres of terrestrial exoplanets by calculating their reflected spectra, transmission spectra, and polarization phase curves. For the reflection spectra, we considered both present and prebiotic Earth-like exoplanets orbiting stars of F, G, K, and M spectral types, as well as nine known terrestrial exoplanets. The transmission spectra are modeled for present and prebiotic Earth-like exoplanets using the Beer-Bouguer-Lambert's law and a general law of multiple scattering, which accounts for diffused radiation. We also model the polarization phase curves of terrestrial exoplanets orbiting Sun-like stars. Various planetary surface types were considered, including water worlds, present and prebiotic Earth-like surfaces, and different sky conditions, such as clear and cloudy atmospheres. Additionally, we modeled atmospheres with increased greenhouse gas abundances.

Methodology: The reflected spectra and geometric albedo is computed by solving the equation applicable for multiple scattering radiative transfer problem. The atmospheric abundance is assumed to be analogous to that of the present Earth-like exoplanets. The Temperature - Pressure profiles for the known exoplanets are derived using hydrostatic equilibrium and the energy balance equation. The transmission spectra is calculated using Beer-Bouguer-Lambert's law as well as using multiple scattering radiative transfer equation. We numerically solve the 3D vector radiative transfer equations to calculate the phase curves of albedo and disk-integrated polarization by using appropriate scattering phase matrices and integrating the local Stokes vectors over the illuminated part of the planetary disks along the line of sight.

Results: Firstly, we present the reflected spectra and the geometric albedo for the present and prebiotic Earth-like exoplanets orbiting around F, G, K and M spectral types of stars and also for the nine known terrestrial exoplanets. We note the effect of the globally averaged surface albedo, clouds and the greenhouse gases abundance on the reflectivity. Secondly, we present the transmission spectra for Earth-like exoplanets, both with and without diffused scattering. We see the effect of the clouds on the transmission spectra and note the absorption lines of the bio-molecules present in the planetary atmospheres. Our models demonstrate that the effect of the diffusely transmitted radiation can be significant, especially in the atmospheres with clouds. Thirdly, we explore the effects of the Bond surface albedo on the polarization and albedo phase curves. The surface features of such planets are known to significantly dictate the nature of these observational quantities. We also determine the effect of the inclination angle and the clouds for two different wavebands i.e. visible and infrared. Our findings indicate that the clouds serve as an indicator for the polarization due to scattering for the terrestrial exoplanets.

More information can be extracted through the synergistic observations of spectra and phase curves. Additionally, the degeneracy among the estimated parameters of terrestrial exoplanets can be reduced by characterizing the atmospheres through various methods like, reflection spectra, transmission spectra and polarization phase curves. Consequently, our models will be instrumental in guiding future observations and enhancing the precision of exoplanetary atmospheric characterization.

Contents

1	Introduction	1
1.1	Historical Background	1
1.2	Relevant new results from JWST	2
1.3	Types of exoplanets	3
1.4	Detection techniques	4
1.4.1	Transit Method	4
1.4.2	Direct Imaging Method	5
1.4.3	Orbit Brightness Modulation	5
1.4.4	Radial Velocity Method	6
1.4.5	Astrometry	7
1.4.6	Gravitational Microlensing	7
1.5	Atmosphere characterization techniques	8
1.5.1	Reflection Spectroscopy	8
1.5.2	Transmission Spectroscopy	10
1.5.3	Emission Spectroscopy	10
1.5.4	Polarization due to scattering	11
1.6	Aim of the work	11
1.7	Plan of the thesis	12
2	Overview of the Atmospheres of Terrestrial Exoplanets	15
2.1	Atmospheres	17

2.1.1	Atmospheric scattering	18
2.1.2	Polarization due to scattering	19
2.2	Habitability conditions	20
2.2.1	Host-star and planet conditions	22
2.2.2	Reflectivity	23
2.2.3	Greenhouse effect	24
2.2.4	Biosignatures	25
3	Reflection Spectroscopy for terrestrial exoplanets	27
3.1	Introduction	27
3.2	Methodology	32
3.2.1	Numerical Methodology	32
3.2.2	Absorption and Scattering Opacity	39
3.2.3	Temperature-Pressure profile	40
3.3	Results and Analysis	42
3.3.1	The Reflection Spectra	42
3.3.2	Reflected spectra of known terrestrial exoplanets	52
3.4	Conclusions and Discussion	62
4	Effect of multiple scattering on transmission spectra for Earth-like exoplanets	65
4.1	Introduction	65
4.2	Transit Depth	67
4.3	Transmission spectra using "Beer-Bouguer-Lambert's law"	68
4.3.1	Atmospheric model	69
4.3.2	Results	70
4.4	Effect of multiple scattering on the transmission spectra	74
4.4.1	Atmospheric model	74
4.4.2	Results	75

4.5	Summary and Conclusions	77
5	Modelling Polarization and Albedo phase curves for Earth-like Exoplanets	79
5.1	Introduction	79
5.2	Atmospheric models for Earth-like exoplanets	83
5.3	The Phase Curve Models	84
5.4	Analysis and Discussion	87
5.5	Conclusions	94
6	Summary and Conclusions	95
6.1	Highlights	97
6.2	Present work limitations and future aspects	99

List of Figures

1.1	This schematic diagram illustrates the primary and secondary eclipses of an exoplanet as it orbits its host star. During the primary eclipse (transit), transmission spectra are computed, providing valuable information about the planet’s atmosphere. In contrast, just before and after the secondary eclipse, the reflected spectra reach their peak, providing insights into the planet’s reflective properties and atmospheric composition. Image credit: Sara Seager	9
2.1	Diagram for showing the habitable zone of a star. The green shaded region represents the habitable zone, which shows that as the temperature of the host star increases, the habitable zone shifts farther away from the host star. Credit: Chester Harman	21

3.1	Comparison of the model reflected spectrum (cyan) for an Earth-like exoplanet that orbit around a Sun-like star with the observed reflected spectrum (green) for the Earth obtained by Galileo spacecraft (Sagan et al. 1993). Blue color represents the model spectra at a spectral resolution same as NIMS in Galileo spacecraft. There is an overall good match except at the lower wavelengths, which is due to the differences in scattering in the Earth’s atmosphere. Red dotted plot represents a comparison between the modelled spectra and the observed spectra.	36
3.2	Comparison of the modeled reflected spectra for TRAPPIST-1e (blue) with the spectra calculated by (Lin and Lisa Kaltenegger 2020) (orange) with the same chemical abundances. The slight variations are due to the differences in the opacities.	37
3.3	(a) Comparison of our model reflected spectrum (blue) calculated by using opacity from Exo-Transmit package and observed atmospheric T-P profile of the Earth with the theoretical spectrum (dashed yellow) provided by S. Ranjan (priv. comm.) as well as with the spectrum calculated by our radiative transfer code using the same opacity and T-P profile as used by S. Ranjan (red) for a prebiotic Earth-like exoplanet orbiting around a solar-type of star. Yellow and red curves are essentially the same. (b) Comparison of the geometric albedo for the above three cases.	38

3.4	Atmospheric Temperature-Pressure (T-P) profile for the Earth's atmosphere (Atmosphere 1976). Temperature first decreases with altitude upto the tropopause following ideal gas law, then increases (thermal inversion) due to the presence of ozone gas in stratospheric region, decreases again, and finally increases due to the absorption of solar radiation. . . .	41
3.5	Input stellar flux at the surface of a habitable terrestrial planet that orbit around stars of several sub-classes of F, G, K and M spectral types. The peaks shift towards the higher wavelength as we go from early to late type stars.	43
3.6	(a) Reflected spectra for present Earth-like exoplanets orbiting around solar type star for different surface compositions (or different surface albedo). Blue line represents the spectra with zero surface albedo, orange line is for 100% ocean cover (surface albedo = 0.06), green line is for 50% ocean cover and the remaining 50% covered with trees and grass (0.1), red line is for present Earth-like surface composition (0.14), purple line is for prebiotic Earth-like surface composition (0.16) and brown line represents the spectra for 83% ocean and the remaining is snow (0.2). (b) Geometric albedo for the same.	45
3.7	Reflected spectra for present Earth-like exoplanets orbiting around stars of spectral types F, G, K and M. The absorption lines of H ₂ O, O ₂ and CH ₄ are clearly visible. And the magnitude of reflected flux decreases with the increase in wavelength due to Rayleigh scattering.	47
3.8	Geometric albedo for present Earth-like exoplanets with Earth-like atmospheric composition (blue) versus geometric albedo with increased abundances of greenhouse gases (red). . . .	48

3.9	Reflected spectra (top panel) and Geometric albedo (bottom panel) for the Earth-like exoplanets that orbit around the Sun-like stars at a resolution of 300. The blue plot is for the clear sky while the orange plot is for the cloudy atmosphere. The absorption lines of O ₂ and H ₂ O are shown.	50
3.10	Same as Figure 3.7 but for early Earth-like exoplanets.	51
3.11	Geometric albedo for early Earth-like exoplanets for surface albedo 0.16. The absorption lines of only CH ₄ and CO ₂ are present because of different atmospheric abundance as compared to present Earth's atmosphere.	51
3.12	Geometric albedo for present (blue) and prebiotic (orange) Earth-like exoplanets for zero surface albedo case. The absorption lines of the potential bio-molecules are shown in the plot.	52
3.13	(a) Possible range of T - P profile; Effect of the surface albedo on (b) the reflected spectra; and (c) geometric albedo for Kepler-442b, Kepler-62e, Kepler-22b and TOI-700d. Green curve is for the Earth-like surface composition (surface albedo = 0.14), orange for 50% ocean and 50% land consisting of trees and grass only (0.1) and blue for zero surface albedo (i.e., no solid/liquid surface)	56
3.14	Same as Figure 3.13 but for Kepler-1649c, Teegarden's Star b, Proxima Centauri b, TRAPPIST-1d and TRAPPIST-1e.	59
3.15	Comparison of the (a) input stellar flux, (b) reflected spectra and (c) geometric albedo for the nine planets in habitable zone.	63

4.1	Transmission spectra of present (blue) and early (orange) Earth-like exoplanets. In the first panel, the transmission spectra up to a wavelength of $4.5 \mu\text{m}$ is shown, and in the second panel, it is shown up to the wavelength $30\mu\text{m}$. The absorption lines of O_2 , H_2O , CO_2 and O_3 are marked. For the early Earth-like exoplanets, the absorption lines of only CO_2 molecules are seen.	71
4.2	Transmission spectrum of the present Earth but with increased greenhouse gas abundance (green). For a comparison, transmission spectrum (blue) of the Earth with actual atmospheric abundance is also presented.	72
4.3	Transit spectra for present Earth with clear sky (blue) and for 100 percent cloud coverage at three different heights i.e. 2.2 km (pink), 9.5 km (brown) and 17.0 km (yellow) from the surface of the planet.	73
4.4	Transmission depth for the Earth-like exoplanets with (solid) and without (dashed) multiple scattering for cloudy and cloud-free atmospheres (see Section 4.4.1). However, scattering opacity is also included even for cloud-free atmosphere case.	76
5.1	Effect of surface albedo on the phase curves of albedo (or flux ratio, $F(\alpha_{\text{orb}})/F_0$) and net polarization (P) integrated over the illuminated planetary disk at a wavelength of $0.6 \mu\text{m}$ and at an orbital inclination = 90° . We have used surface albedo 0.14 for our calculations. And 0.9 surface albedo is for the case of snowball (fully covered with snow) planet. . .	86

5.2	The phase curves of albedo (or flux ratio, $F(\alpha)/F_0$) and polarization (P) integrated over the illuminated disk at a wavelength of $0.6 \mu\text{m}$ (visible) and at orbital inclinations angle 90° (solid) and 45° (dashed) for both cloud-free and cloudy atmospheres.	88
5.3	Same as figure 5.2 but at a wavelength of $1.0 \mu\text{m}$ (near infrared).	89
5.4	Same as figure 5.2 but with single scattering of the incident radiation.	90

List of Tables

3.1	Molecular abundance for the Earth’s atmosphere (Sagan et al. 1993).	40
3.2	Surface Bond albedo for various surface compositions considered in our calculations for the modeled reflected spectra.	44
3.3	$T_{\text{eq,max}}$ is the maximum temperature at the top of the planet’s atmosphere and $T_{\text{surf,max}}$ is the maximum temperature at the bottom of the atmosphere after considering greenhouse effect. $A_{\text{B,max}}$ is the maximum possible Bond albedo, ESI is the Earth similarity index, R_p and M_p are the radius and mass of the planet and a is the orbital separation. [1] https://exoplanets.nasa.gov/exoplanet-catalog/ [2] https://phl.upr.edu/projects/earth-similarity-index-esi *estimate value	57

Chapter 1

Introduction

The planets which lie outside our solar-system and orbit any host star are known as Extra-Solar planets (or Exoplanets). The exploration of exoplanets represents one of the most exciting and rapidly evolving fields in the modern astronomy. This study has reshaped our understanding of the planetary systems and the potential for life elsewhere in the universe.

There are various types of extra-solar planets depending on their size, surface, planetary compositions, etc. and several detection methods are described later in this chapter. Besides detecting the planets, their atmospheric characterization is also important to understand the habitability conditions for the extra - terrestrial life and to go one step further towards the discovery of the first habitable exoplanet and hence finding life outside Earth.

1.1 Historical Background

The idea that other stars might host planets originated in the ancient times. Philosophers like Giordano Bruno in the 16th century proposed the existence of an infinite universe with countless worlds. However, without observational evidence, his ideas remained hypothetical.

In the early 20th century, astronomers like Otto Struve proposed that planets could be detected through their gravitational effects on their host stars. He suggested that large planets close to their host stars could be found by observing the star's wobble caused by the gravitational pull of the planet (Struve 1952).

The notion of planets existing around other stars has fascinated humanity for centuries, but it remained in the realm of speculation until the late 20th century. A significant breakthrough came in 1992 when Aleksander Wolszczan and Dale Frail discovered the first exoplanet orbiting the pulsar PSR B1257+12, using precise radio wave measurements. This finding marked the beginning of the exoplanetary era by proving that planets can exist in the most extreme environments (Wolszczan and Frail 1992).

Since the finding of 51 Pegasi b (Mayor and Queloz 1995), the first confirmed exoplanet around a Solar type star, more than 5000 exoplanets have been discovered¹. It is a gas giant exoplanet which orbits very close to its host star, which is detected by Radial velocity method.

1.2 Relevant new results from JWST

The James Webb Space Telescope (JWST) has made groundbreaking advancements in the study of exoplanet atmospheres. Notably, JWST's observations of the exoplanet WASP-39 b, a gas giant similar to Saturn, have identified a diverse array of atmospheric molecules, including sodium, potassium, water, carbon dioxide, carbon monoxide, and sulfur dioxide. The detection of sulfur dioxide, in particular, is significant as it suggests the presence of photochemical processes within the planet's atmosphere, similar to those occurring on Earth (Rustankulov et al. 2023; Ahrer et al. 2023).

¹<https://exoplanetarchive.ipac.caltech.edu/>

Furthermore, JWST has examined K2-18 b, an exoplanet, which is approximately 8.6 times the mass of the Earth, revealing substantial amounts of methane and carbon dioxide. These findings indicate the possibility of a hydrogen-rich atmosphere and a water ocean beneath it, which places K2-18 b within the habitable zone of its host star. This discovery highlights the potential of Hycean planets as promising candidates for habitability studies (Madhusudhan et al. 2023).

These discoveries highlight the capabilities of JWST in providing the detailed molecular and chemical analyses of the exoplanetary atmospheres. Thus providing a way forward for future research in enhancing the understanding of the potential for life on other worlds. However, JWST also has its limitations in characterizing the atmospheres of Earth-like exoplanets, which is a central focus of this thesis.

1.3 Types of exoplanets

In a vast diversity of exoplanets, there is a broad variety in the exoplanetary masses, atmospheres and their orbital parameters. The planets of our solar system are often split into two groups: terrestrial planets and giant planets. Four inner planets are the terrestrial planets, while the remaining outer planets are the giant planets. Further, ice giants (Uranus and Neptune) and gas giants (Jupiter and Saturn) constitute up the giant planets.

The exoplanets are categorized as Gas Giants, Hot Jupiters (a subclass of gas giants), Super-Earths, Mini-Neptunes, Terrestrial planets, etc (Jonathan J Fortney et al. 2007; N. M. Batalha et al. 2013; Rogers 2015). Terrestrial exoplanets generally have rocky surface and referred as rocky planets. The planet which has radius, mass and temperature similar to that of the Earth is known as an Earth-like planet. Also, the planets which are physically similar to Jupiter but are referred to as hot Jupiters because

they orbit very close to their host stars. Likewise, there are several other types of exoplanets such as water worlds, carbon planets, super Earths, etc.

We are mainly interested in Earth-like exoplanets which lie in the habitable zone (explained in [chapter 2](#)) of their host stars as these are the candidates for the potentially habitable planets. On top of that, if they have atmospheric and surface composition similar to the Earth, they can be the future targets for the search of habitable planets (Anglada-Escudé et al. [2016](#)). For example, the planets like Trappist-1e and Proxima Centauri b are Earth-like exoplanets which orbit around stars of spectral types M8V and M5.5V respectively.

1.4 Detection techniques

Exoplanets can be detected by various direct and indirect methods depending on the type of planet, type of the host-star, etc. Most of the detection methods are indirect because the distant planets are faint and the planets are detected by the planet's influence on the host-star's light. Some of the important and commonly used methods are as follows:

1.4.1 Transit Method

When an exoplanet transits a host star, part of the stellar radiation gets blocked by the planet and thus a dip in the brightness of the star is observed. Also, at the transit position (primary eclipse), the star's radiation penetrates through the planet's atmosphere and contains the information of the atmospheric composition through the absorption lines. Besides the atmosphere, we also get the information about the size of the planet, orbital inclination, orbital semi-major axis, etc. This method is valid when

the planet is orbiting at the edge-on view and we observe at the primary eclipse position. Also, the transit detectability is higher for the larger size planets. Using this technique, the first extra-solar planet i.e. HD 209458 b was detected around a Sun-like star (Charbonneau et al. 1999). NASA's Kepler Space Telescope has discovered thousands of exoplanets using this technique (Borucki, D. Koch, et al. 2010).

1.4.2 Direct Imaging Method

As the brightness of the extra-solar planets are very faint as compared to their host stars, it becomes very difficult to image them. By this method, the planet can be imaged directly by blocking the host star using coronagraphs. The planet and host star should have a relatively large orbital separation for that ($\gtrsim 2$ au). The first exoplanet which was detected by using this method is 2M1207 b. Till now, more than 50 exoplanets² have been detected by using this technique (Marois et al. 2008).

Using this method, one can measure the reflected flux of the planet as the planet reflects part of the starlight along our line of sight. The reflection spectra has been explained in detail in the next section.

1.4.3 Orbit Brightness Modulation

Orbit brightness modulation, also known as phase curve variations, refers to the periodic changes in the observed brightness of a star-planet system caused by the planetary orbit around the star. As the planet orbits, the amount of reflected starlight and emitted thermal radiation reaching the observer varies. This results in predictable fluctuations in the brightness of the star-planet system (Knutson et al. 2007; Esteves, De Mooij, and Jayawardhana 2013). The key factors which influence these variations

²<https://exoplanetarchive.ipac.caltech.edu/exoplanetplots>

include the reflectivity of the planet, atmospheric properties, and orbital inclination. By analyzing these brightness modulations, we can get insights into the exoplanet's atmospheric composition, temperature distribution, and surface properties, hence enhancing our understanding of distant planetary systems as well as their atmospheres (S. R. Kane et al. 2011; Cowan and E. Agol 2011; B. O. Demory et al. 2013; M. Zhang and Showman 2017; D. J. Armstrong et al. 2016).

1.4.4 Radial Velocity Method

For a star and a planet system, the barycenter is located inside the star. While the planet orbits, the host-star wobbles around the barycenter. If we take the edge-on component of the star motion, there is a "to" and "fro" motion of the star (towards and away from the observer) from our line of sight. This is known as the radial motion of the star and hence its radial velocity can be calculated. The equation below gives the amplitude (K) of the fluctuations in radial velocity caused by the orbiting planet.

$$K = \left(\frac{2\pi G}{P_{orb}} \right)^{1/3} \frac{M_p \sin i}{(M_* + M_p)^{2/3}} \frac{1}{\sqrt{1 - e^2}} \quad (1.1)$$

where M_p and M_* are the masses of the planet and the host-star respectively, P_{orb} is the orbital period of the planet, i represents the angle made by our line of sight and normal to the orbital plane of the planet. The exoplanet is detected by noting down the Doppler's shift in the spectra of the host star. This method is most-suited for massive planets (eg. Jupiter-like) orbiting around late-type stars so that the motion of the star is easily detectable. It can also be used for Earth-like planets which orbit their host stars very closely. This technique led to the detection of the first exoplanet, 51 Pegasi b, a Jupiter-like planet orbiting a star similar to the Sun (Mayor

and Queloz 1995).

1.4.5 Astrometry

Because the Earth orbits around the Sun, the star positions appear to oscillate and each oscillation period corresponds to one year. If a planet orbits the host star, the star's motion gets perturbed by the planet. Thus, the planet is detected by observing the minute changes in the position of the star because of the wobbling of star around the barycenter of the planetary system (Perryman 2011). The magnitude of the perturbation ($\Delta\theta$) is given as:

$$\Delta\theta \leq \frac{M_p a}{M_* r_\odot} \quad (1.2)$$

Here, M_p and M_* represent the mass of the planet and the star respectively, star's separation from our solar system is represented by r_\odot and a is orbital semi-major axis. Like radial velocity method, this method is also best-suited for the massive exoplanets.

1.4.6 Gravitational Microlensing

As we know that according to general theory of relativity, light bends around the massive object that lies between the source and the observer. The light from the distant star bends around an intervening star which acts as a lens and this leads to the formation of Einstein ring. The light from the background star gets amplified due to the lens. Now, suppose there is a planet that orbits the star (which is acting as a lens), a bump will appear in the smooth light curve, revealing the presence of a planet (Gaudi 2012). Using this technique, we can detect planets of a broad range of masses ($0.005 M_J$ - $18 M_J$) and semi-major axis (0.2 au - 18 au). By this method, a list of exoplanet candidates has been produced such as rogue planets (Dai

and Guerras 2018), planet in our nearest galaxy i.e. Andromeda (An et al. 2004), etc. The limitation of this method is that the two stars should be in alignment so that the detection probability can be enhanced.

There are many other methods for planetary detection like Transit Timing Variations, disk kinematics, etc. We will not go into the details of these methods as the atmospheric study is not possible by these techniques, thus beyond the scope of the present work. Also, Astrometry, Gravitational lensing and Radial Velocity methods are mainly for planetary detection, but their review has been included for the completeness of the thesis.

1.5 Atmosphere characterization techniques

The detection of the planets are not enough for moving towards the quest for the habitable worlds. We should go one step further and probe their atmospheres to recognize the potentially habitable planets. Some of the methods for the atmospheric characterization are described below.

1.5.1 Reflection Spectroscopy

The stellar radiation after getting reflected from the planet and then reaching to us along our line of sight is known as the reflected radiation. The radiation gets reflected from the atmosphere as well as from the planetary surface. For the case of Earth and Mars, it depends on the reflectivity of the clouds, surface, aerosols, dust particles, etc. present in the planetary atmosphere. But for Titan, Venus and giant planets, the stellar radiation is basically reflected from clouds and hazes.

The scatterers present in the planetary atmosphere absorb and scatter the stellar radiation which leads to diffuse reflection. The reflectivity depends on the wavelength and the shape of the reflected spectrum is ap-

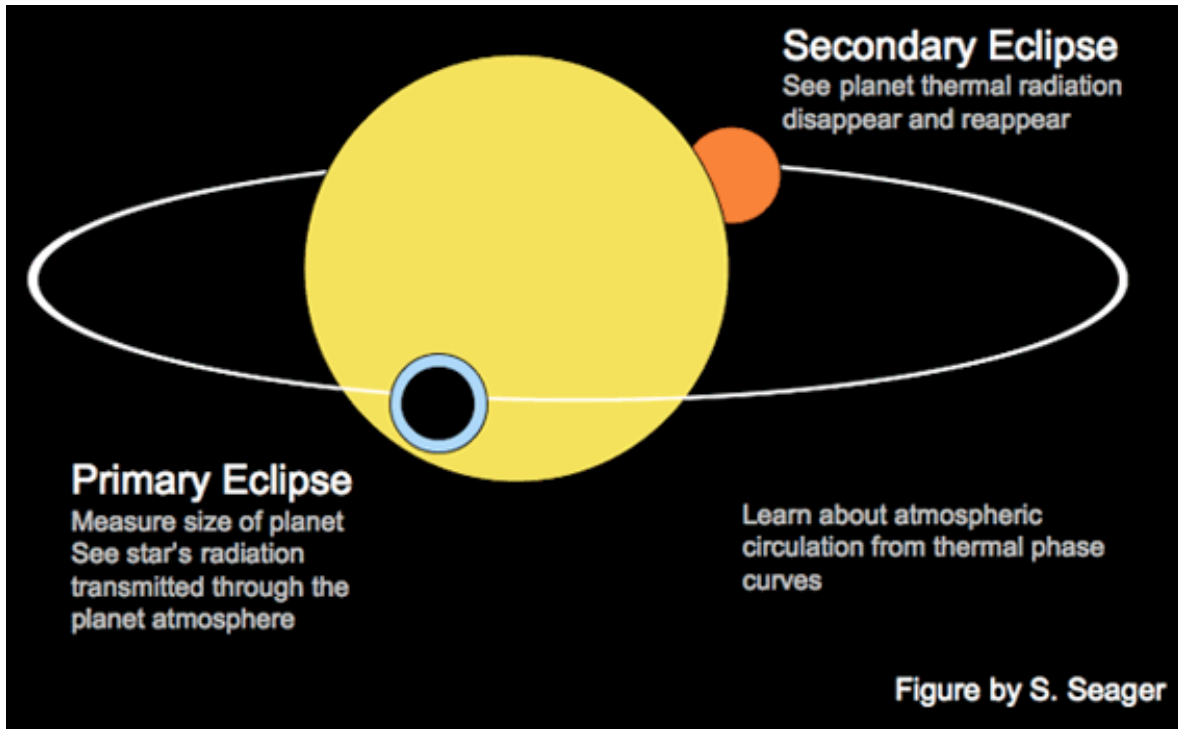


Figure 1.1: This schematic diagram illustrates the primary and secondary eclipses of an exoplanet as it orbits its host star. During the primary eclipse (transit), transmission spectra are computed, providing valuable information about the planet's atmosphere. In contrast, just before and after the secondary eclipse, the reflected spectra reach their peak, providing insights into the planet's reflective properties and atmospheric composition. Image credit: Sara Seager

proximately same as the host star's blackbody spectra. Hence the reflected spectra contains the information of the planetary atmospheric constituents, surface composition, clouds, etc in the form of absorption lines. The observable reflected flux is maximum when the planet is at secondary eclipse position (behind the star). It keeps on decreasing till it reaches the primary eclipse position (see Fig. 1.1).

1.5.2 Transmission Spectroscopy

When the planet is at primary eclipse position, it blocks some part of the star's radiation depending on the ratio of the planet's and star's surface areas. Also, the star's radiation transmits through the atmosphere of the planet and then reaches to us along our line of sight. Thus, it contains the fingerprints of the atmospheric constituents in the form of absorption lines. It is driven by the multiple scattering that takes place in the atmosphere of the planet. It is also affected by the clouds, haze, etc. present in the planetary atmosphere. By this technique, one can effectively probe only the upper atmospheres of the planet because of the high optical depth of the lower atmosphere. Transmission spectra has been calculated for Earth-like exoplanets and discussed in detail in [chapter 4](#).

1.5.3 Emission Spectroscopy

The thermal radiation of a planet is assumed to be like a blackbody which emits as the Plank radiation law given by:

$$B_{\lambda}(T) = \frac{2hc^2}{\lambda^5(e^{hc/\lambda k_B T} - 1)} \quad (1.3)$$

Here, $B_{\lambda}(T)$ is brightness (or specific intensity), T is the equilibrium temperature of planetary atmosphere, k_B and h are Boltzmann and Planck constants and c is speed of light in vacuum.

The planets, like hot Jupiters, have very high internal temperature, emit radiation in near infrared. The absorption lines in this radiation also serve as the fingerprints of the molecules that are present in the atmosphere. It is calculated by subtracting the stellar spectra (obtained at secondary eclipse position) from the star-planet combined spectra. For terrestrial exoplanet, it is very insignificant due to the rocky core and very low internal temper-

ature of the planet. Thus we are not considering the emission spectra for our study of the Earth-like exoplanets.

1.5.4 Polarization due to scattering

Mostly, the stellar radiation is unpolarized (if star is assumed to be a sphere) but it gets polarized after scattering from the planetary atmosphere. It is generally linearly polarized. Due to atmospheric gas particles and the dust particles, Rayleigh scattering polarization is observed for a range of wavelengths. Polarization is also dependent on the planet's orbital phase angle. From the polarization "phase curve", we can tell about the atmospheric composition, size of the scatterers, clouds, etc. By determining the planet star contrast ratio in the polarized light, we can detect the exoplanets and characterize their atmospheres. This has been discussed in detail in [2.1.2](#) and for Earth-like exoplanets, the albedo and polarization phase curves have been calculated in [chapter 5](#).

1.6 Aim of the work

We aim to model the atmospheres of the terrestrial exoplanets by reflection spectroscopy, transmission spectroscopy and by polarization phase curves. We calculate the reflected spectra for present and prebiotic Earth-like exoplanets orbiting around stars of F, G, K and M spectral types. And the transmission spectra is calculated for the Earth-like exoplanets orbiting around Sun-like stars. The multiple scattering is also considered for more realistic study of the atmospheres. Finally, we note the effect of the surface albedo, clouds and the inclination angle on the albedo and the polarization phase curves. Mainly, two models are considered for our study, i.e., planetary atmospheres with and without clouds. The discovery of exoplanets

has profound implications for our understanding of planetary systems. It has shown that planets are common in the galaxy, and the diverse range of planetary environments suggests that the conditions for life might exist in many places. Future missions, such as the James Webb Space Telescope (JWST) and the European Space Agency's PLATO, aim to expand our knowledge by characterizing the atmospheres of these distant worlds and searching for signs of habitability and life (Gardner et al., 2006).

In conclusion, the study of exoplanets is a rapidly advancing field that continues to unveil the complexities and wonders of planetary systems beyond our own. As technology progresses, the dream of finding a world like our own becomes even more achievable.

1.7 Plan of the thesis

The chapter - wise plan of the thesis is given as:

1. **Chapter 2:** In this chapter, we discuss the basics about the terrestrial exoplanets (Earth-like), their atmospheres, habitability conditions and the scattering mechanisms in their atmospheres.
2. **Chapter 3:** In this chapter, we model the reflection spectra and the geometric albedo for the terrestrial exoplanets orbiting around stars of F, G, K and M spectral types. We also calculate it for the nine known Earth-like planets including Teegarden's Star b, Proxima Centauri b and Trappist-1e. We estimated their maximum possible value of the Bond Albedo and determined a range of their Temperature - Pressure profiles. The effect of the surface albedo and the change in the greenhouse abundance is also noted on the reflectivity of the planet.

3. **Chapter 4:** Here, we calculate the transmission spectra for the Earth-like exoplanets that orbit around Sun-like stars. We also determine the effect of multiple scattering due to diffused radiation on the transmission spectra. For that, the multi-scattering radiative transfer equation is solved instead of using "Beer-Bouguer-Lambert's law". Additionally, the effect of water clouds on the transmission spectra is studied.
4. **Chapter 5:** In this chapter, we discuss about polarization due to scattering for the Earth-like exoplanets which orbit around the Sun-like stars. We show the albedo and the polarization phase curves for the Earth-like exoplanets that orbit around Sun-like stars for different inclination angles. We also study how the clouds and the Bond surface albedo affect the phase curves.
5. **Chapter 6:** In the final chapter, we summarize our work and conclude the results covered in all the chapters. We also present the future prospects of this work.

Resource Summary:

In this chapter we presented a brief introduction about the extra-solar planets from the literature. After that, we discussed our aim followed by the plan of the thesis. The resources that we have used here are:

1. Exoplanetary Atmosphere by Sara Seager (2010)
2. Exoplanets by Sara Seager (2010)
3. Fundamental Planetary Science by Jack J. Lissauer & Imke de Pater (2013)
4. Extrasolar Planets and Astrobiology, Caleb A. Scharf (2009)

5. An Introduction to Planetary Atmospheres, Sanchez-Lavega (2011)
6. Tinetti et. al. 2013, The Astronomy and Astrophysics Review volume 21, Article number: 63 (2013)
7. Exoplanet Atmospheres, Seager & Deming (2010), Annual Review of Astronomy and Astrophysics (Sara Seager [2010](#))

Chapter 2

Overview of the Atmospheres of Terrestrial Exoplanets

Terrestrial exoplanets are the planets which resemble Earth in terms of size or composition, for instance, which are composed of rocks, silicates, carbon or water. Earth-like planets are those rocky planets with radii from half to twice the size of the Earth. Other rocky planets which are greater than or equal to twice the Earth's size are known as Super-Earths. Our solar system's terrestrial planets include Earth, Mercury, Venus, and Mars and some of the terrestrial exoplanets are Proxima Centauri b, Trappist-1 d, Teegarden's star b, TOI-700d, Kepler-1649c, etc.

The identification of terrestrial exoplanets has significantly broadened our understanding of planetary systems and the potential for life elsewhere in the universe. A key aspect of assessing the habitability of these exoplanets is the characterization of their atmospheres, which influences surface conditions, climate stability, clouds and the presence of potential biosignatures.

The field of exoplanetary atmospheric characterization gained momentum with the observation of transiting exoplanets, where a planet crosses in front of its host star as we observe from the Earth. This technique,

known as transit spectroscopy, has been instrumental in detecting atmospheric components like water vapor, carbon dioxide, and methane (Sara Seager 2010). Enhancements in ground-based telescope capabilities and space missions such as the Hubble Space Telescope and the James Webb Space Telescope have significantly improved our ability to analyze exoplanetary atmospheres (Tinetti, Drossart, et al. 2018).

Studying the atmospheres of terrestrial exoplanets is particularly challenging due to their smaller size and the faintness of their atmospheric signals compared to gas giants. However, technological progress has enabled the study of these smaller planets. The Kepler mission's discovery of the first Earth-sized planets within the habitable zone of their stars was a pivotal moment, emphasizing the feasibility of atmospheric studies for terrestrial exoplanets (Borucki, D. Koch, et al. 2010). Techniques such as reflection spectroscopy, transmission spectroscopy and polarization due to atmospheric scattering can provide detailed atmospheric analysis, which will be discussed extensively in the upcoming chapters.

Furthermore, advancements in atmospheric modeling and simulations are crucial for predicting the spectra and determining the habitability of these distant worlds (Hu, Sara Seager, and Bains 2012). The effects of clouds, greenhouse gases, multiple scattering, inclination angle, etc. on the spectra and the phase curves provides important information about the habitability of the exoplanet.

Various physical processes in the exoplanetary atmosphere and the habitability conditions like presence of water clouds, oceans, potential biomolecules, etc. have been discussed in the following sections.

2.1 Atmospheres

After the detection of terrestrial exoplanets, characterization of their atmospheres is the next step in determining their habitability. A planetary atmosphere gets formed or developed by two major processes. One is by the capture of primitive atmosphere from the gas-rich stellar nebula. And the other one is from the outgassing of the gases by volcanic eruptions. The lighter elements escape from the atmosphere over a period of time, while the heavier ones stay (Chamberlain and Hunten 1987; Hunten, Pepin, and Walker 1987; Pepin 1991; Ahrens 1995; James F. Kasting and David Catling 2003; Lammer and S. J. Bauer 2003; D. C. Catling and James F. Kasting 2017).

The abundance of the elements forms the basis of the atmospheric composition. Depending on the temperature and pressure distribution in the atmosphere, a few dominant molecules are formed from the elements. Although nitrogen doesn't react with the surface and makes up a large portion of the Earth's atmosphere, it cannot escape because it is very heavy. The second most abundant component is Oxygen gas which gets generated through photosynthesis by photosynthetic bacteria and plants. Another important gas is Ozone gas, which exists in the Earth's stratospheric region (Walker 1977; James F. Kasting and Donahue 1980; Fowler et al. 1999; Jacob 1999).

Clouds also play a very crucial role for the atmospheric characterization. In the planetary atmosphere, clouds form at a height from the surface, where a gas can be condensed into a solid or a liquid form. For terrestrial exoplanets, they are mostly water clouds. Warm air and water vapour rise, expand, and cool as the temperature drops with the increase in the altitude. Apart from the atmospheric gases and the clouds, there are also other components present in the planetary atmosphere like dust, haze, etc.,

which are important for the scattering of the stellar radiation (Ackerman and Mark S. Marley 2001; Pierrehumbert 2010; Gao et al. 2021).

2.1.1 Atmospheric scattering

When starlight traverses the planetary atmosphere, it interacts with the atmospheric gases, dust particles, clouds, haze, etc. Some part of the radiation gets absorbed by the planetary atmosphere and surface while some gets scattered (Sara Seager 2010). After multiple scattering of the stellar radiation, part of it comes along our line of sight. Considering multiple scattering of the diffused radiation is more realistic as compared to considering only single scattering because of the presence of many scatterers in the planetary atmosphere such as the atmospheric gases, dust particles, haze, clouds, etc (Hansen and Larry D Travis 1974; Mishchenko, Joop W. Hovenier, and Larry D. Travis 2000). And this scattering is incorporated in the calculations of reflected or transmitted flux and the polarization phase curve through scattering phase function and the scattering phase matrix respectively (Chandrasekhar 1960).

Clouds also affect the results in several ways. The composition of the clouds is different on different planets. Terrestrial exoplanets usually have water clouds, whereas on Venus, clouds are mainly composed of sulfuric acid (Knollenberg and Hunten 1980). Typically, water clouds are present on Earth and the size of clouds droplets is in several microns ($\sim 20\mu\text{m}$). We have considered thin clouds (few microns) or haze for our calculations. The height at which clouds lie in the planetary atmosphere, also affect the spectra. Also, scattering of the radiation varies with the height, and consequently with temperature, pressure, chemical compositions, etc.

2.1.2 Polarization due to scattering

The light reaching to us after getting reflected from the exoplanetary atmosphere or surface should be polarized. In the atmosphere of the planet, the incident stellar radiation gets scattered in many directions which depend on the scattering mechanism and the single scattering albedo (ω). Due to the atmospheric gas particles, dust grains, clouds, etc., the Rayleigh scattering polarization is observed for a range of wavelengths and the radiation gets polarized through scattering (Coulson 1988; Goody and Yung 1989; Daphne M. Stam 2008).

Electromagnetic radiation (polarized or unpolarized) is divided into the two components of vibration, i.e. ξ_l and ξ_r that are along the two directions l and r, which are perpendicular to each other ((Chandrasekhar 1960)):

$$\xi_l = \xi_l^{(0)} \sin(\omega t - \epsilon_l) \quad (2.1)$$

$$\xi_r = \xi_r^{(0)} \sin(\omega t - \epsilon_r) \quad (2.2)$$

Here, ω is circular frequency of vibration, ϵ_l , ϵ_r , $\xi_l^{(0)}$ and $\xi_r^{(0)}$ are the constants. Depending on the direction of the electric vector, which is a function of time, the polarised radiation can be divided into several classes. They are:

1. **Linearly polarized:** The two components ξ_l and ξ_r must be in phase for the radiation to be linearly polarized but they may or may not have the same relative amplitudes. Thus the electric field vector traces a line in the plane of propagation.
2. **Circularly polarized:** The radiation is said to be circularly polarized if both the components are of same magnitude and are at 90° out of phase. In this case, the electric field vector traces a circle in the propagation plane. According to the direction of rotation of the field,

circularly polarized radiation is divided into two cases, i.e., right and left circularly polarized radiation.

- 3. Elliptically polarized:** Elliptical polarization, of which linear and circular polarisation are special cases, is the most common type of polarisation. For elliptical polarization, ξ_l and ξ_r do not have same amplitudes and they are not in phase and also not 90° out of phase.

For the planetary atmospheres, mostly the radiation is linearly polarized. However, the circularly polarized radiation can yield information about a planetary atmosphere and the surface. It can also directly probe the existence of life on the Earth by detecting homochiral molecules (the foundations of life on Earth), which reflect the circularly polarized radiation (Loic Rossi and Daphne M Stam 2018). But linear polarization is dominant and the circular polarization is measured to be very small for the solar system planets.

2.2 Habitability conditions

The area surrounding a host star, where a planet's surface temperature is ambient for liquid water to reside on the planet's surface is known as the habitable zone (James F Kasting, Daniel P Whitmire, and Ray T Reynolds 1993). Figure 2.1 shows that for hotter stars, the habitable zone lies farther than for the cooler stars and vice versa. The surface temperature also depends on the amount of the stellar radiation that gets reflected by the planet and the atmospheric greenhouse effect of the planet. Thus, there is a competition among these parameters and finally the habitable zone is determined.

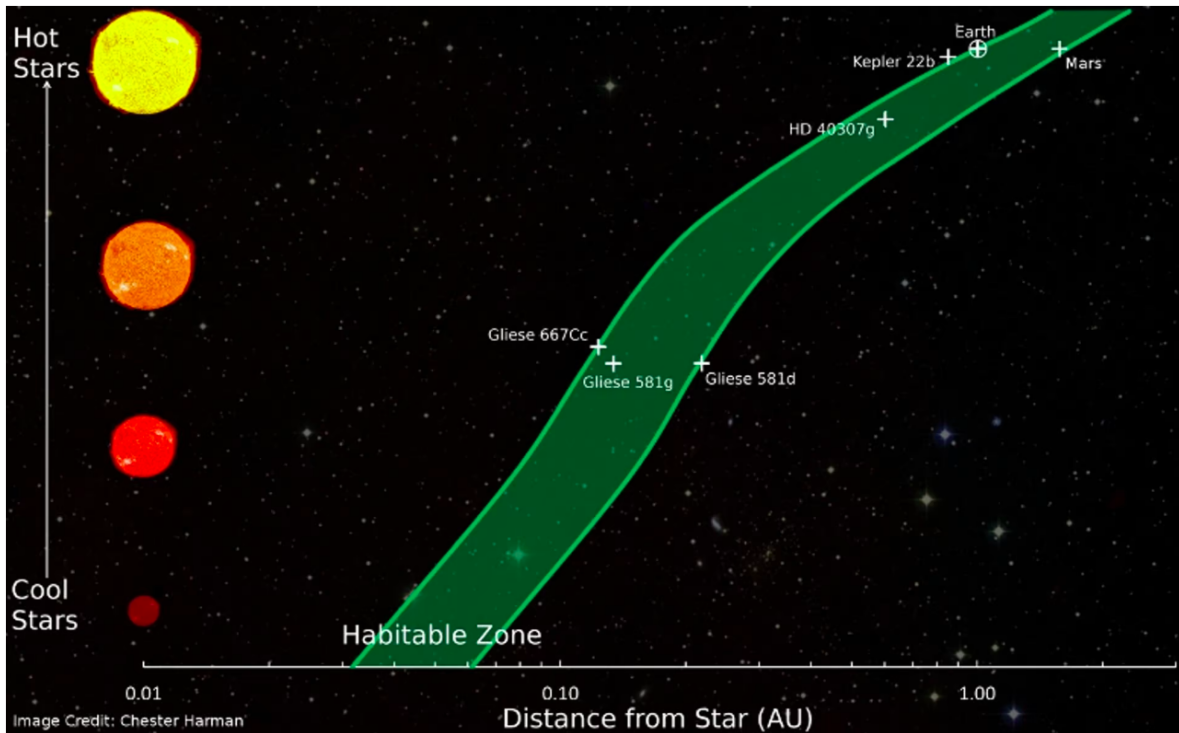


Figure 2.1: Diagram for showing the habitable zone of a star. The green shaded region represents the habitable zone, which shows that as the temperature of the host star increases, the habitable zone shifts farther away from the host star. Credit: Chester Harman

2.2.1 Host-star and planet conditions

A planet that can support life is much less probable to exist around stars with spectral types earlier than F0 because they have main sequence lifetimes of less than 2 Gyr (Antigona Segura, Krellove, et al. 2003). For the hotter stars, the habitable zone lies farther as compared to the cooler stars because the planet's surface temperature depends directly on the host star's effective temperature.

Also, M-dwarf stars are less probable of having habitable planets orbiting around them because their habitable zones are much nearer and narrower and consequently, the planets that are in the habitable zone are subject to intense UV radiation and intense flares (Huang 1959; Huang 1960; Hart 1979). Also the planets lying in the inner habitability zone of M-dwarfs are tidally locked (James F Kasting, Daniel P Whitmire, and Ray T Reynolds 1993; Antigona Segura, Krellove, et al. 2003) and the planet's permanent day or night side have hostile environmental conditions for life. However, nearly 70 percent of all the stars in our Galaxy are M-dwarf stars. Also, it may happen that most rocky planets orbit M-dwarfs in the universe (Shields, Ballard, and Johnson 2016; Victoria S Meadows et al. 2018; Lin and Lisa Kaltenegger 2020). Therefore, it is important to include the exoplanets orbiting M-dwarf stars as well in any investigation.

The potentially habitable planets should be rocky, Earth-like or super Earth-like. They should have a higher value of ESI¹ (Earth Similarity Index). It is a parametric quantity of the Earth-likeness of the exoplanets or the Solar-system planets. It is a number which lies between zero (not similar to Earth) and 1 (identical to Earth). Its value for the known planets that we have considered is given in [chapter 3](#).

¹<https://phl.upr.edu/projects/earth-similarity-index-esi>

2.2.2 Reflectivity

The surface temperature also depends on the amount of radiation that is reflected back either by the planetary surface or the atmosphere (Chandrasekhar 1960; Sara Seager 2010). The reflection happens through scattering by the atmospheric gases, dust particles, haze, clouds, aerosol, etc (Hansen and Larry D Travis 1974; Kokhanovsky 2006). The ratio between the reflected flux and the input stellar flux, at planetary surface, is known as the geometric albedo. And the radiation scattered from the planet in all the directions and at all frequencies is known as the Bond albedo (or the bolometric albedo). The fraction of the scattered radiation by the surface is known as the surface Bond albedo (Sudarsky, A. Burrows, and Pinto 2000; Cahoy, Mark S. Marley, and Jonathan J. Fortney 2010; Imke de Pater and Jack J. Lissauer 2010).

The surface Bond albedo is calculated by doing weighted sum of all the components' reflectivity or albedo. And the weight factors are the respective fractions of the planetary surface coverage. It is ~ 0.14 for the present Earth where the surface composition is 70% ocean, 2% coast and 28% land which is divided into 30% grass, 30% trees, 9% granite, 9% basalt, 15% snow and 7% sand (Lisa Kaltenegger, Traub, and Jucks 2007).

The energy balance equation for a planetary atmosphere tells us that either the host star or the planetary interior supplies the energy to the atmosphere of the planet. The energy is given by the equation (Sara Seager 2010):

$$E_{\text{out}}(t) = (1 - A_B)E_{\text{inc}}(t) + E_{\text{int}}(t) \quad (2.3)$$

where, $E_{\text{out}}(t)$ is the rate of energy emitting from the planet, A_B is the Bond albedo, $E_{\text{inc}}(t)$ is the rate of energy incident at the planet and $E_{\text{int}}(t)$ is the rate of energy that gets transferred from the interior of the planet to the planetary atmosphere. The internal luminosity is insignificant, for

the terrestrial exoplanets, as compared to the incident stellar luminosity. By using Stefan-Boltzmann Law the equation 2.3 (at a particular time) reduces to:

$$T_{\text{eq}} = T_{\text{eff},*} \left(\frac{R_*}{a} \right)^{1/2} \left(\frac{f}{4} (1 - A_B) \right)^{1/4} \quad (2.4)$$

Here, T_{eq} is the planet's equilibrium temperature, $T_{\text{eff},*}$ and R_* is the effective temperature and the radius of the star respectively, a is the separation between the planet and the host star and f is the correction factor to 4π (Sara Seager 2010). Thus, the equilibrium temperature (planet's) depends on the star's effective temperature, orbital separation and the Bond albedo of the planet.

2.2.3 Greenhouse effect

If an atmosphere, which is optically thick in infrared waveband, envelops a planet, the surface temperature can be considerably higher from the planet's equilibrium temperature. As the star's radiation falls on the planetary atmosphere, some part of it gets scattered (trapped) by the greenhouse gases in the atmosphere and some gets absorbed by the surface. Hence, infrared radiations are emitted by the gases and the surface which leads to the heating of the planet's atmosphere (Houghton 2002; Pierrehumbert 2010; T. D. Robinson and D. C. Catling 2014).

The greenhouse gases that are behind the heating of the atmosphere of the Earth are N_2O , CH_4 , CO_2 , water vapours, etc. These are very strong absorbers, or they have much stronger absorption cross-sections as compared to the most abundant gases, i.e. N_2 and O_2 (Andrews 2010).

To calculate the difference between the flux at the top of the planetary atmosphere and the surface due to the greenhouse effect, radiative transfer equation in the infrared region is used. For a simple model (ignoring convection), the surface temperature can be determined from the temperature

at the top of the atmosphere (J. Lissauer and I. de Pater 2013),

$$T_{\text{surf}}^4 = T_{\text{eq}}^4 \left(1 + \frac{3}{4}\tau_g\right) \quad (2.5)$$

Here, T_{eq} is the planet's equilibrium temperature or temperature at the top of the planetary atmosphere (T_{eq}), T_{surf} is the temperature at the surface of the planet with greenhouse effect and τ_g is the optical depth of the atmosphere at infrared wavelengths. For Earth, its value is ~ 0.83 in infrared. Consequently, the greenhouse effect rises the surface temperature of the Earth by 30-40 K due to the infrared opacity (J. Lissauer and I. de Pater 2013).

2.2.4 Biosignatures

The characteristics for an ideal biosignature gas are: first, it should not be naturally present in the atmosphere of the planet; second, its production should not be through geophysical processes or by photochemistry; and third, it should show a strong spectral signature. The key basis for biosignature is that the amount of gas present should be sufficiently more in amount than that can be generated by any abiotic process (Scharf 2009).

Oxygen gas comprises of 21% of the atmosphere of the Earth. As it is a highly reactive gas, it can be in a significant quantity only when it is being continuously produced. It is generated by biotic sources through photosynthesis. Ozone is produced by photolysis of oxygen in the presence of UV radiation of Sun. O_2 and O_3 are the most significant biosignature gases of the Earth. Nitrous oxide is also generated by life forms, although in very small quantity. O_2 and N_2O are also produced by photochemistry, but in negligible amounts. Although CH_4 and CO_2 are not biosignatures, but their detection can give the evidence of the presence of life on the exoplanet (Sara Seager 2014; Lisa Kaltenegger 2017; Victoria S. Meadows

2017).

Besides the atmospheric biosignatures, photosynthetic vegetation is a very strong surface biosignature. As it reflects strongly, the albedo increases suddenly at about $0.75 \mu\text{m}$, which is also known as the "red edge". Also, the detection of clouds (not a biosignature) can suggest the presence of liquid water oceans which is treated as a crucial signal for life (Sagan et al. 1993; Victoria S. Meadows and Crisp 1996; Arnold et al. 2002; Sara Seager et al. 2005; Tinetti, Rashby, and Yung 2006).

This thesis focuses on the various modelling techniques to characterize the terrestrial exoplanet atmospheres, analyze notable exoplanet case studies, and discuss the implications of these findings for our understanding of planetary habitability. By combining observational data with theoretical models, and verifying with previous models, this research aims to contribute to the broader field of exoplanetary science and the search for extraterrestrial life.

Resource Summary:

1. Exoplanetary Atmospheres by Sara Seager (2010)
2. Extrasolar Planets and Astrobiology by Caleb A. Scharf (2009)
3. Radiative Transfer by S. Chandrasekhar (1960)
4. Fundamental Planetary Science by Jack J. Lissauer and Imke de Pater (2013)
5. An Introduction to Planetary Atmospheres, Sanchez-Lavega (2011)

Chapter 3

Reflection Spectroscopy for terrestrial exoplanets¹

3.1 Introduction

Using a variety of techniques, more than 5000 exoplanet candidates have been detected since the finding of 51 Pegasi b (Mayor and Queloz 1995), yet very little has been investigated about their atmospheres. According to S. Bryson et al. 2020, around half of the Solar-type stars in our Galaxy might host rocky and potentially habitable planets within their habitable zones. But still we are far from finding any exoplanet that may have an ambient environment similar to that of the Earth. We will be a step closer to finding out such planets if we can characterize the atmospheres of terrestrial exoplanets (F. Selsis 2004; Morley et al. 2015; Lisa Kaltenegger 2017; Alonso 2018; Ravi Kumar Kopparapu, Wolf, and Victoria S Meadows 2020; Quanz et al. 2021).

The region around a star where a planet's surface temperature is suitable for water to exist in a liquid form is known as the classical circumstellar habitable zone (Huang 1959; Huang 1960; D. Whitmire, R. Reynolds, and

¹This chapter presents the work from the published papers - Singla et al. 2023, ApJ, 944 155 and Singla & Sengupta 2023, NewA, Volume 102, August 2023, 102024.

J. Kasting [1991](#); James F Kasting, Daniel P Whitmire, and Ray T Reynolds [1993](#); Ravi Kumar Kopparapu, Ramirez, et al. [2013](#)). A few of the planets detected by NASA's "*Kepler* space mission", possibly located in the habitable zone of their host stars (Covone et al. [2021](#)), are also of great interest. The recent TESS ("Transiting Exoplanet Survey Satellite") discoveries include Super-Earth and Sub-Neptunes orbiting around HD 108236 (G3V), GJ 3929 b, which is a hot Earth-sized planet that orbit around M3.5V star (Daylan et al. [2021](#); Kemmer et al. [2022](#)). Many Earth-like planets, including TOI-700d, which lie in their host star's habitable zone, discovered by TESS are also important (Kaltenegger, Pepper, et al. [2021](#)). Many potentially habitable exoplanets have also been discovered by RV Spectrographs (Jurgenson et al. [2016](#); Wildi et al. [2017](#), and many more).

When stellar radiation is incident on the surface of a planet, parts of it get reflected, absorbed and transmitted depending on the wavelength of the radiation and the incidence angle of the stellar flux (Sara Seager [2010](#); Perryman [2018](#)). The planetary reflected spectra are generated by the fraction of the incident stellar radiation reflected along our line of sight (Franck Selsis, Lisa Kaltenegger, and Paillet [2008](#)). The matter in the planet's upper atmosphere interacts with incoming stellar radiation to produce traces of the atmospheric chemical composition in the reflected spectra. However, when an exoplanet moves in front of the host star, a tiny portion of the star's disk is blocked yielding into a reduction in the stellar flux. At the same time, a fraction of star-light passes through the planetary atmosphere, if any, and brings the information about the planet's atmospheric abundance. This is known as the transmission spectrum (Enric Pallé et al. [2009](#); Wunderlich, Mareike Godolt, et al. [2019](#)). The signatures of the molecules present in the planetary atmosphere are revealed in the absorption features of reflected and transmitted spectra (Tinetti, Encrenaz, and Coustenis [2013a](#)). If a combination of biosignatures, such as oxygen, ozone,

water, methane, etc. were detected in the atmosphere of rocky exoplanets lying in the habitable zone, there would be a high possibility that the planet harbours life (Owen 1980; Sagan et al. 1993; Selsis 2004; Scharf 2009; John L Grenfell et al. 2014; Fujii et al. 2018; Claudi and Alei 2019).

Previous studies suggested that the potentially habitable planets can orbit stars of F, G, K and M spectral types (Selsis 2000). According to James F Kasting, Daniel P Whitmire, and Ray T Reynolds 1993, the most potentially habitable planets orbit around late F, G and early K type main-sequence stars. Stars whose spectral type is earlier than F0 have less than 2 Gyr main sequence lifetimes and hence are very less likely to have planets that can harbour life (Antigona Segura, Krelove, et al. 2003). On the other hand, M dwarfs have much less probability of having life supporting planets orbiting around them because their habitable zones are much nearer and narrower and so the habitable zone planets are subjected to strong UV radiation and strong flares (Huang 1959; Huang 1960; Hart 1979). Also, most planets which lie in the inner habitable zone of M-dwarfs are tidally locked (James F Kasting, Daniel P Whitmire, and Ray T Reynolds 1993; Antigona Segura, Krelove, et al. 2003; Martinez-Rodriguez et al. 2019) and the planet's permanent day or night side may have hostile environment for life. Nearly 70% of all stars in our Galaxy are M dwarfs and it may be most usual that, most rocky planets orbit M dwarfs (Shields, Ballard, and Johnson 2016; Victoria S Meadows et al. 2018; Lin and Lisa Kaltenegger 2020; Sabotta et al. 2021). Therefore, it is important to include the exoplanets orbiting M dwarfs as well in any investigation and probe.

Exoplanets similar to the prebiotic Earth (~ 3.9 Ga) can also be the potential candidates for supporting life on them. Prebiotic Earth contained no free molecular oxygen but carbon dioxide and nitrogen as the most dominant gases in their atmospheres (Rugheimer et al. 2015). Prevalent oxygenation of the Earth's atmosphere took place somewhere between

2.45 Ga and 2.32 Ga, which is referred to as the "Great Oxidation Event" (GOE) (Holland 2002; Bekker et al. 2004; Guo et al. 2009). Discovery of the biomarkers in sedimentary rocks (banded iron formation) with age 2.7 Ga to 2.8 Ga, which are characteristic of photosynthetic cyanobacteria, indicates the appearance of O₂ in the Earth's atmosphere (Brocks et al. 1999). Before this period, life survived through anoxygenic photosynthesis process. The second oxygenation event took place around 0.8 Ga to 0.5 Ga, which is known as "Neoproterozoic Oxygenation Event" (NOE). During that period, oxygen probably accumulated to the levels that are required for the animal life (G. Shields-Zhou and L. Och 2011; L. M. Och and G. A. Shields-Zhou 2012; Hiatt, Pufahl, and Silva 2020).

About three decades ago, the *Galileo* space mission obtained the reflected spectra of the Earth over a relatively clear sky region of the Pacific Ocean, north of Borneo, which was analysed by Sagan et al. 1993. Previously, many groups have characterized the atmospheres of modern and prebiotic Earth-like exoplanets by calculating reflection and transmission spectra (Ehrenreich et al. 2006; Lisa Kaltenegger and Traub 2009; Daniel Kitzmann et al. 2010; S. D. Domagal-Goldman et al. 2014; Wunderlich, Mareike Godolt, et al. 2019; Lisa Kaltenegger, Lin, and Sarah Rugheimer 2020; Lin, MacDonald, et al. 2021). Studies have also been done for the Earth-like exoplanets orbiting F, G, K and M stars (Antígona Segura, James F Kasting, et al. 2005; John Lee Grenfell et al. 2007; Sarah Rugheimer, Lisa Kaltenegger, et al. 2013; Sarah Rugheimer and Lisa Kaltenegger 2018). An open source radiative transfer model PICASO to calculate the reflected spectra of exoplanets was presented by N. E. Batalha et al. 2019. Earth's transmission spectra through lunar eclipse observations were calculated by Enric Pallé et al. 2009; Pallé et al. 2010 and Yan et al. 2015.

Previously, Kreidberg and Loeb 2016, V. Meadows et al. 2016, Dong

et al. 2017; Lovis et al. 2017; Luger et al. 2017; Victoria S Meadows et al. 2018; Lin and Lisa Kaltenegger 2020; Scheucher et al. 2020 have characterized the atmosphere for Proxima Centauri b and De Wit et al. 2018; Krissansen-Totton et al. 2018; Moran et al. 2018; Z. Zhang et al. 2018; Lustig-Yaeger, Victoria S Meadows, and A. P. Lincowski 2019; Hori and Ogihara 2020; Lin and Lisa Kaltenegger 2020; Martin Turbet, Bolmont, et al. 2020; Wunderlich, Scheucher, et al. 2020; May et al. 2021 have extensively discussed about TRAPPIST-1 system and in particular the planets TRAPPIST-1d and e. Kaltenegger, Sasselov, and Rugheimer 2013, on the other hand, modeled the transmission spectra for the planet Kepler-62e. Clouds also play a pivotal role in the determination of the reflection and transmission spectra (Kitzmann, Patzer, Paris, Godolt, Stracke, et al. 2010; Daniel Kitzmann et al. 2010; Kitzmann, Patzer, Paris, Godolt, and Rauer 2011a; Kitzmann, Patzer, Paris, Godolt, and Rauer 2011b; Kawashima and Rugheimer 2019). T. J. Fauchez, Martin Turbet, Villanueva, et al. 2019 demonstrated the effect of clouds and hazes on the planet's transmission spectra in the habitable zone of TRAPPIST-1, and Pidhorodetska et al. 2020 worked on detectability of molecules through transmission spectroscopy.

Here, we present the new synthetic reflected spectra of exoplanets similar to the modern and prebiotic Earth orbiting around stars of spectral types F, G, K and M. If the atmosphere is optically thick at pressure level much smaller than 10^3 mbar, most of the incident stellar radiation in the optical wavelength region will get absorbed and reflected only by the planetary atmosphere. However, the reflecting properties of the surface play a crucial role in the re-emission of thermal radiation in the infrared. The surface albedo of solid or liquid (ocean) surface is also considered, which provides better and realistic model spectra. We also calculate the spectra for nine Earth-like planets that lie within the habitable zone of their host stars.

In the next Section, we discuss the methodologies adopted to calculate the reflected spectra and the validation of our results. In particular, numerical methodologies are discussed in Section 3.2.1 and the absorption and scattering opacities that are employed are described in Section 3.2.2 and we discuss about Temperature-Pressure profile in Section 3.2.3. Results are presented in Section 3.3. The model reflected spectra for both cases - modern and prebiotic Earth-like exoplanets orbiting around stars of F, G, K and M spectral types are presented in Section 3.3.1 and the model reflected spectra of specific and interesting habitable terrestrial planets are shown in Section 3.3.2. Finally we discuss our results with specific conclusions in Section 3.4.

3.2 Methodology

3.2.1 Numerical Methodology

To calculate the reflected spectra, we solved the multiple- scattering radiative transfer equation for diffused scattering for a plane-parallel geometry and azimuthal symmetry, which is given by (Chandrasekhar 1960; Sen- gupta, Chakrabarty, and Tinetti 2020):

$$\mu \frac{dI(\tau, \mu, \lambda)}{d\tau} = I(\tau, \mu, \lambda) - \frac{\omega}{2} \int_{-1}^1 p(\mu, \mu') I(\tau, \mu', \lambda) d\mu' - \frac{\omega}{4} F(\lambda) e^{-\tau(\lambda)/\mu_0} p(\mu, \mu_0) \quad (3.1)$$

Here, $I(\tau, \mu, \lambda)$ represents the specific intensity of the diffusely scattered radiation in direction $\mu = \cos \theta$, where θ is the angle made by the axis of symmetry and the ray path, ω is the albedo for single scattering, $F(\lambda)$ is the incoming stellar flux along $-\mu_0$ and τ is the optical depth such

that $d\tau = -\chi dz$, where χ is the total absorption coefficient or extinction coefficient, i.e., the sum of true absorption and absorption due to scattering. In the above equation, $p(\mu, \mu')$ represents scattering phase function which tells about the photonic angular distribution before and after the scattering. It depends on the nature of scattering particles. The angular distribution for scattering by atoms and molecules is given by the Rayleigh scattering phase function and represented by Chandrasekhar 1960,

$$p(\mu, \mu') = \frac{3}{4}[1 + \mu^2\mu'^2 + \frac{1}{2}(1 - \mu^2)(1 - \mu'^2)], \quad (3.2)$$

where μ and μ' are the cosine of the angle w.r.t. the normal before and after scattering .

As pointed out by Sengupta, Chakrabarty, and Tinetti 2020, the radiation has two parts in a scattering medium: the reflected and transmitted intensities suffering one or more scattering process, and the direct transmitted flux, which is known as the reduced incident flux (Chandrasekhar 1960), $\pi F(\lambda)e^{-\tau(\lambda)/\mu_0}$ which is in the direction $-\mu_0$. Thus, the second term on the right side of equation 3.1 incorporates the transmitted and reflected intensities, does not contain the reduced incident flux, which is given by the third component.

We solved the multi-scattering radiative transfer equations using the discrete space theory that was thrived by Peraiah and Grant 1973 and Annamaneni Peraiah 2002. The numerical code has widely been used for solving the 3D vector radiative-transfer equations to incorporate scattering polarized spectra of self-luminous exoplanets and brown dwarfs (Sengupta and Mark S Marley 2009; Sengupta and Mark S Marley 2010; Sengupta and Mark S Marley 2016; Mark S Marley and Sengupta 2011; Sengupta 2016b; Sengupta 2018). For this work, the scalar form of the same numerical code has been used by using these steps:

1. As the vertical atmosphere is heterogeneous with respect to temperature, pressure and optical depth, we divided it into many "shells" of small optical depths. The minimum thickness of every shell is equal to a critical thickness τ_{critical} , that is calculated based on the physical properties of the medium. If $\tau \leq \tau_{\text{critical}}$, the reflection and transmission operators have non-negative elements (Peraiah 2001). We assume a constant temperature and pressure over each shell, and then integrate the radiation over all the shells.
2. The transfer equation's integration is carried out on the shells, a two-dimensional grid constrained by $[r_n, r_{n+1}] \times [\mu_{j-1/2}, \mu_{j+1/2}]$, where, $\mu_{j+1/2}$ is the angular grid and r_n is the radial grid:

$$\mu_{j+1/2} = \sum_{k=1}^j c_k, j = 1, 2, \dots, J \quad (3.3)$$

Here, c_k are the weights of "Gauss-Legendre quadrature formula". We used the plane-parallel approximation by making the shell curvature equal to zero.

3. The Gauss' quadrature formula is given as (Chandrasekhar 1960):

$$\int_{-1}^{+1} f(\mu) d\mu = \sum_{j=1}^m a_j f(\mu_j) \quad (3.4)$$

where μ_1, \dots, μ_m are the zeros of $P_m(\mu)$ and

$$a_j = \frac{1}{P'_m(\mu_j)} \int_{-1}^{+1} \frac{P_m(\mu)}{\mu - \mu_j} d\mu \quad (3.5)$$

where, $P_m(\mu)$ is known as the Legendre Polynomial of order m . We used the 8-point Gauss' Quadrature Formula.

4. Shells' transmission and reflection operators are computed when the discrete equations are compared with the canonical equations of the interaction principle, which relates incident and the emergent radiation from a medium of given optical depth.
5. Combining all the shells by star algorithm (Annamaneni Peraiah 2002), we obtained the total radiation field. Star algorithm combines the radiation for two consecutive shells by putting them together and calculating the radiation field as a whole.

The numerical method has been described in detail in Peraiah and Grant 1973, Annamaneni Peraiah 2002, Sengupta and Mark S Marley 2009 and Sengupta, Chakrabarty, and Tinetti 2020.

To verify our numerical calculations, we compared the model reflected spectra of a terrestrial exoplanet that orbit around a Sun-like star with the observed reflected spectra of the Earth obtained by the *Galileo* spacecraft (Sagan et al. 1993). This is presented in Figure 3.1. We found an overall good match of the observed low-resolution spectrum with our model spectrum, in particular the dominant water and oxygen bands. The intensity decreases with wavelength in the infrared region because of the nature of input solar spectra and Rayleigh scattering (which is proportional to λ^{-4}). The deviation towards the lower wavelengths is significant because of the differences in scattering in real Earth's atmosphere and the modeled Earth's atmosphere. In the case of observed spectra, there are other scattering elements as well, such as dust, haze, cloud molecules, etc. Due to which, the amount of reflected radiation along our line of sight is less than the model intensity in shorter wavelength region (because the radiation is scattered away from our line of sight). But for the longer wavelengths, the difference is insignificant because Rayleigh scattering is negligible for higher wavelengths.

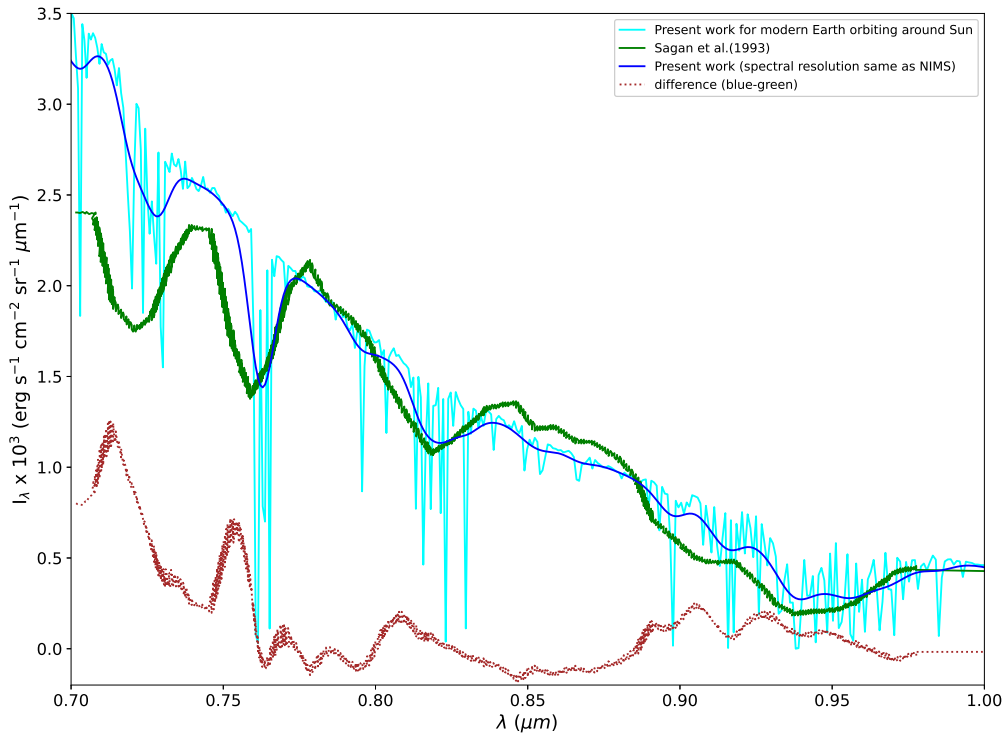


Figure 3.1: Comparison of the model reflected spectrum (cyan) for an Earth-like exoplanet that orbit around a Sun-like star with the observed reflected spectrum (green) for the Earth obtained by Galileo spacecraft (Sagan et al. 1993). Blue color represents the model spectra at a spectral resolution same as NIMS in Galileo spacecraft. There is an overall good match except at the lower wavelengths, which is due to the differences in scattering in the Earth's atmosphere. Red dotted plot represents a comparison between the modelled spectra and the observed spectra.

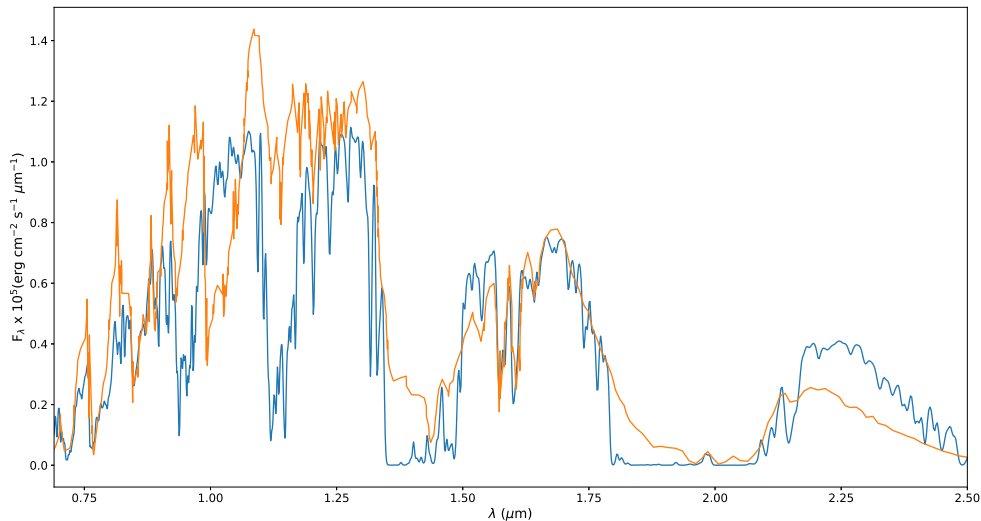


Figure 3.2: Comparison of the modeled reflected spectra for TRAPPIST-1e (blue) with the spectra calculated by (Lin and Lisa Kaltenegger 2020) (orange) with the same chemical abundances. The slight variations are due to the differences in the opacities.

Figure 3.2 shows the comparison between the reflected spectra for TRAPPIST-1e as calculated by our model with that calculated by Lin and Lisa Kaltenegger 2020. We used the same chemical abundance as in Lin and Lisa Kaltenegger 2020 for verification purposes. Temperature - Pressure (T-P) profiles employed for this case were the same as considered by O'Malley-James and Lisa Kaltenegger 2019. Here also, overall nature is the same and the slight variations are due to different opacities used and also they used vertically variable atmospheric abundance, but we used vertically homogenous atmospheric abundance. We also compared our model reflected spectrum for prebiotic Earth-like exoplanets orbiting around Sun-like stars (atmosphere composed of only N_2 and CO_2 ; (Rugheimer et al. 2015)) with the model spectrum calculated by S. Ranjan (priv. comm.). Figure 3.3a demonstrates that the reflection spectrum of prebiotic terrestrial exoplanets calculated by us matches very well with that derived by S. Ranjan.

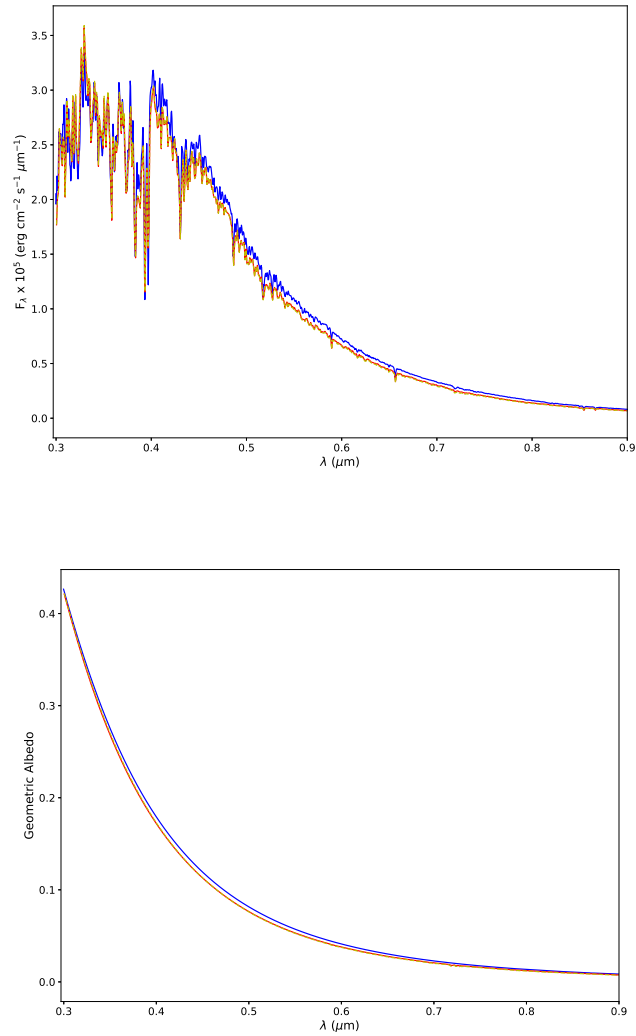


Figure 3.3: (a) Comparison of our model reflected spectrum (blue) calculated by using opacity from `Exo-Transmit` package and observed atmospheric T-P profile of the Earth with the theoretical spectrum (dashed yellow) provided by S. Ranjan (priv. comm.) as well as with the spectrum calculated by our radiative transfer code using the same opacity and T-P profile as used by S. Ranjan (red) for a prebiotic Earth-like exoplanet orbiting around a solar-type of star. Yellow and red curves are essentially the same. (b) Comparison of the geometric albedo for the above three cases.

The slight variation is again due to the differences in opacities used in both models. Figure 3.3b shows the comparison of the geometric albedo, which also matches very well. Here there are no absorption lines because the considered molecules show absorption beyond the limit of the wavelength considered in this work ($2.49 \mu\text{m}$).

3.2.2 Absorption and Scattering Opacity

To calculate the reflection and the transmission spectra, we calculated the absorption coefficients and the scattering coefficients of the atmosphere by using `Exo-Transmit` (Kempton et al. 2017). In this package, the opacities of 30 atomic and molecular species on a fixed temperature-pressure-wavelength grid are tabulated. The range of the wavelength is between 0.3 and $30 \mu\text{m}$ at low spectral resolution of $\mathcal{R} \approx 1000$. The temperature and pressure range at which the absorption coefficients and scattering coefficients were calculated for each wavelength were 100–3000 K and 10^{-6} – 10^6 mbar respectively. The opacities were derived by using the line lists given by Lupu et al. 2014. The gas opacities were taken from the widely used database of Freedman, Mark S Marley, and Lodders 2008; Freedman, Lustig-Yaeger, et al. 2014. The individual opacity sources are the atomic and molecular opacity weighted by their abundances and the total Rayleigh scattering opacity. Since the Earth’s atmosphere is sufficiently cool, we neglected the collision induced absorption of hydrogen. We adopted the molecular abundances of the present Earth (Sagan et al. 1993) as described in Table 3.1. For the prebiotic Earth-like exoplanets, we considered a carbon dioxide dominated atmosphere with the molecular abundance as 10% CO_2 , trace amounts of CH_4 and the remaining N_2 as considered by Lisa Kaltenegger, Traub, and Jucks 2007. The atmospheric abundances of Proxima Centauri b, Kepler-442b, Kepler-62e, Kepler-22b,

Molecule	Abundance (volume mixing ratio)
N ₂	0.78
O ₂	0.21
H ₂ O	0.03 - 0.001
Ar	9×10^{-3}
CO ₂	3.5×10^{-4}
CH ₄	1.6×10^{-6}
N ₂ O	3×10^{-7}
O ₃	$10^{-7} - 10^{-8}$

Table 3.1: Molecular abundance for the Earth’s atmosphere (Sagan et al. 1993).

Kepler-1649c, TOI-400d, Teegarden’s Star b, Trappist-1d and TRAPPIST-1e were considered to be the same as that of the present Earth. For the verification purpose for TRAPPIST-1e, the atmospheric abundance and T-P profile were adopted following O’Malley-James and Lisa Kaltenegger 2019. The molecular abundances were incorporated in the equation of states file in the `Exo-Transmit` package, in which pressure and temperature were also included for the atmospheric layers.

3.2.3 Temperature-Pressure profile

The internal temperature of the terrestrial exoplanets is negligible as compared to the irradiated temperature. Thus the incoming stellar flux at the uppermost layer of the atmosphere and the molecules present in the atmosphere determine the Temperature-Pressure (T - P) profile of terrestrial exoplanets.

Most of the stellar radiation gets reflected from the outer layers of the planet’s atmosphere. So, the temperature profile of the upper layers of the atmosphere mostly determines the reflected spectra. For transmission spectra case, the lower atmosphere cannot be probed for most of the wavelengths (Lisa Kaltenegger and Traub 2009). Hence, for the present Earth-like exoplanets orbiting around stars of F, G, K and M spectral types, we

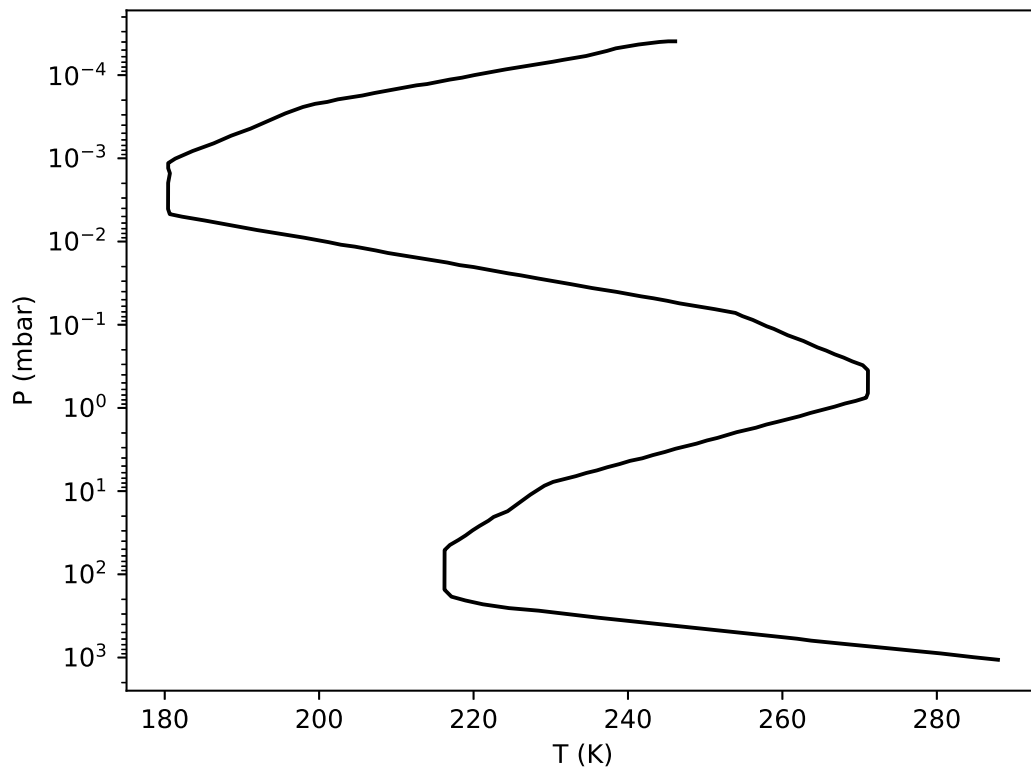


Figure 3.4: Atmospheric Temperature-Pressure (T-P) profile for the Earth's atmosphere (Atmosphere 1976). Temperature first decreases with altitude upto the tropopause following ideal gas law, then increases (thermal inversion) due to the presence of ozone gas in stratospheric region, decreases again, and finally increases due to the absorption of solar radiation.

adopted the Earth’s atmospheric T - P profile (Atmosphere 1976), which is shown in Figure 3.4. As we go upwards from the solid surface of the Earth, the temperature decreases continuously with the decrease in pressure, thus following the ideal gas law in the tropospheric region. This region extends roughly about 9 km at the poles and 17 km at the equator (Caballero et al. 2022). We will roughly consider the height of the tropopause equal to 11 km for our calculations. In the stratospheric region, which extends about 35 km above from the tropopause, the temperature rises with the decrease in pressure because of the presence of ozone gas, which absorbs the ultra-violet radiation. This is known as the temperature inversion (Atmosphere 1976). The atmospheric T - P profile of early Earth-like exoplanets is taken the same as considered in Lisa Kaltenegger, Traub, and Jucks 2007 for Epoch 0 (3.9 Ga).

3.3 Results and Analysis

3.3.1 The Reflection Spectra

While orbiting its host star, an exoplanet reflects part of the starlight along our line of sight. The maximum reflected radiation is observed when the planet is almost at full phase or zero degree phase angle, which is just before or after the secondary eclipse position.

In the present investigation, we considered terrestrial planets around stars of three sub-classes 0, 2 and 5 of F, G, K and M spectral types so that late to early stages of each spectral type are included. All the stars were considered to be of main sequence dwarfs of luminosity class V. The input stellar fluxes at the surface of the planets that orbit within the host star’s habitable zone are shown in Figure 3.5. The fluxes at the stellar surface for F, G and K spectral types were obtained from ESO library

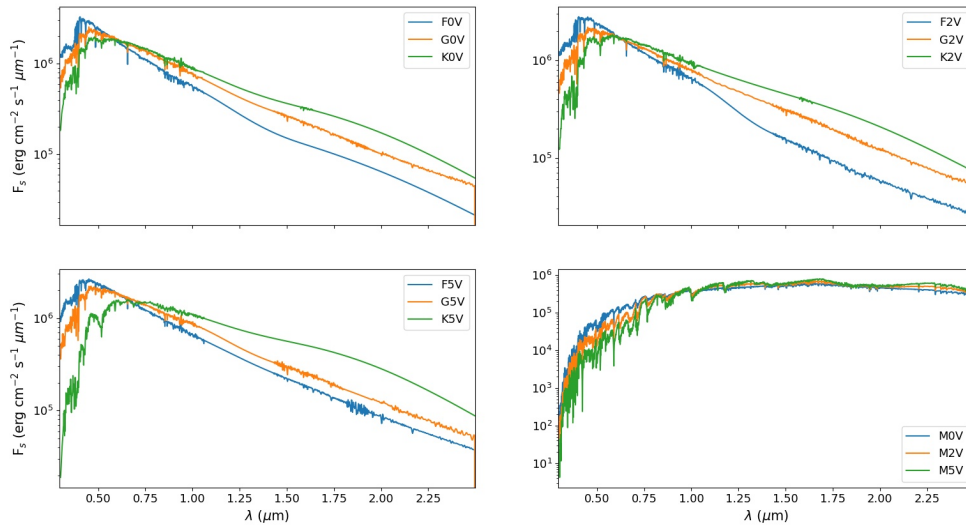


Figure 3.5: Input stellar flux at the surface of a habitable terrestrial planet that orbit around stars of several sub-classes of F, G, K and M spectral types. The peaks shift towards the higher wavelength as we go from early to late type stars.

(Pickles 1998). But for the M spectral type, the stellar fluxes were obtained from PHOENIX model (Husser et al. 2013) generated through publicly available code petitRADTRANS (Mollière et al. 2019). The equilibrium temperatures of the planets were supposed to be same as for the present Earth, i.e. 288 K.

Reflected spectra for present Earth-like exoplanets

We calculated the reflected spectra by solving the multi-scattering radiative transfer equation for the plane-parallel stratification (equation (3.1)). To estimate the surface Bond albedo of the rocky planets, we considered few different types of surfaces with the compositions given in Table 3.2. The surface composition of the present Earth is 70% ocean, 2% coast and 28% land, which is divided into 30% grass, 30% trees, 9% granite, 9% basalt, 15% snow and 7% sand (Lisa Kaltenegger, Traub, and Jucks 2007).

S.No.	Surface composition	Surface albedo
1	Ocean cover (100%)	0.06
2	Ocean (50%), Trees and grass (50%)	0.1
3	Present Earth-like	0.14
4	Prebiotic Earth-like	0.16
5	Ocean (83%) and snow (17%)	0.2
6	No solid or liquid surface	0

Table 3.2: Surface Bond albedo for various surface compositions considered in our calculations for the modeled reflected spectra.

And the surface composition for prebiotic Earth is 70% ocean, 2% coast and 28% land. The land surface consists of 35% basalt, 40% granite, 15% snow and 10% sand with no land vegetation (Lisa Kaltenegger, Traub, and Jucks 2007; Sarah Rugheimer and Lisa Kaltenegger 2018). In the sixth scenario, no solid or liquid surface exists, which means that the atmosphere of the planet is so optically thick, that the incoming stellar radiation gets reflected only from the atmosphere and it does not reach up to the surface. Hence, in this case, surface albedo does not affect the reflected spectra or the geometric albedo. Zero surface albedo may also mean the gaseous planets, which is beyond the scope of this work.

We calculated the surface Bond albedo by weighted sum of all the components' albedo. And the weight factors are the respective fractions of planetary surface coverage. The reflected spectra for present Earth-like exoplanets orbiting around solar type of star for different surface albedo are shown in Figure 3.6. Reflected flux increases with the increase in the surface albedo and it is steeper than the input stellar flux because of Rayleigh scattering. The effect of surface albedo on the geometric albedo for the present Earth-like exoplanets is shown in Figure 3.6b. We can see that geometric albedo increases with the increase in surface albedo. However, it decreases with the wavelength because Rayleigh scattering is not significant at longer wavelength region.

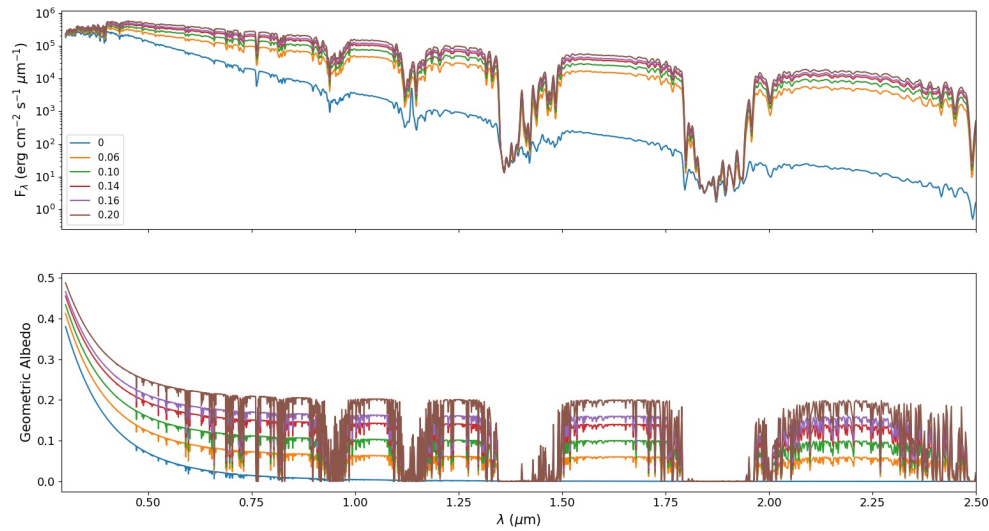


Figure 3.6: (a) Reflected spectra for present Earth-like exoplanets orbiting around solar type star for different surface compositions (or different surface albedo). Blue line represents the spectra with zero surface albedo, orange line is for 100% ocean cover (surface albedo = 0.06), green line is for 50% ocean cover and the remaining 50% covered with trees and grass (0.1), red line is for present Earth-like surface composition (0.14), purple line is for prebiotic Earth-like surface composition (0.16) and brown line represents the spectra for 83% ocean and the remaining is snow (0.2). (b) Geometric albedo for the same.

The reflected spectra for the present Earth-like exoplanets orbiting around stars of F, G, K and M spectral types are shown in Figure 3.7. The absorption lines of H₂O (0.72 μm , 0.82 μm , 0.94 μm , 1.10 μm and 1.87 μm), O₂ (0.63 μm , 0.69 μm , 0.76 μm) and CH₄ (1.60 μm) are also shown in this figure. The flux decreases with the increase in the wavelength in the infrared region. This is because of two reasons: firstly, the input stellar flux also decreases with the increase in wavelength in infrared and secondly Rayleigh scattering dominates in the shorter wavelength region (Ityaksov, Linnartz, and Ubachs 2008). The reflected spectra has the planetary atmospheric features as well as the stellar atmospheric features.

In this study, we have ignored the effects of strong stellar ultra-violet irradiation that may alter the planetary environment by dissociating water molecules and energy limited hydrogen loss (Sanz-Forcada et al. 2011; Sengupta 2016a). Presence of sufficient initial water content at the planetary surface may still avoid the planet to become parched under such situation. However, since most of the planets lying in the habitable zone of M-dwarfs are tidally locked, the presence of an Earth like planet is rare (Martinez-Rodriguez et al. 2019).

In order to examine the effect of various greenhouse gases on the geometric albedo, we increased the abundance of CO₂ by two orders in magnitude, CH₄ by four orders in magnitude and H₂O by one order in magnitude. This increase is compensated by altering the abundance of N₂. The geometric albedo of the present Earth-like exoplanets with higher abundances of atmospheric greenhouse gases is presented in Figure 3.8. We found that the geometric albedo increases slightly in the shorter wavelength region because of the increase in Rayleigh scattering. However, the scattering could have drastic effect in the thermal re-emission in near and far infrared waveband and hence in determining the T_{surf} of the planet (surface temperature) by an increased greenhouse effect.

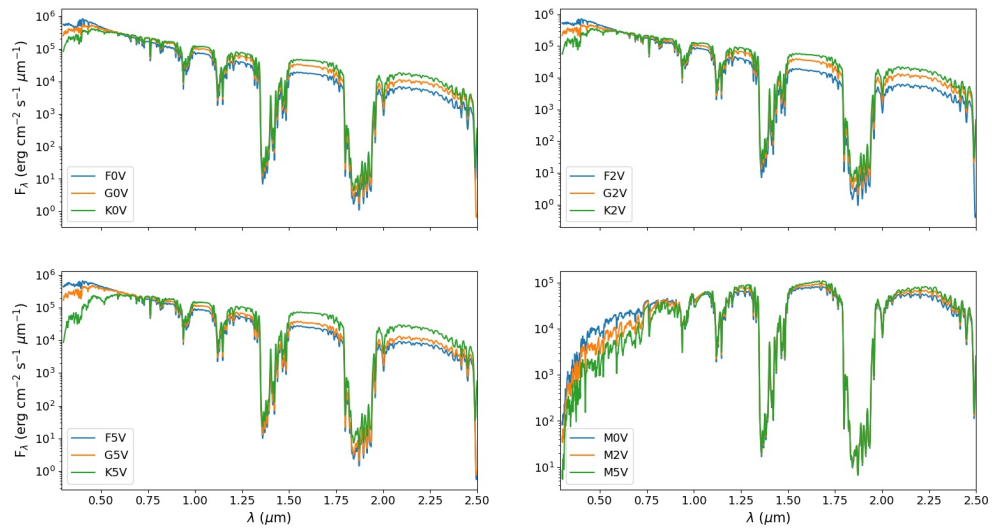


Figure 3.7: Reflected spectra for present Earth-like exoplanets orbiting around stars of spectral types F, G, K and M. The absorption lines of H_2O , O_2 and CH_4 are clearly visible. And the magnitude of reflected flux decreases with the increase in wavelength due to Rayleigh scattering.

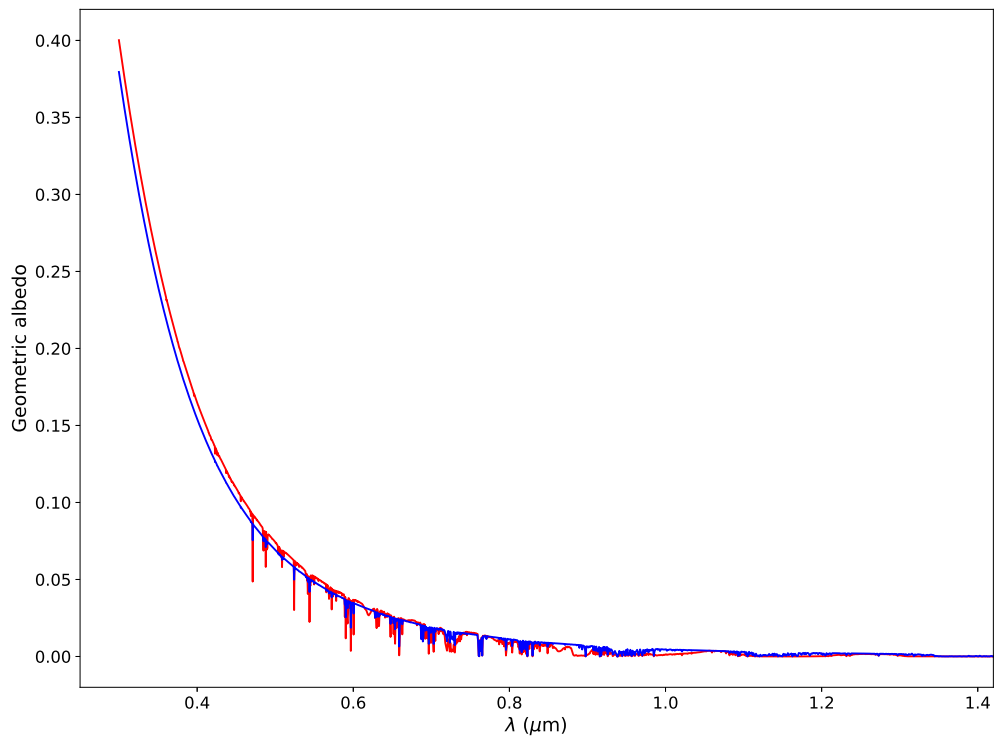


Figure 3.8: Geometric albedo for present Earth-like exoplanets with Earth-like atmospheric composition (blue) versus geometric albedo with increased abundances of greenhouse gases (red).

Effect of clouds

Clouds also play a crucial role in scattering and hence affect the reflected spectra or the geometric albedo. The clouds may increase the reflected spectra by increasing the scattering along our line of sight. We considered very thin clouds or haze with 100% coverage and we used an approximate Rayleigh model to express the effect of these clouds/haze following Sing et al. 2016; Kempton et al. 2017, etc. We considered the cloud position between the pressure levels of 1×10^3 Pa and 5×10^4 Pa with a scattering cross-section equal to 400 times the scattering cross-section of nitrogen gas. Fig. 3.9 shows the reflected spectra for present Earth-like exoplanets (with surface albedo) orbiting around Sun-like stars. There are two models, i.e., with (orange) and without (blue) clouds. We can clearly note that the spectra for the cloudy atmosphere is more than that for the clear sky. The reflected flux is more for the cloudy atmosphere due to the backscattering of the stellar radiation by the clouds.

Early Earth-like exoplanets

The reflected spectra for the prebiotic Earth orbiting around stars of F, G, K and M spectral types are presented in the Figure 3.10. And the geometric albedo (for surface albedo 0.16) is presented in Figure 3.11. We see very less absorption lines because only N_2 , CO_2 and trace amount of CH_4 were considered in the atmospheric composition for the prebiotic Earth. The absorption lines of CO_2 ($1.4 \mu m$, $1.6 \mu m$ and $2 \mu m$) and CH_4 ($1.66 \mu m$) can be seen. The overall nature of spectra remains the same as that for the modern Earth case.

A comparison between the geometric albedo for present and prebiotic Earth with zero surface albedo is shown in the Figure 3.12. Prebiotic Earth-like exoplanets scatter more starlight as compared to the present

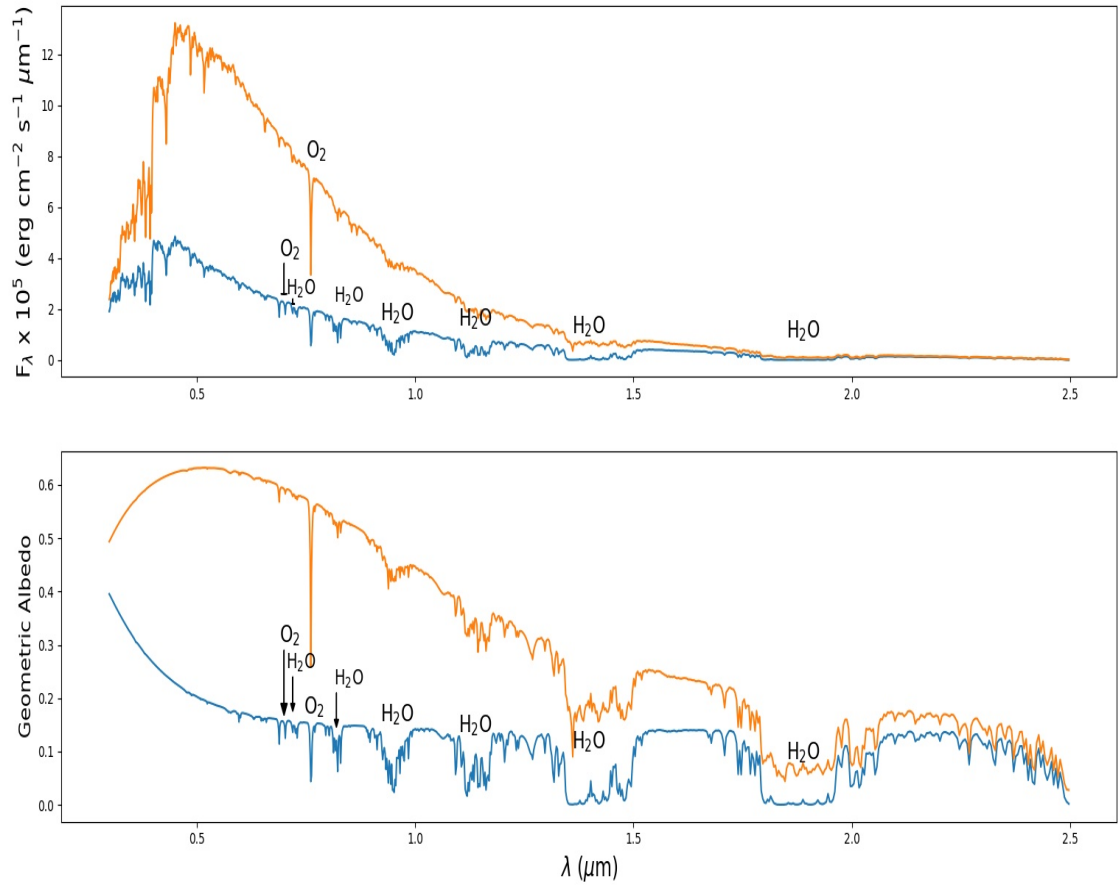


Figure 3.9: Reflected spectra (top panel) and Geometric albedo (bottom panel) for the Earth-like exoplanets that orbit around the Sun-like stars at a resolution of 300. The blue plot is for the clear sky while the orange plot is for the cloudy atmosphere. The absorption lines of O_2 and H_2O are shown.

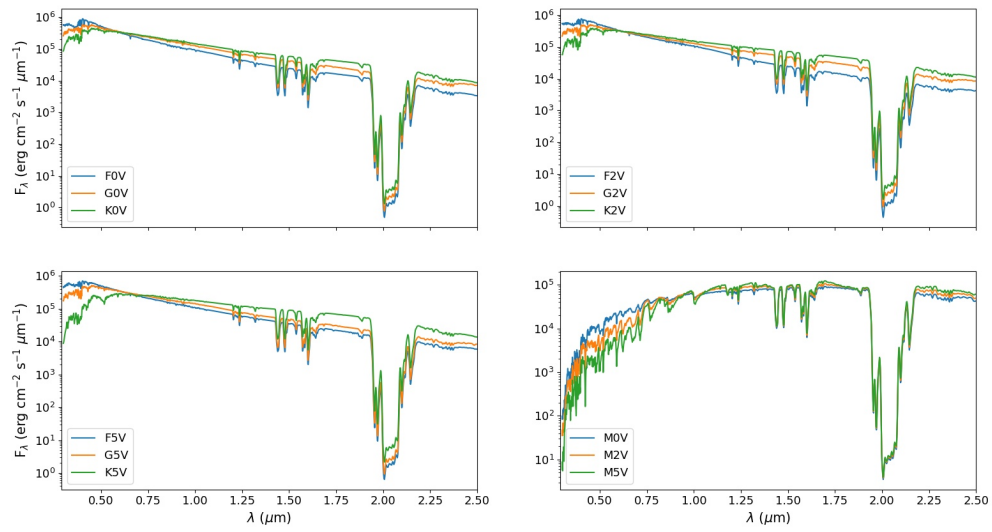


Figure 3.10: Same as Figure 3.7 but for early Earth-like exoplanets.

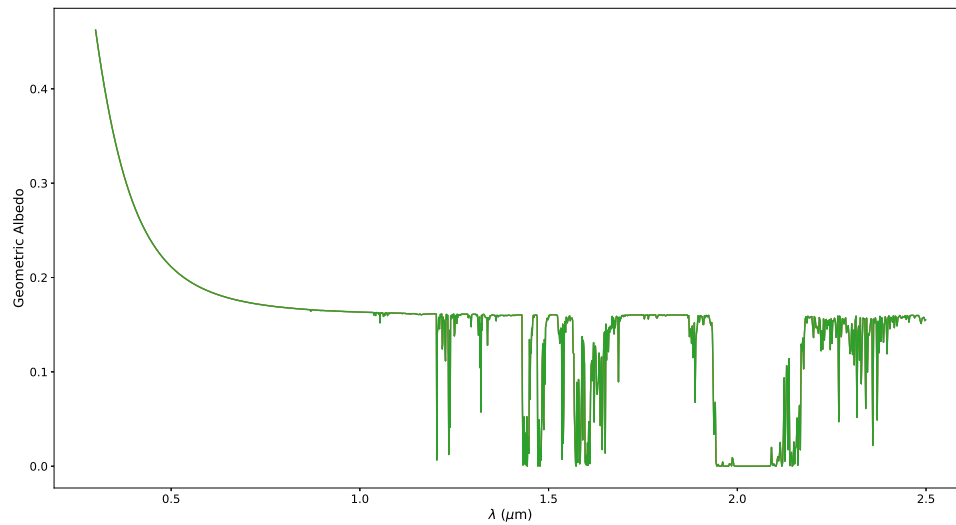


Figure 3.11: Geometric albedo for early Earth-like exoplanets for surface albedo 0.16. The absorption lines of only CH_4 and CO_2 are present because of different atmospheric abundance as compared to present Earth's atmosphere.

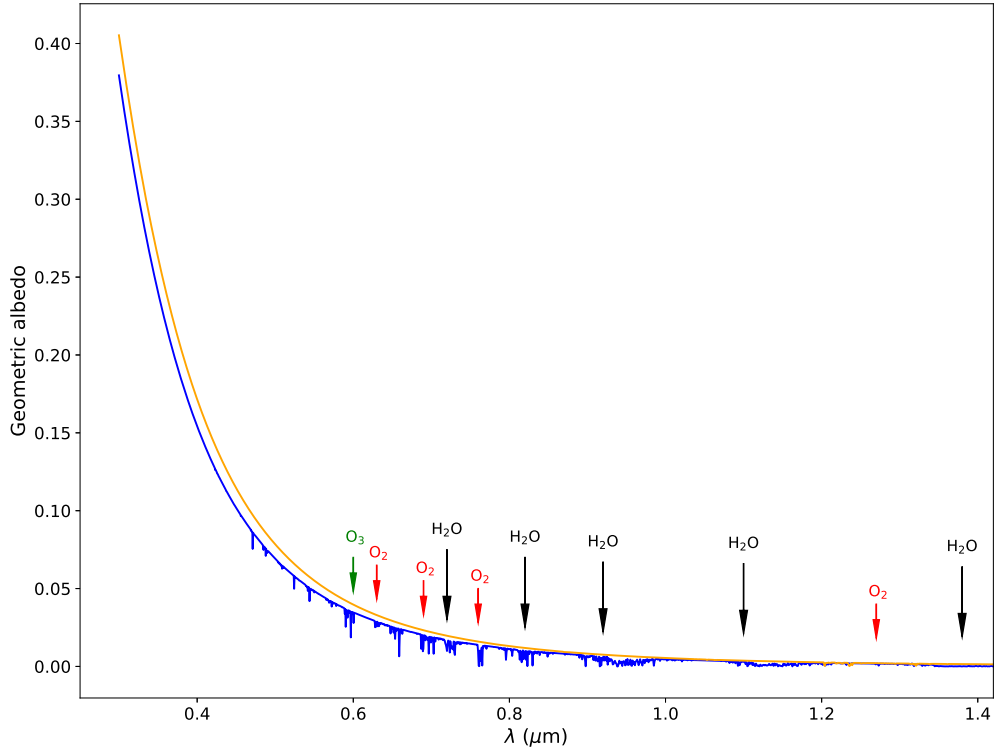


Figure 3.12: Geometric albedo for present (blue) and prebiotic (orange) Earth-like exoplanets for zero surface albedo case. The absorption lines of the potential biomolecules are shown in the plot.

Earth-like exoplanets because of greater abundances of greenhouse gases (mainly CO_2). The absorption lines for the present Earth are also shown in this figure.

3.3.2 Reflected spectra of known terrestrial exoplanets

We also present the reflected spectra for some of the well known habitable planets such as Kepler-442b, Kepler-62e, Kepler-22b, TOI-700d, Kepler-1649c, Teegarden's Star b, Proxima Centauri b, TRAPPIST-1d and

TRAPPIST-1e. These planets orbit stars of spectral types G, K and M. Their radii are in the range of $0.7 R_{\oplus}$ and $2.4 R_{\oplus}$. These planets lie in the habitable planets catalog in Hill et al. 2022. Although very little is known about their atmospheres at present, we expect them to have Earth-like atmospheric compositions with favourable temperature because of greenhouse effect. The input stellar flux at the surface of Kepler-442b, Kepler-62e and Kepler-22b were calculated by taking the stellar flux from Pickles 1998. We used PHOENIX model spectra for the cases of TOI-700d, Kepler-1649c and Teegarden’s Star b. For Proxima Centauri b, the stellar flux is taken from (Lin and Lisa Kaltenegger 2020) and for TRAPPIST-1d and e, we used the spectra from Burgasser, Logsdon, et al. 2015.

Their equilibrium temperature T_{eq} can be derived from the relationship given in equation 3.6 (Sara Seager 2010). The temperature at the atmospheric bottommost region (or surface temperature) with greenhouse effect is given by equation 3.7 (De Pater and Jack J Lissauer 2015).

$$T_{\text{eq}}^4 = (1 - A) \frac{R_s^2}{2a} T_{\text{eff}}^4 \quad (3.6)$$

$$T_{\text{surf}}^4 = T_{\text{eq}}^4 \left(1 + \frac{3}{4} \tau_g\right) \quad (3.7)$$

In equations 3.6 and 3.7, A is the Bond albedo, R_s is the host star’s radius, a is the orbital separation, T_{eff} is the host star’s effective temperature, T_{surf} is the temperature at the planet’s surface with greenhouse effect and τ_g is the optical depth of the planetary atmosphere at infrared wavelengths. We assumed it to be same as that for the Earth, i.e. ~ 0.83 . The surface temperature should not be less than 273 K for the planet to be habitable ($T_{\text{surf,min}} \approx 273 \text{ K}$). And from equation 3.7, the minimum equilibrium temperature or the temperature at the atmosphere’s top ($T_{\text{eq,min}}$) is about 242 K.

Kepler-442b

It is an Earth-like exoplanet that orbits its host star (K5V) within the habitable zone and about 366 pc away from the Earth. It is among all the detected rocky planets that is most similar to the Earth and has a very high habitability index value (Torres et al. 2015; Stephen R Kane, Hill, et al. 2016; Rodriguez-Mozos and Moya 2017). This planet receives an incident stellar flux that is 0.9 times of the flux that is received by the Earth (Torres et al. 2015; D. Armstrong et al. 2016; Rodriguez-Mozos and Moya 2017; Barbato et al. 2018). It is a promising candidate for search of biosignatures as K-type of stars maintain favourable circumstellar conditions for habitability (Cuntz and Guinan 2016). Its density is very similar to the Earth and mean surface gravity is $\sim 12.5 \text{ m/s}^2$, slightly higher than that of the Earth. According to G. N. Arney 2019, K-type stars present an advantage for the detectability of biosignatures. One of the reasons is that K dwarfs offer extended photochemical lifetime of methane as compared to G types stars. And the other reason is better signal to noise ratio (S/N) of K dwarfs than G dwarfs, due to which oxygen and methane can be strongly observed. We calculate the T - P profile by the following method:

1. For tropospheric region (up to 11 km), $T = -mh + T_{\text{surf}}$ where m is the adiabatic lapse rate.

$T_{\text{surf,min}} \approx 273 \text{ K}$; For $h=11 \text{ km}$, $T \approx 242 \text{ K}$ (minimum equilibrium temperature); $m = 2.83 \text{ K/km}$

$T_{\text{surf,max}} \approx 290.1 \text{ K}$; For $h=11 \text{ km}$, $T \approx 257 \text{ K}$ (maximum equilibrium temperature); $m = 3 \text{ K/km}$

$$T_1 = -2.83h + 273; T_2 = -3h + 290.1 \quad (3.8)$$

2. For Stratospheric region and above, $T_1 \approx 242$ K; $T_2 \approx 257$ K.

Similarly, we calculated the T-P profile for all the other planets by calculating their adiabatic lapse rates. The possible range of T-P profile for Kepler-442b is shown in Figure 3.13 and the temperature can lie anywhere in this range. The maximum value of Bond albedo (A_{\max}), temperature at the atmosphere's top (T_{eq}) and temperature at the atmosphere's bottom including green-house effect (T_{surf}) were calculated in the same ways and are shown in Table 3.3. The atmospheric abundance was assumed to be the same as that of the Earth and shown in Table 3.1. We calculated the reflected spectra for the two T - P profiles and found that the spectra does not alter with the variation in T - P profile within the given range. The reflected spectra for the planet Kepler-442b for various surface compositions i.e. different surface albedos is shown in the Figure 3.13.

Figure 3.13 also shows the geometric albedo of Kepler-442b for different surface compositions of the planet. We note that the geometric albedo increases significantly with the increase in the surface Bond albedo or we can say that the surface albedo considerably affects the geometric albedo. This is because the surface also contributes in the total reflectivity of the planet. For example, for the zero surface albedo case, the geometric albedo is the least. And it is maximum for the present Earth-like surface components (0.14 surface albedo).

Kepler-62e

Kepler-62e orbits within the classical habitable zone of the host star (K2V) and the orbital period is about 122 days (Borucki, Eric Agol, et al. 2013; Kaltenegger, Sasselov, and Rugheimer 2013; Torres et al. 2015; D. Armstrong et al. 2016; Stephen R Kane, Hill, et al. 2016). The possible T - P profile was calculated similarly as in the case of Kepler-442b and is pre-

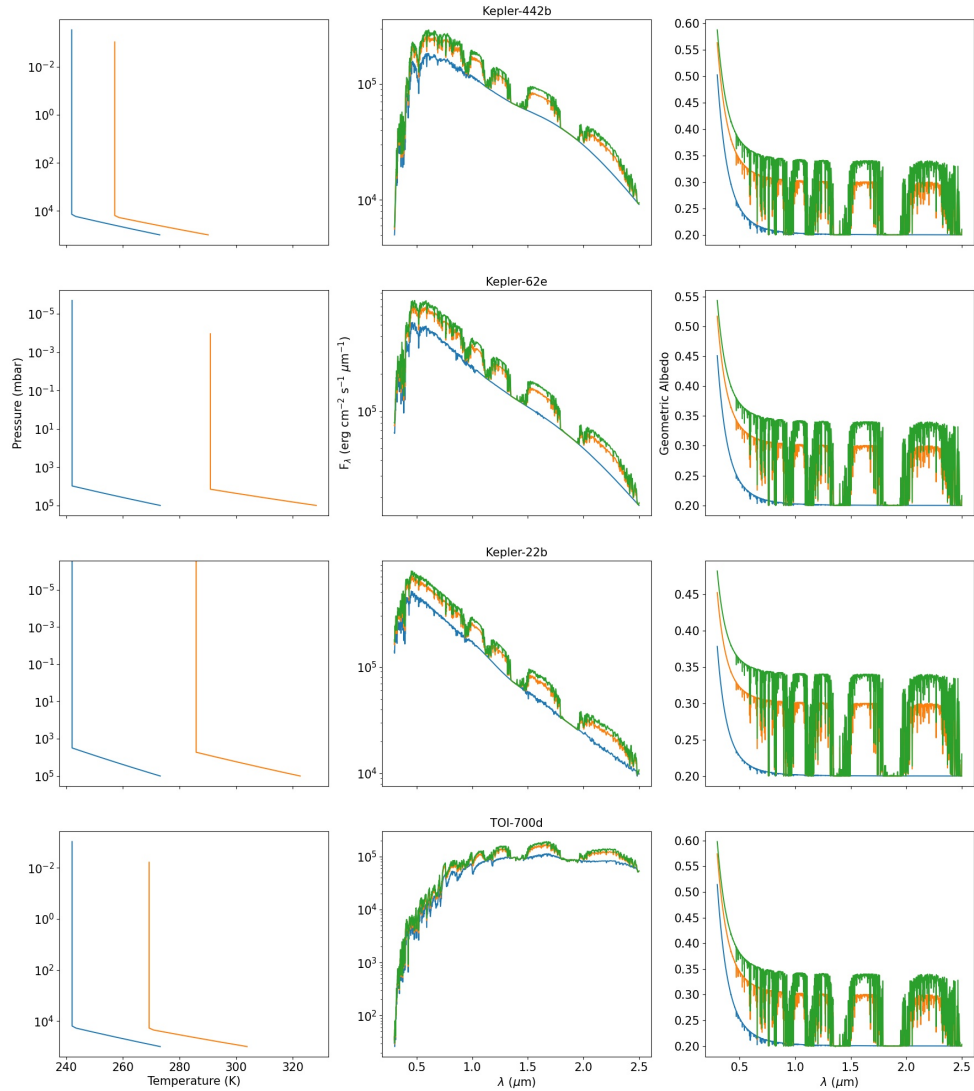


Figure 3.13: (a) Possible range of T - P profile; Effect of the surface albedo on (b) the reflected spectra; and (c) geometric albedo for Kepler-442b, Kepler-62e, Kepler-22b and TOI-700d. Green curve is for the Earth-like surface composition (surface albedo = 0.14), orange for 50% ocean and 50% land consisting of trees and grass only (0.1) and blue for zero surface albedo (i.e., no solid/liquid surface)

Planet	$T_{\text{eq,max}}$ (K)	$T_{\text{surf,max}}$ (K)	$A_{\text{B,max}}$	$R_p^{[1]}$ (R_{\oplus})	$M_p^{[1]}$ (M_{\oplus})	$a^{[1]}$ (au)	ESI ^[2]
Kepler-442b	257	290	0.216	1.34	2.36	0.409	0.84
Kepler-62e	291	328	0.52	1.61	36	0.427	–
Kepler-22b	286	323	0.486	2.33	36	0.849	–
TOI-700d	269	304	0.347	1.144	1.57	0.1633	0.93
Kepler-1649c	296	334	0.55	1.06	1.2	0.0649	0.90
Teegarden b	289	326	0.51	1.02*	1.05	0.0252	0.95
Proxima b	258	292	0.2289	1.08*	1.27	0.0485	0.87
TRAPPIST-1d	286	323	0.49	0.788	0.388	0.0223	0.90
TRAPPIST-1e	250	282	0.12	0.92	0.692	0.0292	0.85

Table 3.3: $T_{\text{eq,max}}$ is the maximum temperature at the top of the planet’s atmosphere and $T_{\text{surf,max}}$ is the maximum temperature at the bottom of the atmosphere after considering greenhouse effect. $A_{\text{B,max}}$ is the maximum possible Bond albedo, ESI is the Earth similarity index, R_p and M_p are the radius and mass of the planet and a is the orbital separation. [1]<https://exoplanets.nasa.gov/exoplanet-catalog/> [2]<https://phl.upr.edu/projects/earth-similarity-index-esi>
*estimate value

sented in Figure 3.13. The temperature and pressure can be anywhere between these limits.

The reflected spectra and the geometric albedo for Kepler-62e are also shown in Figure 3.13 for various surface compositions. It is highest for Earth-like surface composition (surface albedo 0.14) and lowest for no surface albedo at all. The green curve is for 50% ocean cover and the remaining covered with trees and grass. As the ocean cover is reduced from 70% to 50% by increasing the land cover, the geometric albedo decreases.

Kepler-22b

Kepler-22b is a super-Earth orbiting a G5V star, which is about 194.7 pc away from Earth. This planet is also orbiting within the habitable zone of the host star (Borucki, D. G. Koch, et al. 2012; Neubauer et al. 2012; Torres et al. 2015; Stephen R Kane, Hill, et al. 2016). It is the first detected

Earth-like exoplanet within the habitable zone of a solar type star.

The atmospheric T - P profile used to calculate the reflected spectra of the planet is shown in Figure 3.13. It is also calculated by assuming the atmosphere of the planet in hydrostatic equilibrium and considering greenhouse effect.

The effect of the surface Bond albedo (derived from the surface compositions) on the reflected spectra and the variation of the geometric albedo are also shown in Figure 3.13.

TOI-700d

It is TESS's first Earth-size exoplanet, which lies in the habitable zone of its host star TOI-700 (M dwarf). The planet should be tidally locked as its eccentricity nearly zero (Gilbert et al. 2020; Rodriguez et al. 2020; Suissa et al. 2020; Kaltenegger, Pepper, et al. 2021). It receives about 86% of the insolation that the Earth receives (Gilbert et al. 2020). The possible range of the atmospheric T - P profile for this planet is shown in Figure 3.13. The reflected spectra and the geometric albedo are also shown in this figure.

Kepler-1649c

This is an Earth-size planet lying in the habitable zone of its host star, which is of M5V spectral type. It is located at a distance of about 92 pc from the Earth (Vanderburg et al. 2020; Stephen R Kane, Z. Li, et al. 2020; Gvalani 2022). The T - P profile, the reflected spectra and the geometric albedo are presented in Figure 3.14.

Teegarden's Star b

Teegarden's Star is at a distance of about 3.83 pc and is of spectral type M7V (Teegarden et al. 2003; Alonso-Floriano et al. 2015). It has two

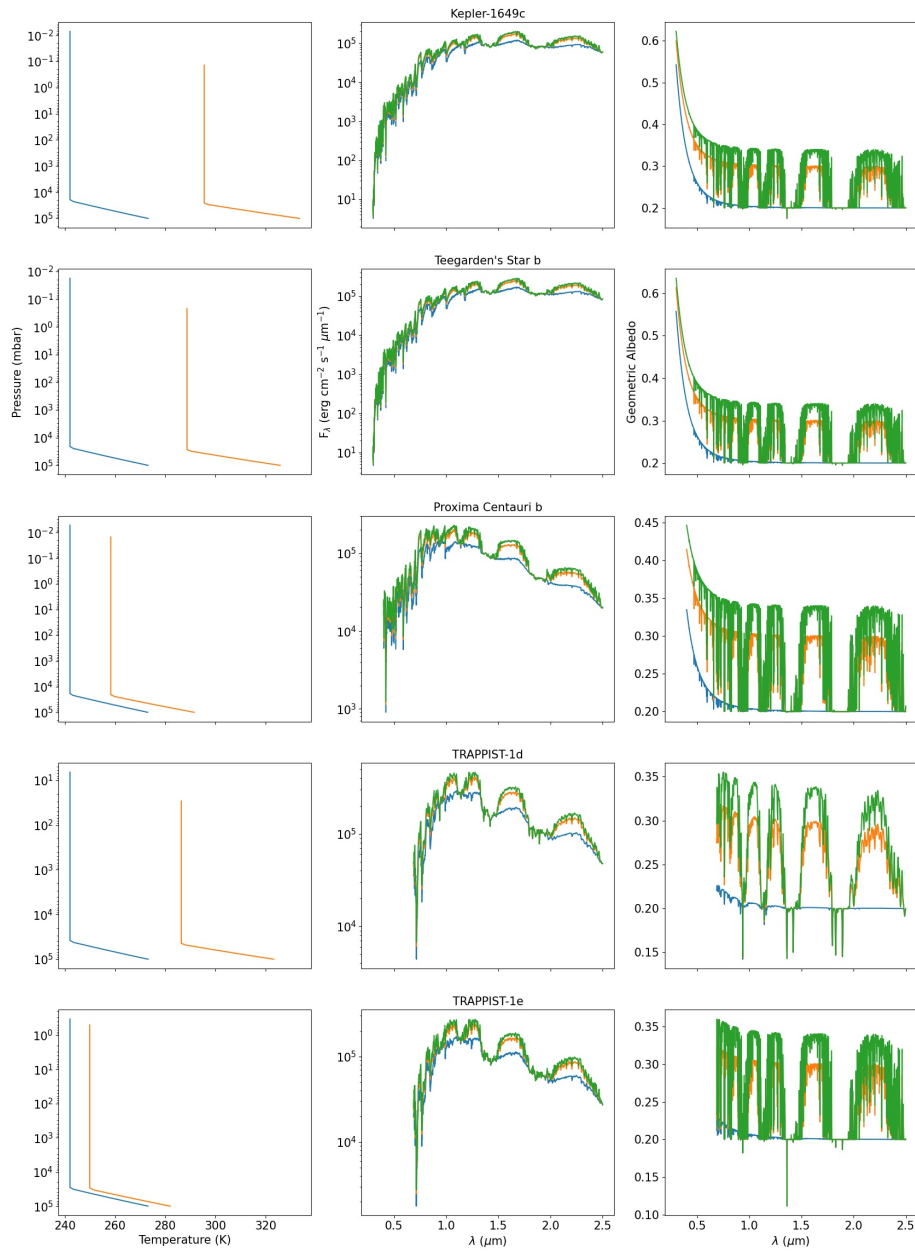


Figure 3.14: Same as Figure 3.13 but for Kepler-1649c, Teegarden's Star b, Proxima Centauri b, TRAPPIST-1d and TRAPPIST-1e.

planets Teegarden’s Star b and c. Both of them are super Earths but Teegarden b is the most Earth-like planet or maximum ESI value (see Table 3.3), discovered till now (Wandel and Lev Tal-Or 2019; Zechmeister et al. 2019). This planet orbits within the habitable zone and it is tidally locked. The T-P profile range, reflected spectra and the geometric albedo are presented in Figure 3.14.

Proxima Centauri b

Proxima Centauri b, a rocky planet, orbits within the habitable zone of our nearest neighbour Proxima Centauri (M5V), which receives about 65% of the total flux which our Earth gets from the Sun (Anglada-Escudé et al. 2016; Garraffo, Drake, and Cohen 2016; Martin Turbet, Leconte, et al. 2016; Ignasi Ribas et al. 2017; Victoria S Meadows et al. 2018; Lin and Lisa Kaltenegger 2020; Galuzzo et al. 2021).

We modeled the reflected spectra of Proxima Centauri b by using the stellar flux presented by Lin and Lisa Kaltenegger 2020. The T - P profile (derived similarly) for the atmosphere of Proxima Centauri b is shown in Figure 3.14 where a range is given. The reflected spectra and the geometric albedo for Proxima Centauri b are shown in Figure 3.14 for various surface Bond albedo determined by different surface compositions. Here also, it is maximum for Earth-like surface composition and minimum for no surface albedo.

TRAPPIST-1d and e

TRAPPIST-1 is another M dwarf of spectral type M8V, which is about 12 pc away from us, hosts seven rocky planets out of which, three are inside the habitable zone of the host-star (Gillon, Jehin, et al. 2016; Burgasser and Mamajek 2017; Gillon, Triaud, et al. 2017; O’Malley-James and Lisa

Kaltenegger 2019; Lin and Lisa Kaltenegger 2020). TRAPPIST-1e is most likely to have habitable surface conditions, as it receives about $\sim 66\%$ of stellar radiation that the Earth receives from the Sun and needs very little greenhouse effect to have a surface temperature such that liquid water can survive on its surface (Ravi Kumar Kopparapu, Ramirez, et al. 2013; Wolf 2017; Wolf 2018; T. J. Fauchez, Martin Turbet, Wolf, et al. 2020). Also, TRAPPIST-1e is quite similar in size to the Earth. On the other hand, TRAPPIST-1d has a very high ESI value of 0.9 (see Table 3.3). So it becomes important to model both the planets.

The T - P profile, the reflected spectra and the geometric albedo are presented in Figure 3.14 for both the cases. The reflected spectra and the geometric albedo were calculated for various surface materials. As the surface albedo increases, the reflected flux increases because the surface also contributes to the reflected flux. The geometric albedo is decreasing with the increase in wavelength because scattering becomes negligible at longer wavelengths. Also it decreases significantly with the decrease in the surface Bond albedo. For the zero surface albedo case, all the radiation is reflected only from the atmosphere.

Comparisons

The input stellar flux at the surface of the above planets is shown in Figure 3.15a. The reflected spectra for these planets for Earth-like surface albedo are shown in Figure 3.15b and the geometric albedo is shown in the Figure 3.15c. We can see that the reflected spectra follows the input stellar spectra in the visible wavelength region. The geometric albedo is highest for Kepler-22b and lowest for TRAPPIST-1e in the infrared. But in the optical, it is highest for the case of Teegarden's Star b and lowest for Kepler-22b.

The geometric albedo in the optical region is not estimated for any of the

planets around TRAPPIST-1 because it is a late M dwarf whose effective temperature is about 2400K. Its blackbody spectra peak lies at around $1\ \mu\text{m}$ and thus the flux in the optical is very less in magnitude as compared to the flux in NIR. The nature of geometric albedo depends on the opacity data of the planetary atmosphere or the T-P profile and the atmospheric composition of the corresponding planet.

3.4 Conclusions and Discussion

We presented the numerical models of the reflection spectra (in visible) for both the present and prebiotic Earth-like exoplanets that orbit within the habitable zone of main sequence stars of F, G, K and M spectral types. The model reflected spectra for the known exoplanets, which are orbiting around the stars of G, K and M spectral types is also presented.

We found that the nature of the reflected spectra is similar to the incident stellar spectrum i.e., the reflected flux peaks in the optical waveband but decrease significantly at longer wavelengths. However, Rayleigh scattering in the planetary atmosphere makes the reflected spectra comparatively steeper. The geometric albedo also decreases with the increase in wavelength because of the same reason i.e. Rayleigh scattering. The amount of reflected flux for the planets orbiting M dwarfs is significantly less compared to the stars of F, G and K spectral types. This is because the input stellar spectra peaks in the infrared where Rayleigh scattering is very less. The absorption lines of the biomolecules like O_2 , H_2O , O_3 , etc. are dominant in the geometric albedo. Owing to the fact that prebiotic early Earth-like exoplanets have a greater percentage of greenhouse gas CO_2 , they scatter more radiation than the present Earth-like exoplanets do. A present Earth-like exoplanet with higher abundance of greenhouse gases also have greater albedo. We also estimated the maximum possible

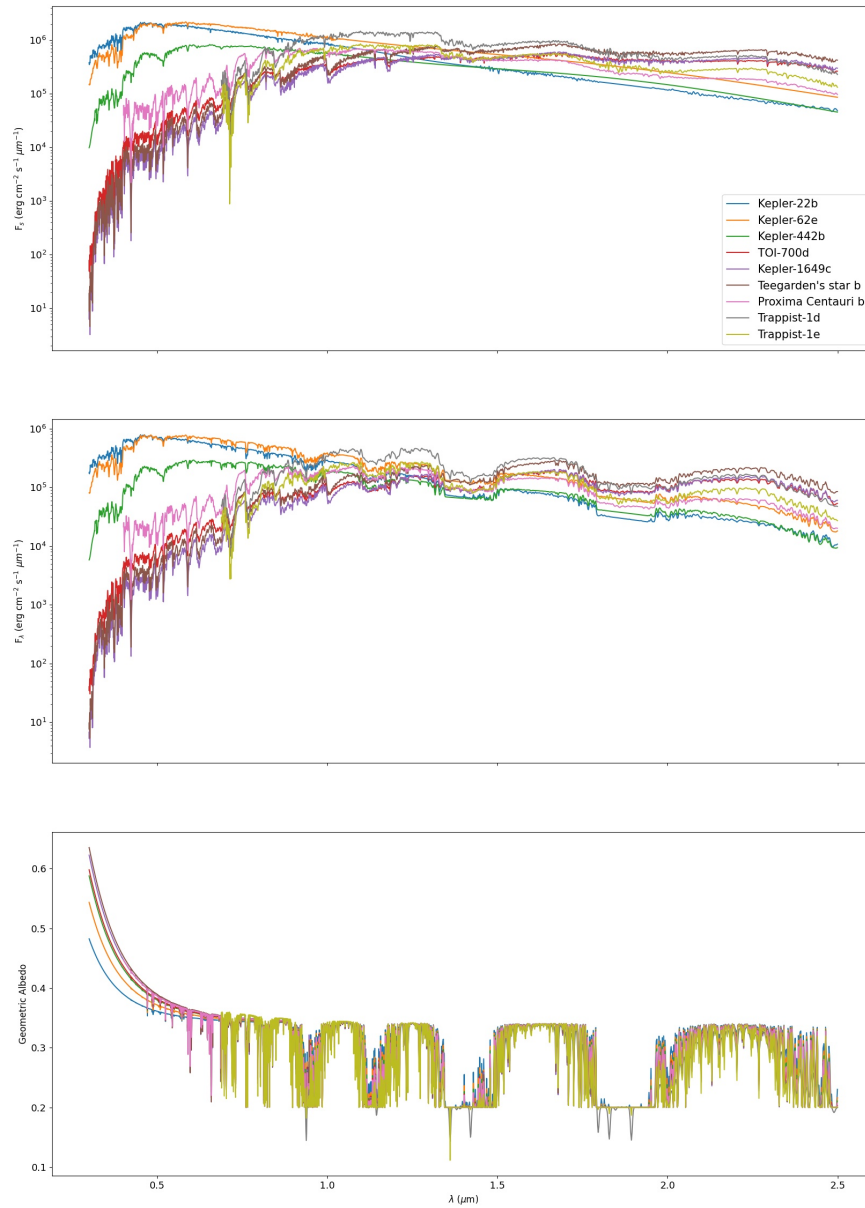


Figure 3.15: Comparison of the (a) input stellar flux, (b) reflected spectra and (c) geometric albedo for the nine planets in habitable zone.

values of Bond albedo for the known exoplanets and thus given a limit on Bond albedo for the planets to remain habitable.

We also investigated the effects of surface Bond albedo on the reflected spectra and geometric albedo for various solid and liquid surface composition. We considered several kinds of solid and liquid surfaces e.g., (1) present Earth-like surface composition, (2) early Earth-like surface composition, (3) 100% ocean cover, (4) 50% ocean and remaining with trees and grass and (5) 83% ocean and remaining with snow. The reflected flux and the geometric albedo increases with the increase in surface albedo. It is minimum for no surface albedo at all. The effect of the surface albedo becomes negligible for an atmosphere thick enough to obstruct the incident stellar radiation to reach the solid or liquid surface. Thus, surface composition plays a pivotal role in calculating the reflectivity of the planet. In the infrared region, the planetary surface with ocean, vegetation, desert etc. play important role in determining the reflected as well as the re-emitted thermal radiation. However, here we did not consider the thermal radiation that gets re-emitted.

In the future, since many big-budget missions are coming like 6 m class space telescope operating in the ultraviolet, optical and NIR, GMT, TMT, Extremely Large Telescope (ELT), etc., our models will play a crucial role in the habitability study of the Earth-like exoplanets. By knowing the planet's reflectivity, Bond albedo and the transmission spectra, we would be able to know about the factors like planet's surface and atmospheric composition, T-P profile of the atmosphere, presence of clouds, greenhouse gases, etc., which play a vital role in finding the habitability of the planet.

Chapter 4

Effect of multiple scattering on transmission spectra for Earth-like exoplanets¹

4.1 Introduction

When an extra-solar planet passes in front of the host star, some fraction of the stellar radiation gets transmitted from the planet's atmosphere. The radiation interacts with the atmosphere through scattering and absorption and provides the spectral fingerprints on the transmitted flux. Transmission spectra of the Earth through lunar eclipse observations have been calculated by Enric Pallé et al. [2009](#); Pallé et al. [2010](#); Yan et al. [2015](#). Wunderlich, Mareike Godolt, et al. [2019](#) calculated the transmission spectra of terrestrial exoplanets that orbit around M-dwarfs within the habitable zone. Ehrenreich et al. [2006](#); Lisa Kaltenegger and Traub [2009](#) also calculated the transit-depth for Earth-sized planets and Lin, MacDonald, et al. [2021](#) calculated the same for the prebiotic and present Earth. Ehrenreich et al. [2006](#); Wunderlich, Scheucher, et al. [2020](#); Madden and

¹This chapter presents the work from the published papers - Singla et al. 2023, ApJ, 944 155 and Singla & Sengupta 2023, NewA, Volume 102, August 2023, 102024.

Lisa Kaltenegger 2020; Gialluca et al. 2021, etc also presented some model transmission spectra for Earth-like exoplanets.

In these models, only the total extinction of the incident stellar flux is considered by the use of "Beer-Bouguer-Lambert's law" (Tinetti, Encrenaz, and Coustenis 2013a). These models, albeit include the scattering opacity to the true absorption opacity, do not incorporate the angular distribution of the transmitted photons due to scattering in planetary atmosphere. Sengupta, Chakrabarty, and Tinetti 2020 have considered the in and out scattering for the hot Jupiters while modeling the transmission spectra. The single scattering albedo and the scattering co-efficient is negligible for wavelengths beyond visible. Thus, for that wavelength region, that assumption works fine. There can be two phenomena possible due to multiple scattering. One, the transmitted flux may increase due to the contribution of the multiple scattering along our line of sight; two, the transmitted flux may decrease due the multiple scattering of the radiation in other directions except along our line of sight. Thus the resultant is the increase in the transmission flux or the decrease in the transit-depth. Hence, for the smaller wavelengths (visible), this method overestimates the transmission depth. Here, the diffused reflection and transmission because of multiple scattering become crucial.

We model the transmission spectra for Earth-like exoplanets that orbit around Sun-like stars (for with and without multiple scattering). Surface albedo of the planet is not considered for calculating the transmission spectra as it predominantly convey the information of the upper atmosphere. Firstly, we calculate it for the case of zero scattering albedo (without multiple scattering). For this, we use "Beer-Bouguer-Lambert's law" for the present and prebiotic Earth-like exoplanets using publicly available code `Exo-Transmit`² (Kempton et al. 2017). A study of the transmission spec-

²https://github.com/elizakempton/Exo_Transmit

tra which is calculated by using the `Exo-Transmit` code and the `TauREx` software package (Waldmann et al. 2015) has been compared in Sengupta, Chakrabarty, and Tinetti 2020. Secondly, we calculate the transmission spectra for Earth-like exoplanets, which orbit around Sun-like stars, by including multiple scattering. For that, the multi-scattering radiative transfer equation for diffused reflection and transmission is solved following Sengupta, Chakrabarty, and Tinetti 2020. This includes the use of discrete space theory (Peraiah and Grant 1973). We see the dissimilarities in the transit depth when the scattering albedo is included versus when it is not included. We also study the effect of the clouds with various scattering cross-sections on the transit depth.

We determine that diffuse transmission radiation due to scattering can affect the overall broad natures of the transmission spectra, especially when the single-scattering albedo increases in the presence of clouds.

In the upcoming section, we discuss about the basic idea of the transit depth. In Section 4.3, we present the transmission spectra for present and prebiotic Earth-like exoplanets without including multiple scattering (using "Beer-Bouguer-Lambert's law"). The effect of multiple scattering on the transit-depth spectra is shown in section 4.4. In section 4.5, we summarize and conclude our results.

4.2 Transit Depth

When the exoplanet is at the primary eclipse position, it blocks some of the starlight along our line of sight resulting into a reduction in the observed stellar flux. While transiting, a fraction of the star's light passes from the planet's atmosphere providing signature of the gas present there. The stellar radiation that is subjected to absorption and scattering in the planet's atmosphere is known as the transmission or transit spectra. The

transmission spectra is usually presented by a wavelength dependent quantity called the transmission or transit depth. Like reflected spectra, it also contains a lot of information about the planetary atmosphere.

Transit depth is the ratio between the stellar flux obtained with and without transit. It can be expressed as

$$D = 1 - \frac{F_{\text{trans}}}{F_{\text{star}}} \quad (4.1)$$

where F_{trans} is the star's flux obtained during the planetary transit epoch and F_{star} is the unblocked stellar flux or the stellar flux during the out of transit epoch. F_{trans} is given as (Kempton et al. 2017; Sengupta, Chakrabarty, and Tinetti 2020):

$$F_{\text{trans}} = [1 - (\frac{R_{\text{pl,atm}}}{R_{\text{star}}})^2] F_{\text{star}} + F_{\text{atm}} \quad (4.2)$$

where, $R_{\text{pl,atm}}$ is the planet's radius including its atmosphere and R_{star} is the host star's radius, F_{atm} is the stellar flux which gets transmitted from the planetary atmosphere along our line of sight.

4.3 Transmission spectra using "Beer-Bouguer-Lambert's law"

In order to calculate the transmitted flux, we used "Beer-Bouguer-Lambert's law" (Tinetti, Encrenaz, and Coustenis 2013b) that is given as:

$$I(\lambda) = I_0(\lambda)e^{-\tau_\lambda/\mu_0} \quad (4.3)$$

where $I(\lambda)$ is the transmitted stellar intensity through the planetary atmosphere and $I_0(\lambda)$ is the incoming stellar intensity on the planet. In the above equation, μ_0 is the cosine of the angle between the direction of the

incident radiation and the normal and τ_λ is the optical depth along the path of the ray. The expression for the optical depth along the line of sight ($\tau(\lambda, z)$) is given by:

$$\tau(\lambda, z) = 2 \int_0^{l(z)} \chi(\lambda, z) \rho(z) dl \quad (4.4)$$

where $\chi(\lambda, z)$ is the extinction coefficient (sum of the scattering and the absorption coefficient), $\rho(z)$ is the density of the planetary atmosphere, z is the height of the atmosphere from the planetary surface, l is the distance covered by the radiation in the planetary atmosphere given by (Tinetti, Encrenaz, and Coustenis 2013a):

$$l(z) = \int dl = \sqrt{(R_p + z_{\max})^2 - (R_p + z)^2} \quad (4.5)$$

where R_p is the planet's radius below which the medium becomes opaque at all wavelength and z_{\max} is the maximum height (on the top of R_p) above which photons don't suffer any absorption or scattering. We calculate the transmission spectra by using `Exo-Transmit` package (Kempton et al. 2017).

4.3.1 Atmospheric model

The Earth's atmospheric T-P profile is used which is same as that used for calculating the reflection spectra in [chapter 3](#). In order to calculate the transmission spectra, we first compute the absorption and scattering coefficients of the atmosphere by using `Exo-Transmit` (Kempton et al. 2017), which is same as that used for the reflected spectra case (for details, refer [3.2](#)). Since the Earth's atmosphere is sufficiently cool, here also we have neglected the collision induced absorption (CIA) of hydrogen. We have adopted the molecular abundances of the present Earth's atmosphere

(Sagan et al. 1993). For the cloudy atmosphere, the cloud height is considered to be at three different heights of about 2.2 km, 9.5 km and 17 km from the surface of the planet.

4.3.2 Results

We calculated the transmission spectra for the present and prebiotic Earth-like exoplanets using "Beer-Bouguer-Lambert's law". Fig. 4.1 shows the transmission spectra for the present and prebiotic Earth-like exoplanets. Fig. 4.1a presents the transmission spectra up to a wavelength of $4.5 \mu\text{m}$ while Fig. 4.1b shows the same up to the wavelength $30 \mu\text{m}$. The transmission depth due to absorption by O_2 , H_2O , CO_2 and O_3 are marked in the spectra. For the early or prebiotic Earth-like exoplanets, the absorption lines of only CO_2 molecules are seen.

By studying the absorption lines in the spectra can help us in detecting the bio-molecules or the volatiles present in the planetary atmospheres. In the transmission spectrum of prebiotic Earth presented in Fig. 4.1, signatures of CO_2 can be found at $1.4 \mu\text{m}$, $1.6 \mu\text{m}$, $2.0 \mu\text{m}$, $2.7 \mu\text{m}$ and at $4.3 \mu\text{m}$. On the other hand, the signatures of H_2O at $0.72 \mu\text{m}$, $0.82 \mu\text{m}$, $0.94 \mu\text{m}$, $1.1 \mu\text{m}$, $1.87 \mu\text{m}$ and $2.7 \mu\text{m}$ are clear in the transmission spectrum of modern Earth. In the case of modern Earth, signatures of O_2 can also be found at $0.63 \mu\text{m}$, $0.69 \mu\text{m}$, $0.76 \mu\text{m}$ and that of CO_2 at $1.4 \mu\text{m}$, $2.7 \mu\text{m}$, $4.3 \mu\text{m}$. The signature of O_3 is visible at $3.3 \mu\text{m}$.

Fig. 4.2 shows the transmission spectra for the increased abundances of greenhouse gases in the atmosphere of the terrestrial exoplanet. Here we notice that the transmission depth increases with the increase in the abundances of greenhouse gases in the planetary atmosphere. The differences arise due to the different amounts of scattering in both the cases. However, this increase in the transmission depth is found to be confined

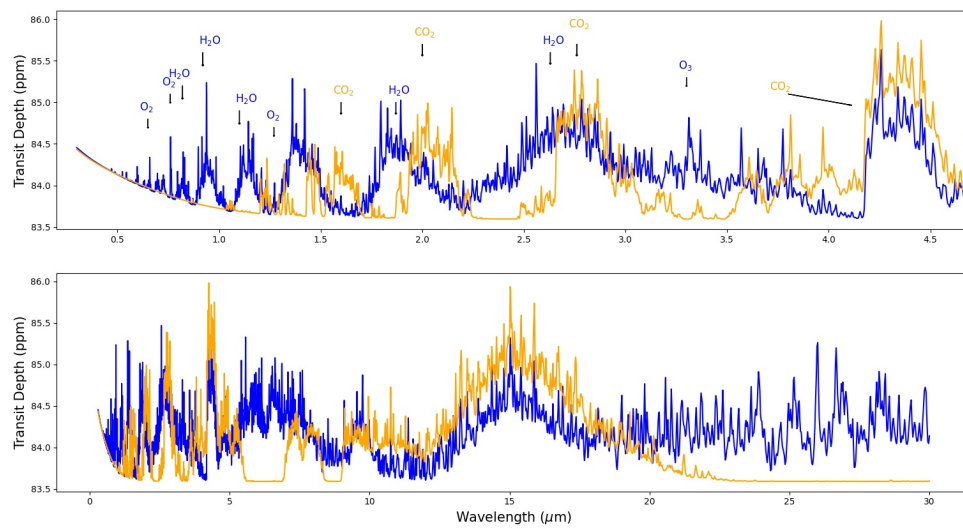


Figure 4.1: Transmission spectra of present (blue) and early (orange) Earth-like exoplanets. In the first panel, the transmission spectra up to a wavelength of $4.5 \mu\text{m}$ is shown, and in the second panel, it is shown up to the wavelength $30 \mu\text{m}$. The absorption lines of O_2 , H_2O , CO_2 and O_3 are marked. For the early Earth-like exoplanets, the absorption lines of only CO_2 molecules are seen.

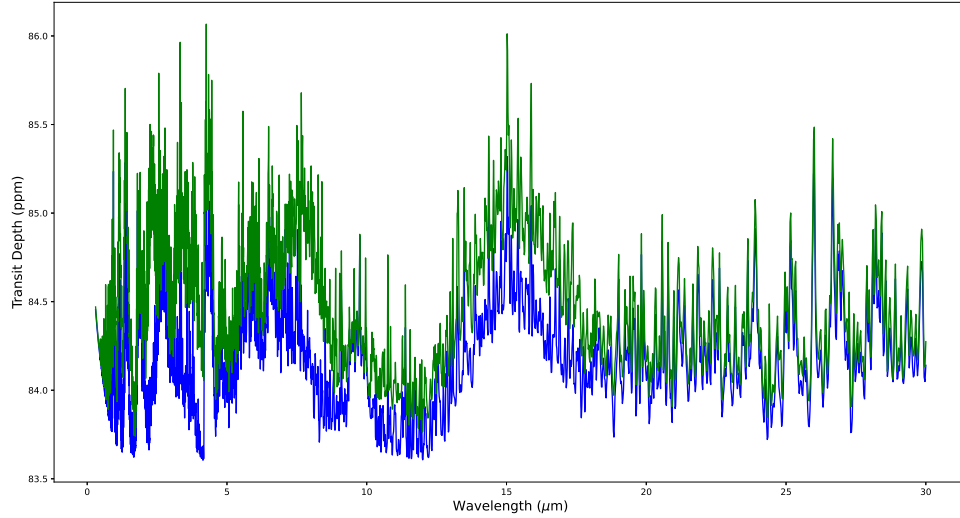


Figure 4.2: Transmission spectrum of the present Earth but with increased greenhouse gas abundance (green). For a comparison, transmission spectrum (blue) of the Earth with actual atmospheric abundance is also presented.

only up to a certain wavelength region. This happens due to the Rayleigh scattering which is dominant in smaller wavelength region. Due to scattering, less transmitted flux reaches along our line of sight. In infrared, both the curves seem to merge where the effect of Rayleigh scattering is insignificant. In the next section, we will improve upon this by including the multiple scattering.

The observations of the various exoplanetary atmospheres indicate that the presence of clouds or hazes are a typical occurrence in the planetary atmospheres (Kreidberg, Jacob L Bean, et al. 2014; Sing et al. 2016). This is one of the reasons for weak or no molecular feature observed in the transmitted spectra of quite a few hot Jupiters (Sánchez-López et al. 2020). The same situation may arise for the terrestrial exoplanets if the upper atmosphere is covered by clouds or hazes. The presence of clouds or hazes however, increases the Rayleigh scattering.

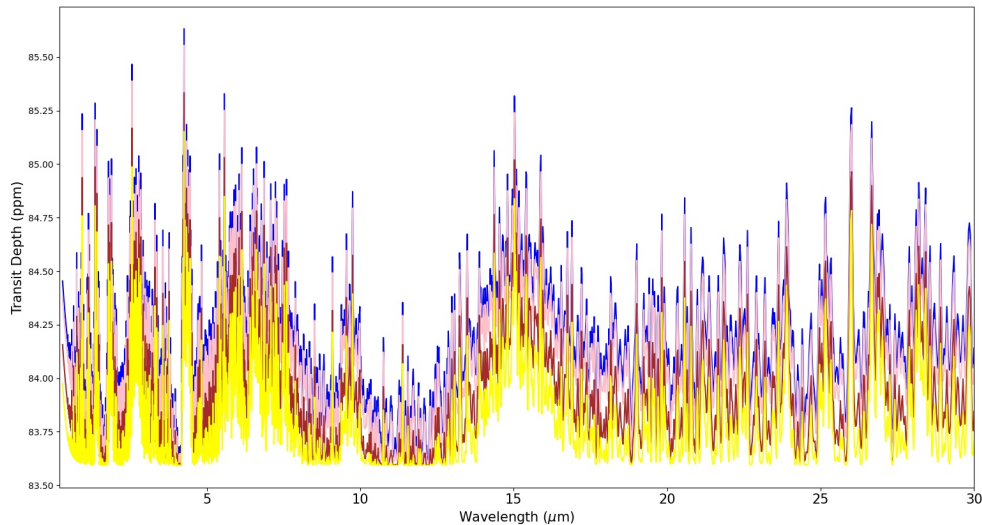


Figure 4.3: Transit spectra for present Earth with clear sky (blue) and for 100 percent cloud coverage at three different heights i.e. 2.2 km (pink), 9.5 km (brown) and 17.0 km (yellow) from the surface of the planet.

For gray cloud calculations, we selected a pressure layer in the atmosphere at which the cloud’s top is optically thick. We provided a threshold pressure within the pressure range of the T-P profile and performed the radiative transfer calculations for pressures below than the pressure at cloud deck. We used `Exo-Transmit` package (Kempton et al. 2017) for the calculation of cloud optical depth. In Figure 4.3, we see that the transmission spectra for clear sky and for the sky with 100% coverage of clouds at three different atmospheric heights i.e. 2.2 km, 9.5 km and 17.0 km from the surface of the planet.

The transmission depth reduces in magnitude with the increase in the height of the cloud level. Since the `Exo-Transmit` code does not incorporate diffused radiation by multiple scattering, it just reduces the magnitude of the transmission depth. As the height of the cloud increases, the threshold pressure decreases. As a consequence, a comparatively smaller

atmospheric region above the clouds yields a featureless transmission spectra. Since we assume a vertically homogeneous abundance, the spectral feature remain the same with the change in the cloud height. The effect of multiple scattering by including clouds has been incorporated in the next section.

4.4 Effect of multiple scattering on the transmission spectra

Multiple scattering becomes essential in computing the reflected or the transmission spectra. Presence of clouds, haze, dust particles, the gas molecules, etc. is responsible for multiple scattering of the stellar radiation. If we include multiple scattering, the spectra becomes one step closer to the realistic situation. To calculate the transmission spectra, the multi-scattering radiative transfer equation in one dimension is solved following Sengupta, Chakrabarty, and Tinetti 2020 (refer section 3.2.1 for the equation). Discrete space theory is used for the calculations where the atmosphere is divided into several layers (For details, see section 3.2).

4.4.1 Atmospheric model

For calculating the transmission spectra by including multiple scattering, we take the atmospheric chemical composition for the modern Earth-like exoplanets same as taken by Kawashima and Rugheimer 2019 and opacity data, i.e. absorption and scattering cross-sections for all the molecules that have been taken in the planet's atmospheric abundance, from the database for PICASO (Batalha et al. 2020). The observed temperature-pressure profile of the Earth's atmosphere is considered for the calculations. Here also we consider two types of atmosphere cloudy and cloud-free. In the

case of cloudy atmospheres, we consider very thin clouds or haze and we have used an approximate Rayleigh model to express the effect of these clouds/haze following Sing et al. 2016; Kempton et al. 2017, etc.

We have included thin clouds with scattering cross-sections (σ) equal to 100, 200 and 400 times the scattering cross-section (σ_R) of the dominant atmospheric constituent i.e. nitrogen in this case. The cloud deck and base have been fixed at 5×10^2 Pa and 5×10^3 Pa. The cloud position of the case of reflected spectra was kept at deeper layers of the atmosphere (in [chapter 3](#)) while for the case of the transmission spectra, the clouds are considered at the upper layers of the atmosphere. It is because we can probe only the outer atmosphere by transmission spectra. Also, we will probe complementary portions of the atmosphere in terms of the altitude. A terrestrial exoplanet usually should have water cloud in the upper atmosphere.

4.4.2 Results

Using the atmospheric models described in section [4.4.1](#), the transmission depth for modern Earth-like exoplanets orbiting around Sun-like stars at wavelengths up to $2.0 \mu\text{m}$ is shown in [Figure 4.4](#). We can see that the transit depth reduces with the inclusion of diffuse radiation due to scattering as explained by Sengupta, Chakrabarty, and Tinetti 2020. The transmission depth increases with the inclusion of clouds as the cloud particles block the transmitted flux through the atmosphere. Clouds also suppress the absorption features of the molecules in shorter wavelengths. The effect of diffusion due to scattering on the broadband continuum can be noteworthy with respect to the levels of the individual absorption features, especially when the atmospheric clouds are present. This calls for more accurate modeling of the transmission spectra by solving the complete radiative transfer equation. Otherwise detecting the features of the biosignatures of

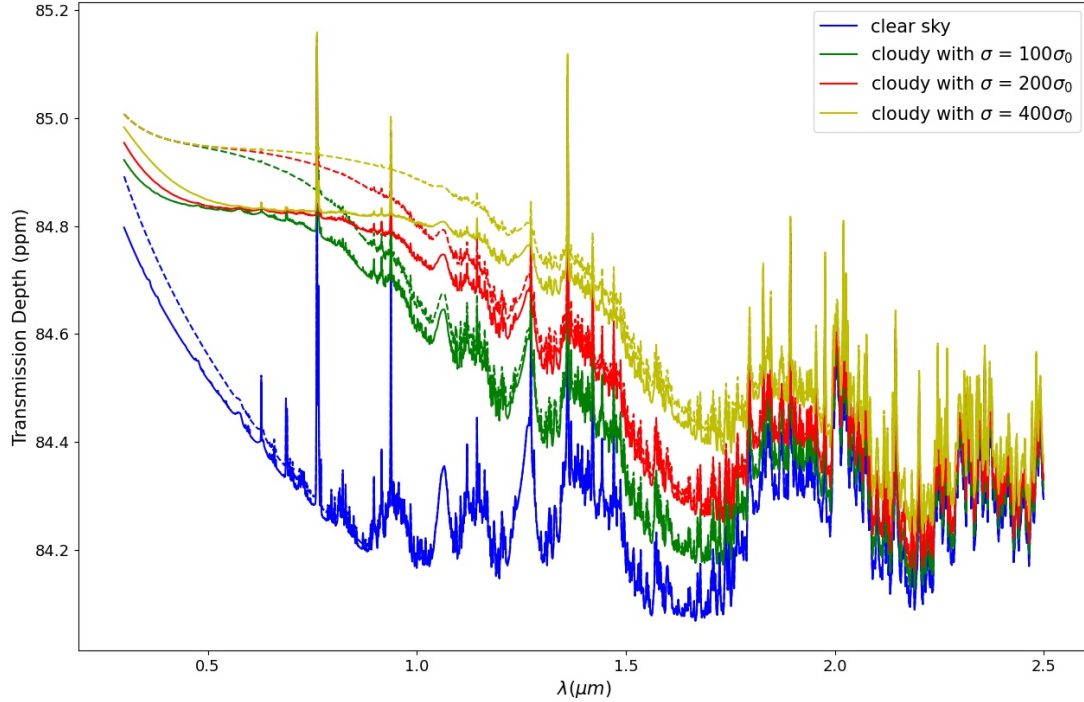


Figure 4.4: Transmission depth for the Earth-like exoplanets with (solid) and without (dashed) multiple scattering for cloudy and cloud-free atmospheres (see Section 4.4.1). However, scattering opacity is also included even for cloud-free atmosphere case.

the Earth-like planets can be confusing and may be erroneous. Of course, at longer wavelength regions, all the plots are found to merge because Rayleigh scattering is negligible in that range.

When multiple scattering is not considered, especially in the longer wavelengths where the values of ω are extremely low ($\omega \approx 0$), we can use the "Beer-Bouguer-Lambert's law" instead of solving the radiative transfer equations. Note that even when the diffuse radiation because of multiple scattering is not incorporated, total atmospheric optical depth is computed by both the absorption and the scattering opacities.

4.5 Summary and Conclusions

In the first part of the chapter, we presented the transmission spectra for present and prebiotic Earth-like exoplanets using "Beer-Bouguer-Lambert's law". In the shorter wavelength region, the transmission depth increases with an increase in the abundances of greenhouse gases. Also, the transmission depth reduces in magnitude with the increase in the height of the cloud level from the planetary surface.

In the second part, we improvised the transmission spectra results by including the multiple scattering. For that, we solved the multiple scattering radiative transfer equation. We found that the transit depth reduces with the inclusion of diffuse radiation due to multiple scattering. But it increases if we include the clouds as the cloud particles block the transmitted flux through the atmosphere. Also, it increases with the increase in the scattering coefficient of the clouds. Clouds suppress the absorption features of the molecules in shorter wavelengths but at longer wavelengths, all the plots are found to merge because the effect of multiple scattering is negligible.

One might note that with the inclusion of clouds, the transit depth reduces in magnitude for the first work. But in the second work, it increases when the clouds are considered. Clouds affect the transmission spectra in two opposite ways for the two cases due to the different models used for the calculations. In one case, we have used the vertically homogenous atmosphere, while in the other case, we used height dependent abundances. Also, the cloud model is different for both the cases. And we can say that the second model is more accurate and precise than the first one.

Chapter 5

Modelling Polarization and Albedo phase curves for Earth-like Exoplanets¹

5.1 Introduction

Over 5000 extra-solar planets have been detected till date and many techniques are being developed to study their atmospheres in detail. Techniques such as reflection, transmission and emission photometry and spectroscopy (Tinetti 2006; Sara Seager 2010) help in characterizing the planetary atmospheres. Characterizing the terrestrial exoplanets is extremely challenging because of their very small size and low planet to star flux ratio (Franck Selsis, Lisa Kaltenegger, and Paillet 2008; Rice 2014). We will only be able to detect the biosignatures on extra-terrestrial planets unambiguously if we can precisely characterize the Earth-sized planets which lie in the circumstellar habitable zone of their host stars (Huang 1959; Huang 1960; D. Whitmire, R. Reynolds, and J. Kasting 1991; James F Kasting, Daniel P Whitmire, and Ray T Reynolds 1993; Ravi Kumar Kopparapu, Ramirez, et al. 2013; Torres et al. 2015; Stephen R Kane, Hill, et al. 2016;

¹This chapter presents the work from the published paper - Singla et al. 2023, ApJ, 944 155

Fujii et al. 2018; Covone et al. 2021). Presence of the biosignatures like oxygen, water, methane, etc. signals the high chances of the existence of life on these planets. The presence of oxygen and ozone is the result of an extended biomass production through oxygenic photosynthesis (Owen 1980; Sagan et al. 1993; Selsis, Despois, and Parisot 2002; Selsis 2004; Segura et al. 2007; Seager 2008; Franck Selsis, Lisa Kaltenegger, and Paillet 2008; Scharf 2009; John L Grenfell et al. 2014; Fujii et al. 2018; Claudi and Alei 2019).

Several polarimetric techniques are increasingly being used for the study of exoplanetary atmospheres. Polarimetric studies for planets were initiated with the observation of the Solar system objects and are still being continued (David L Coffeen 1969; D. Coffeen and Gehrels 1969; Hall and Riley 1974; Michalsky and Stokes 1977; West et al. 1983; Joos and Schmid 2007, etc.). Mallama 2009 characterized the terrestrial exoplanets based on the phase curves of some solar system planets. Daphne M Stam, Joop Hovenier, and Waters 2003; Daphne M Stam 2003; Loic Rossi, Berzosa-Molina, and Daphne M Stam 2018, etc. studied the polarization spectra for the extra-solar planets. By studying the polarization profiles, we can extract information about the atmospheric as well as physical properties such as cloud distribution, mean size of cloud particulate as well as rotation-induced oblateness etc. as demonstrated by Sengupta and Krishan 2001; Sengupta and Maiti 2006; Sengupta 2008; Sengupta and Mark S Marley 2009; Sengupta and Mark S Marley 2010; Sengupta and Mark S Marley 2011; Sengupta and Mark S Marley 2016; Sengupta 2016b for brown dwarfs and self-luminous exoplanets. In addition, phase dependent polarization of reflected planetary radiation can help understanding more atmospheric composition including biosignatures, surface constituents like ocean, ice, forest etc and thus the evidence of a habitable environment in exoplanets (Zubko, Baba, and Murakami 2008; Kedziora-Chudczer and Bailey 2010;

Loic Rossi, D. Stam, and Turbet 2017). The traces of exomoons are also being searched by means of polarization (Sengupta and Mark S Marley 2016; J. Molina, D. Stam, and Rossi 2017; J. B. Molina, Loic Rossi, and Daphne M Stam 2018).

The reflected light can be polarized because of the various scattering processes which depend on the types of scatterers and the scattering mechanism (Sara Seager 2010). Linear polarization signals from the starlight reflected from the horizontally inhomogeneous Earth-like planets is presented in Karalidi and D. Stam 2012. Groot et al. 2020; Loic Rossi and Daphne M Stam 2018 studied the linearly or circularly polarized signals from the sunlight that gets reflected from the model Earth. Polarization signals from the stellar light reflected by the Earth-like exoplanets have been studied by D. Stam 2008; T. Fauchez, Loic Rossi, and Daphne M Stam 2017; Wei and Zhong-quan 2017; Muñoz 2018; Sterzik et al. 2019; Patty et al. 2021; Gordon et al. 2022, among others. Wang, Qu, and H. Li 2019 have used PARASOL data to calculate the variation of the disk-integrated polarization. Karalidi, D. Stam, and Hovenier 2011; Karalidi, D. Stam, and Hovenier 2012; Michael F. Sterzik and Manev 2020 have modeled the polarized signal from the clouds on exoplanets and Michael E Zugger et al. 2010; M. Zugger et al. 2011 from the exoplanetary oceans and atmospheres. D. Stam and Hovenier 2005 have estimated the errors in the calculated phase functions and albedos of planets if polarization is neglected.

Detecting the polarization signals of the reflected radiation is, however, extremely difficult because of the very low signal to noise (S/N) ratio as compared to that of the planets from our Solar-system. Some of the upcoming telescopes will unravel the polarimetric properties of the Earth and the exoplanets. LOUPE ("Lunar Observatory for Unresolved Polarimetry of the Earth"), a small spectropolarimeter is being developed to observe the Earth (as an exoplanet) from the Moon (Klindžić et al. 2021; Kara-

lidi, D. Stam, Snik, et al. 2012) and also ELF (Exo-Life finder) Telescope (Berdyugina et al. 2018) will be used for the direct detection of exoplanet biosignatures. Other big-budget missions like HabEx, LUVOIR, Roman Space Telescope, etc. will also have imaging polarimetric facility. These missions will additionally have coronagraphic instruments onboard which will allow us to detect polarimetric signals from the exoplanets in the habitable zones directly.

Most of the above mentioned polarization models either use Monte Carlo method or solve 1-D vector radiative transfer equations and invoke generalized spherical harmonic expansion to integrate the scattering polarization over the visible disk. In the present work we compute the azimuth-dependent intensity vectors by solving 3-D vector radiative transfer equations. The disk integrated flux and polarization are calculated by integrating the intensity vector at each local point over the illuminated disk. The 1-D version of the same numerical code has also been used to solve the radiative transfer equations in their vector form for the calculation of polarized spectra of rotation-induced oblate self-luminous exoplanets and cloudy brown- dwarfs (Sengupta and Mark S Marley 2009; Sengupta and Mark S Marley 2010; Mark S Marley and Sengupta 2011; Sengupta 2016b; Sengupta and Mark S Marley 2016; Sengupta 2018). However, in those research, the spherical harmonic expansion approach was employed to compute the polarisation over the object's rotation-induced oblate disk. This scalar version of this code has also been used for the transmission spectra calculations for the hot Jupiters (Sengupta, Chakrabarty, and Tinetti 2020; Chakrabarty and Sengupta 2020). Chakrabarty and Sengupta 2021 have presented the polarization models for hot Jupiters by solving 3D vector radiative transfer equations. In this work, we employ the same methodology to calculate the polarization for the Earth-like exoplanets. Study of the albedo and polarization phase curves can add to the information that is

obtained from the transmission and the reflection spectroscopy. Moreover, these techniques can be used to characterize the planets with arbitrary orbital alignment w.r.t. the line of sight.

In the next section, we discuss about the necessary inputs used to calculate the albedo and polarization phase curves for Earth-like exoplanets. In section 5.3, vector phase curve models are presented. In section 5.4, we describe the results and finally, in the last section, we present the conclusions of this work.

5.2 Atmospheric models for Earth-like exoplanets

We present the models for phase curves for geometric albedo and linear polarization for the Earth-like exoplanets that orbit around Sun-like stars. For calculating that, we take the atmospheric chemical composition for the modern Earth-like exoplanets from Kawashima and Rugheimer 2019 and opacity data, which is, absorption and scattering cross-sections for the molecules that have been taken in the planetary atmospheric composition (abundances from Kawashima and Rugheimer 2019), from the database for PICASO (Batalha et al. 2020). The observed T-P profile of the Earth's atmosphere is considered for the calculations. We consider two types of atmosphere in all of our model calculations: cloudy and cloud-free. In the case of cloudy atmospheres, we consider very thin clouds or haze and we have used an approximate Rayleigh model to express the effect of these clouds/haze following Sing et al. 2016; Kempton et al. 2017, etc.

We considered the cloud position between the pressure levels of 1×10^3 Pa and 5×10^4 Pa with a scattering cross-section equal to 400 times the scattering cross-section of nitrogen gas. A terrestrial exoplanet usually should have water cloud in the upper atmosphere. For large cloud particulates, Mie scattering phase matrix should be appropriate to describe the angular

distribution of photons before and after the scattering. But for small size of cloud particles, Rayleigh phase matrix serves the purpose reasonably well. In the present work we have used Rayleigh phase matrix for water droplets (Sengupta and Maiti 2006).

5.3 The Phase Curve Models

The reflected light observable from the planets depends on their orbital phase and the study of phase curves conveys valuable information of the atmospheres and surfaces of the Earth-like exoplanets. The orbital phase (α_{orb}) is 0° when the maximum area of the illuminated disk is viewed and 180° when the minimum or no illuminated part of the planetary disk is viewed. However, modeling these phase curves is cumbersome and requires us to invoke three-dimensional radiative transfer models as explained by (Chakrabarty and Sengupta 2021). Here, we solve the 3-D vector radiative transfer equation to calculate both the albedo (total reflectivity of the disk) phase curves and the disk-integrated polarization phase curves. The 3-D vector radiative transfer including multiple scattering is expressed as:

$$\begin{aligned} \mu \frac{dI(\tau, M, \Phi, \mu, \phi)}{d\tau} = I(\tau, M, \Phi, \mu, \phi) \\ - \frac{\omega(\tau)}{4\pi} \int_0^{2\pi} \int_{-1}^1 P_m((\mu, \phi; \mu', \phi')) I(\tau, M, \Phi, \mu', \phi') d\mu' d\phi' \\ - \frac{\omega(\tau)}{4\pi} F_0 e^{-\tau/\mu_0} P_m(\mu, \phi; -\mu_0, \phi_0) \end{aligned} \quad (5.1)$$

Here, \mathbf{I} is the Stokes vector,

$$\mathbf{I} = \begin{bmatrix} I \\ Q \\ U \\ V \end{bmatrix} \quad (5.2)$$

P is the scattering phase matrix and (M, Φ) is an arbitrary point on the illuminated disk grid, at which the reflected radiation can be calculated. ϕ_0 is the zero point of ϕ at every location (M, Φ) . It is described in Chandrasekhar 1960 and Chakrabarty and Sengupta 2021.

The partial illumination of a planetary disk yields net non-zero disk-integrated scattering polarization of the reflected light. A study of this polarization can provide us information about the atmospheric clouds in detail, surface composition, and also the light absorbers present in the atmospheres (Chakrabarty and Sengupta 2021). The incident stellar radiation is assumed to be unpolarized and the polarization of the planet's reflected light is solely caused by the scattering process. We ignore polarization due to strong magnetic field if any.

The state of polarization of each beam of ray after scattering is determined by the scattering phase matrices which depend on the scattering mechanism. We follow the methods prescribed by Chakrabarty and Sengupta 2021 for solving the vector radiative transfer equations and for the calculation of the phase dependent reflected flux and the polarization (P) averaged over the illuminated planetary disk.

We noted how surface albedo affects the overall disk albedo and polarization as depicted in Figure 5.1. For the rest of the calculations, we considered the value of surface albedo to be 0.14 (surface Bond albedo for present Earth-like exoplanets). Figure 5.2-5.3 show the the total albedo and

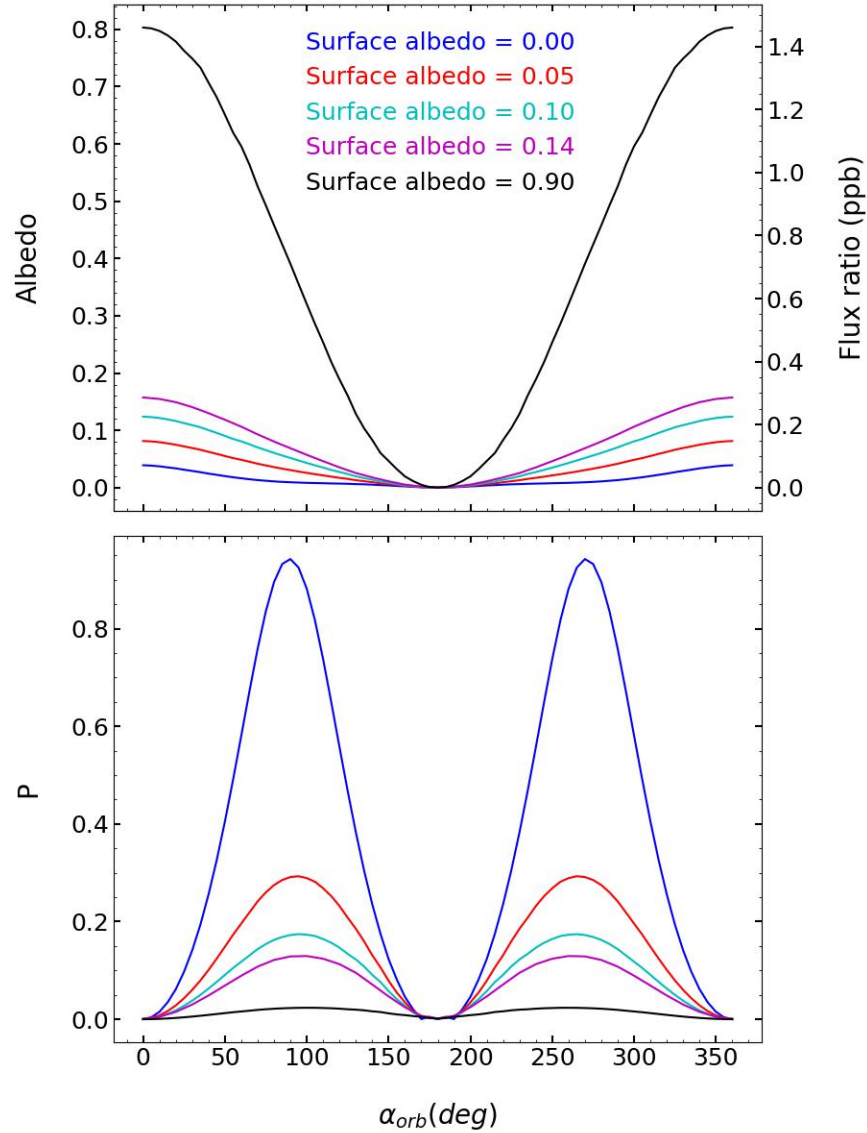


Figure 5.1: Effect of surface albedo on the phase curves of albedo (or flux ratio, $F(\alpha_{orb})/F_0$) and net polarization (P) integrated over the illuminated planetary disk at a wavelength of $0.6 \mu\text{m}$ and at an orbital inclination = 90° . We have used surface albedo 0.14 for our calculations. And 0.9 surface albedo is for the case of snowball (fully covered with snow) planet.

the disk polarization (P) at $\lambda = 0.6 \mu\text{m}$ and $\lambda = 1 \mu\text{m}$ for cloudy as well as cloud-free atmospheres, by considering multiple scattering of incident radiation. Figure 5.4 shows the same for visible wavelength ($\lambda = 0.6 \mu\text{m}$), if only single scattering is considered. These phase curves can be detected with the next-generation polarimetric missions which will use their coronagraphic instruments to resolve the Earth-like exoplanets from their host stars. The observable flux ratio i.e. ratio of the observable reflected flux of the planet to the observable starlight is shown in the figures. This indicates the contrast required by those instruments to directly detect the reflection spectra from such planets. Since the flux ratios are in the order of parts per billion (ppb), detecting the polarization of the planets without resolving them separately amidst the stellar glare will be impossible with the current technology and hence not shown in the figures.

5.4 Analysis and Discussion

The transmission depth for modern Earth-like exoplanets orbiting around solar type stars at wavelengths up to $2.0 \mu\text{m}$ is shown in Figure 4.4. We can see that the transit depth reduces with the inclusion of diffuse radiation due to scattering as explained by Sengupta, Chakrabarty, and Tinetti 2020. The transmission depth increases with the inclusion of clouds as the cloud particles block the transmitted flux through the atmosphere. Clouds also suppress the absorption features of the molecules in shorter wavelengths. The effect of diffusion due to scattering on the broadband continuum can be noteworthy with respect to the levels of the individual absorption features, especially when the atmospheric clouds are present. This calls for more accurate modeling of the transmission spectra by solving the complete radiative transfer equation. Otherwise detecting the features of the biosignatures of the Earth-like planets can be confusing and may be erro-

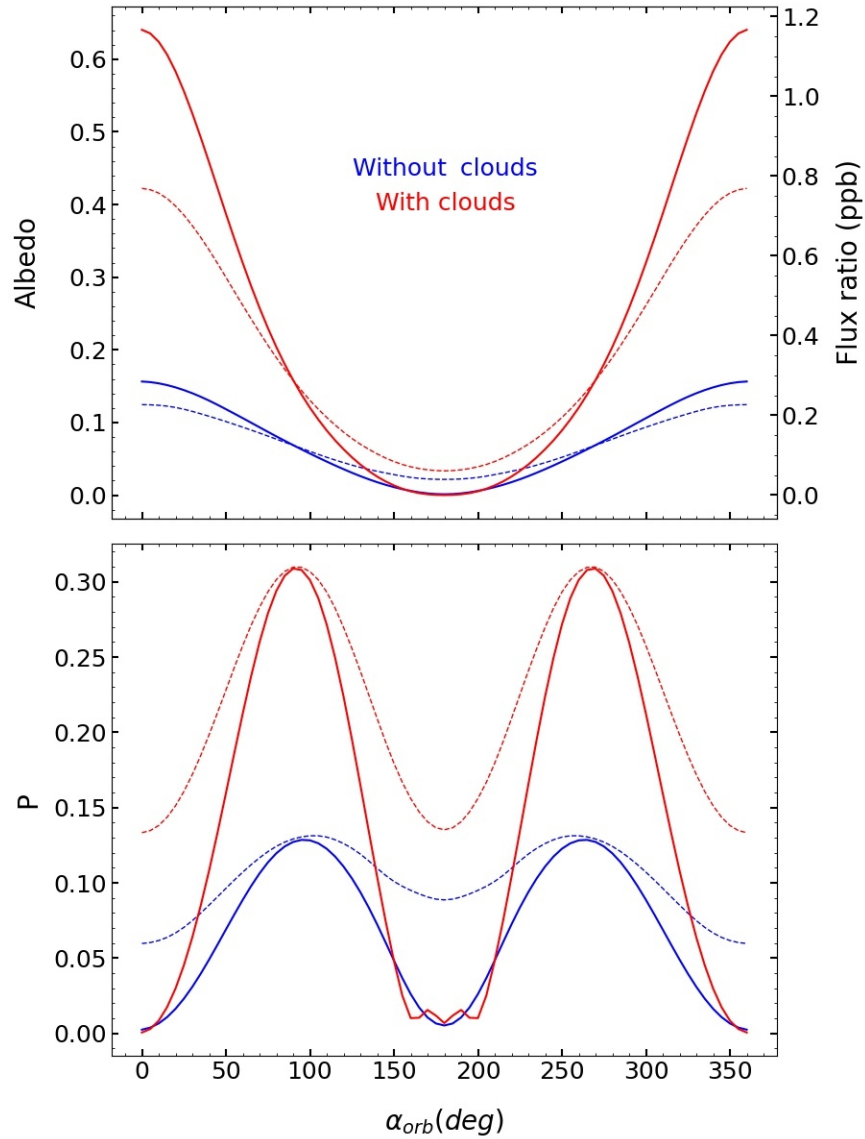


Figure 5.2: The phase curves of albedo (or flux ratio, $F(\alpha)/F_0$) and polarization (P) integrated over the illuminated disk at a wavelength of $0.6 \mu\text{m}$ (visible) and at orbital inclinations angle 90° (solid) and 45° (dashed) for both cloud-free and cloudy atmospheres.

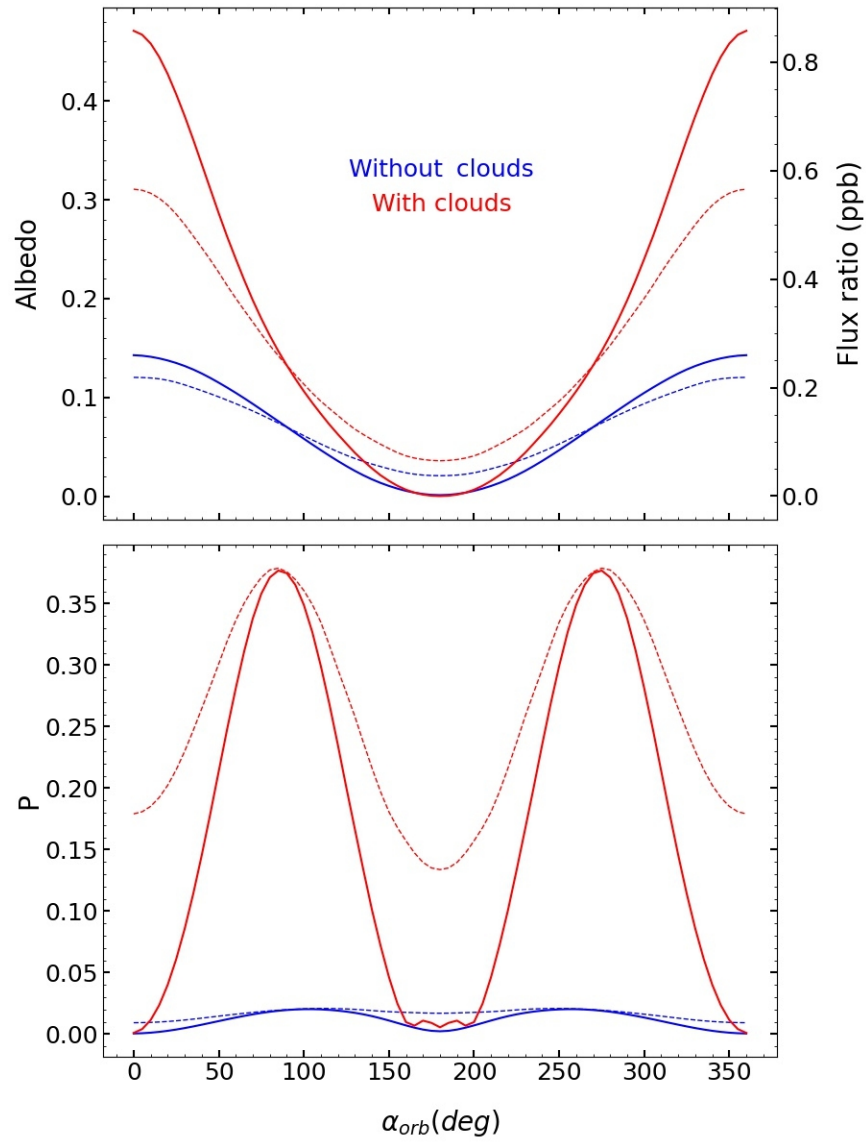


Figure 5.3: Same as figure 5.2 but at a wavelength of $1.0 \mu\text{m}$ (near infrared).

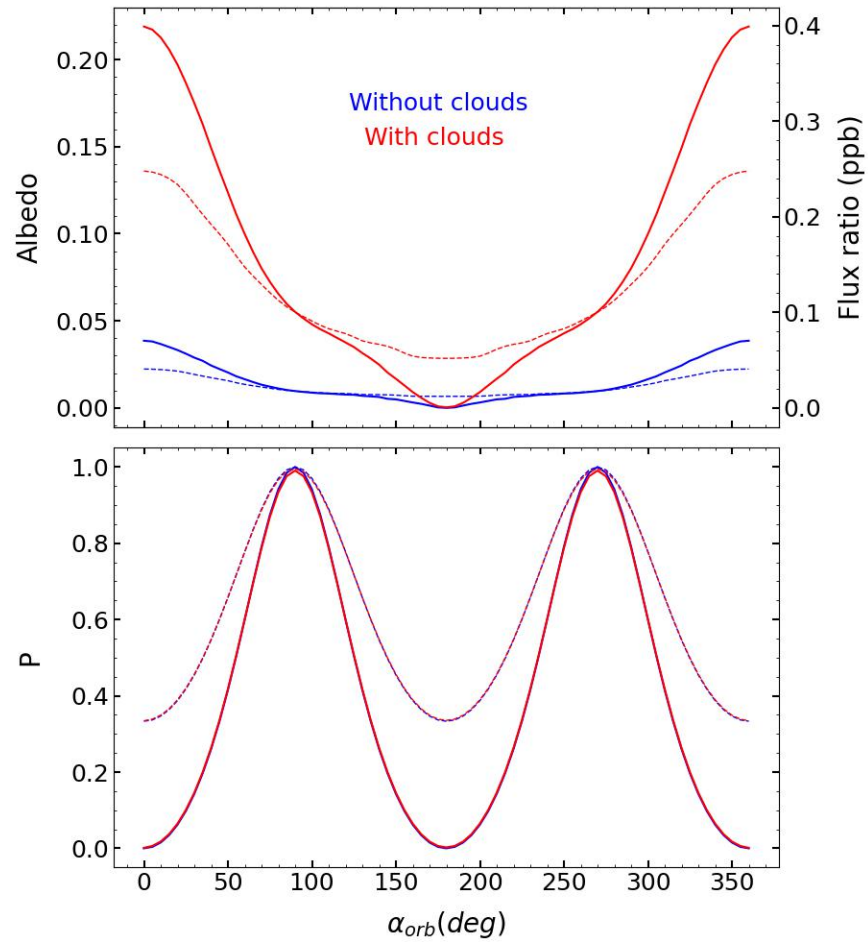


Figure 5.4: Same as figure 5.2 but with single scattering of the incident radiation.

neous. Of course, at longer wavelength regions, all the plots are found to merge because the effect of scattering is negligible.

The relatively stronger absorption lines such as O_2 , H_2O are easily detectable in the reflection spectra (see Figure 3.9). Clearly, the geometric albedo increases with the decrease in wavelength because of the dominance of Rayleigh scattering ($\propto \frac{1}{\lambda^4}$) at shorter wavelength. Also, because of increased back scattering of the incident stellar radiation, the presence of clouds significantly increases the geometric albedo and hence the reflected flux at the visible wavelength region.

In Figure 5.1, we can see that the variation of the albedo and the disk-averaged polarization (P) for different orbital phase at a fixed wavelength ($\sim 0.6\mu\text{m}$) and an orbital inclination angle of 90° (edge-on view) for different surface albedos. The value of surface albedo depends on the surface composition of the extra-solar planet i.e. amount of ocean cover, land cover, trees, ice, etc. The surface albedo of 0.9 corresponds to the case where the whole surface of the planet is covered with snow. The intermediate surface albedo of 0.05 in the figure corresponds to the case where almost the whole surface is covered with ocean and 0.1 corresponds to the case where half of the surface is covered with ocean and the remaining half with trees and grass. As the surface reflection is assumed to be Lambertian, it completely depolarizes the light that is reflected in the upward direction from the planet's surface, i.e., from the bottom of atmosphere (BOA) (Loic Rossi, Berzosa-Molina, and Daphne M Stam 2018). As a result, with an increase in the surface albedo, the overall albedo increases but the polarization (P) decreases. P is evidently found to peak at around 90° orbital phase. The phase dependent polarization profile presented here is consistent with that presented by (Sengupta and Maiti 2006; Daphne M Stam, Joop Hovenier, and Waters 2003).

Figures 5.2 and 5.3 show the phase dependent light curves at wave-

lengths of $0.6 \mu\text{m}$ and $1.0 \mu\text{m}$ respectively for a planet with two orbital inclinations, e.g., 45° and 90° . Evidently, the peak-to-peak fluctuations of the light curves decrease with a decrease in the orbital inclination. Moreover, these figures also demonstrate the effects of clouds. The presence of clouds and non-zero surface albedo increase the total albedo of the disk as expected.

Figure 5.4 show the phase dependent light curve at a wavelength of $0.6 \mu\text{m}$ for the same orbital inclinations by considering only single scattering at each atmospheric layer. Clouds affect the albedo in the same way as the multiple scattering affect. But clouds do not affect the disk averaged polarization because angle of scattering at each layer is the same. We note that the peak polarization (i.e. at 90° phase angle) is 1 for clear sky as well as cloudy atmosphere. This happens because we have approximated the effects of clouds with the Rayleigh phase matrix and for the case of Rayleigh scattering, the degree of single-scattering polarization is 1 at 90° phase angle (see Fig. 3 of Chakrabarty and Sengupta 2021). Basically, the single-scattering approximation overestimates the observable polarization and underestimates the total albedo.

Although, we see opposite behaviour of disk averaged polarization with the clouds in case of hot-Jupiters (see Fig. 15 of Chakrabarty and Sengupta 2021). For hot-Jupiters, the polarization is controlled by the single scattering albedo, but for the Earth-like exoplanets, it depends on both the single scattering albedo and the surface albedo as explained in the next paragraph.

However, to understand the total degree of polarization for a planet with a Lambertian surface with non-zero surface albedo, we divide the total upward (towards us) radiation at the top of atmosphere (TOA) into two streams: (i) the downward incident radiations that get scattered back to the upward direction and get polarized, especially at disk locations away

from the substellar point (e.g., D. Stam, De Rooij, et al. 2006; Chakrabarty and Sengupta 2021), and (ii) the upward radiations from BOA that get transmitted in the same direction which are predominantly unpolarized. For the case of cloud-free atmosphere, as the wavelength increases, the intensity of stream-i decreases since the atmospheric single-scattering albedo decreases, whereas the intensity of stream-ii remains almost constant as we have assumed the same surface albedo at both the wavelengths. Hence, the relative dominance of stream-ii increases at higher wavelengths, and the polarization (P) drops significantly at $\lambda = 1 \mu\text{m}$ compared to that at $\lambda = 0.6 \mu\text{m}$. For the same reason, the total disk albedo at $0.6 \mu\text{m}$ is only slightly higher than that at $1 \mu\text{m}$ for the cloud-free case which is also suggested by Figure 3.9.

The effect of clouds is twofold. For a very low value of surface albedo, as for the case of the gaseous planets, presence of clouds increases the depolarization of radiations due to multiple scattering as the atmospheric single-scattering albedo increases (Chakrabarty and Sengupta 2021). Due to this, the total disk polarization drops with the presence of clouds while the disk albedo rises (Figures 15-17 of Chakrabarty and Sengupta 2021). On the other hand, for a rocky planet with relatively high surface albedo, we find that stream-ii dominates over stream-i at the TOA in the absence of any cloud particle which causes a low value of disk polarization. However, the presence of a cloud layer tends to strengthen stream-i by reflecting back more of the downward radiations to the upward direction and weaken stream-ii by reflecting them back in the downward direction. As a result, the presence of clouds increases the overall disk-integrated degree of polarization and also increases the albedo of the disk. Thus, polarization acts as a measure of the presence of clouds and helps us understand the thickness and the properties of the cloud layers when combined with the scalar spectrum of the planet.

5.5 Conclusions

In this chapter, we demonstrate that the atmospheric clouds and surface albedo can significantly affect both the albedo and the polarization phase curves. The use of polarimetry can allow us to study the properties of the clouds in great detail and reduce the overshadowing effects of clouds. The coronagraphic instruments of those upcoming missions in the upcoming decades will be able to directly image the Earth-like planets in the habitable zones around their host stars. Leveraging the polarimetric instruments in conjunction with these coronagraphic instruments, we will be able to conduct a phase curve study of such planets. Our vector phase curve models show the contrast required to resolve these planets from their host stars and also predict the maximum observable reflected flux and degree of polarization.

Evidently, the surface albedo and the clouds significantly dictate the nature of the phase dependent light curves. Our approximate globally averaged Lambertian representation of the surface albedo has allowed us to simplify the calculations to some extent and develop an understanding of the effect of surface albedo on the reflected spectra and phase dependent light curves. However, in our upcoming works, we will consider individual surface components and their wavelength-dependent reflection matrices to calculate the spectra and the light curves more accurately.

Finally, our models should be useful in designing the instruments onboard the upcoming missions, selecting the science targets, as well as extracting the planetary properties from the spectra and phase curves, once obtained.

Chapter 6

Summary and Conclusions

We characterized the Earth-like exoplanetary atmospheres by modelling their reflection spectra, transmission spectra and the polarization phase curves.

In the first project, we model the reflection spectra for both the present and prebiotic Earth-like exoplanets that orbit within the habitable zone of main-sequence stars of F, G, K and M spectral types. These are calculated by including non-zero globally averaged surface albedo. And these spectra carry information about the biosignatures like O₂, H₂O, O₃, etc., volatiles, surface compositions etc. The effect of clouds and the increased greenhouse gases abundance on the reflection spectra is also considered. We found that the clouds and the surface albedo contribute to the reflectivity of the planet. We also determined that prebiotic Earth-like exoplanets scatter more radiation than the present Earth-like exoplanets because they have a higher abundance of greenhouse gases.

We also calculated the reflected spectra and geometric albedo for various solid and liquid surface compositions of the planet. Several kinds of solid and liquid surfaces were considered such as: (1) present Earth-like surface composition, (2) early Earth-like surface composition, (3) 100% ocean cover, (4) 50% ocean and remaining with trees and grass and (5)

83% ocean and remaining with snow. The reflectivity increases with the surface albedo and it is minimum for no surface albedo at all. Therefore, surface composition plays a significant role in determining the reflectivity of the planet.

We noted that the nature of the reflected spectra is similar to the incident stellar spectrum i.e., the reflected flux peaks in the optical waveband but decrease significantly at longer wavelengths. Also, the geometric albedo decreases with wavelength because of Rayleigh scattering. Specifically for the planets orbiting M-dwarfs, the amount of reflected flux is significantly less because the input stellar spectra for this case peaks in the infrared where Rayleigh scattering is negligible.

We also calculated the reflectivity for the nine known terrestrial exoplanets and estimated the maximum possible value of the Bond albedo for the planets to remain habitable.

In the second project, we presented the transmission spectra for present and prebiotic Earth-like exoplanets. As the transmission depth is more for the shorter wavelengths (due to scattering), increase in the greenhouse gases abundance yields into greater transmission depth. Also, the magnitude of the transmission depth reduces with the increase in the height of the clouds since we assumed a vertically homogeneous atmospheric abundance for the first case.

We also demonstrated how the inclusion of diffused radiation due to multiple scattering can improve the transmission spectra model over the traditional approach of invoking the "Beer- Bouguer-Lambert's law". The difference is significant with respect to the molecular absorption features that can serve as biosignatures especially in the presence of atmospheric clouds. Clouds suppress the absorption features of the molecules in the shorter wavelength region as Rayleigh scattering is negligible in the longer wavelength region.

In the last project, we model the albedo and polarization phase curves for cloudy and cloud free atmospheres for the Earth-like exoplanets. The increase in surface albedo decreases the disk averaged polarization, but increases the overall albedo. Clouds serve as an indicator for the polarization for terrestrial exoplanets. As the inclination angle varies from 90° , the phase curves broaden.

This thesis focuses on the various existing techniques that may be used synergically for the characterization of the Earth-like exoplanets. However, obtaining the transmission or reflection spectra from such small-sized planets with thin atmospheres is extremely challenging at present but will be possible in the era of the upcoming big-budget missions like HabEx, LUVOIR, TMT, ELT, etc. Our models would play a significant role in the habitability study of the potentially habitable candidates using transmission, reflection spectra and phase dependent linear polarization by giving targets to the future missions.

6.1 Highlights

The summary and the highlights of all the chapters are given below:

- **Chapter 1** In this chapter, the general overview about the exoplanets, types of exoplanets, their detection techniques and their atmosphere characterization techniques are presented. In the end, the aim of the work and the plan of the thesis has been discussed.
- **Chapter 2** Here we discuss particularly about the terrestrial exoplanets, about their atmospheres, scattering in the atmosphere, polarization, habitability, etc. The basic idea about how the stellar radiation is being reflected, transmitted or polarized before reaching to Earth is explained. We also discuss about the habitability conditions for the

exoplanets like habitable zone, surface temperature, greenhouse effect, reflectivity, presence of the biomolecules, etc.

- **Chapter 3** We present the reflected spectra and the geometric albedo for the present and prebiotic Earth-like exoplanets orbiting around stars of F, G, K and M spectral types. We calculate this using multiple scattering radiative transfer equation for plane-parallel geometry and azimuthal symmetry. With the increase in wavelength, the reflectivity decreases in the optical due to the dominance of Rayleigh scattering in the shorter wavelength region. It also increases with the increase in the surface albedo. We also note that presence of water clouds also increases the magnitude of the reflected spectra or the geometric albedo. In the end, we model the reflection spectra and the geometric albedo for the nine known terrestrial exoplanets by considering three different planetary surfaces. We also give maximum value of the Bond albedo for these planets.
- **Chapter 4** In this chapter, transmission spectra for the present and prebiotic Earth-like exoplanets is modeled. First, we calculate it by using "Beer-Bouguer-Lambert's law", where multiple scattering is not included. We note that the transit depth increases with the increase in the greenhouse gases abundance whereas it decreases with the increase in the height of the clouds from the surface. After that we improvise upon that by including the multiple scattering. That is calculated by solving the multi-scattering radiative transfer equation. Here, we see that the transmission depth decreases if multiple scattering is included. Also, it increases with the increasing cross-section of the cloud particles.
- **Chapter 5** Here we calculate the albedo and the polarization phase curves for the Earth-like exoplanets for both cloudy as well as clear

sky atmospheres. Three dimensional vector radiative transfer equation is solved and the appropriate phase matrices are used. Finally, the phase curves of albedo and the disk-integrated polarization are calculated. The disk integrated polarization decreases with increase in the surface albedo but increase with the presence of thin clouds. Also, only the partially illuminated planetary disk gives non-zero polarization. We also see the effect of the inclination angle on the albedo and the polarization phase curves. Thus, the surface and the atmospheric features of such planets significantly dictate the nature of the observational quantities.

6.2 Present work limitations and future aspects

1. Presently, we are limited to the thin clouds/haze model, but in our future works, we will have a more detailed model for the cloudy atmospheres of the Earth-like exoplanets.
2. For now, we have averaged the reflectivity for the various surface components. In the future, we will consider individual surface components and their wavelength dependent reflection matrices to calculate the spectra and light curves more accurately.
3. We can extend our study to model the transmission spectra and the polarization phase curves for the known exoplanets like Proxima Centauri b, Teegarden's Star b, TOI-700d, etc., which have a very high value of ESI (Earth Similarity Index).
4. Our models are very important for the observational perspective as they will help in giving the targets to the upcoming telescopes for probing habitable exoplanets.

Bibliography

Book Sources

- Ahrens, Thomas J., ed. (1995). *Global Earth Physics: A Handbook of Physical Constants*. Washington, D.C.: American Geophysical Union. ISBN: 978-0875908519.
- Andrews, David G. (2010). *An Introduction to Atmospheric Physics*. 2nd. Cambridge: Cambridge University Press. ISBN: 978-0521693189.
- Atmosphere, US Standard (1976). *US standard atmosphere*. Vol. 76. National Oceanic and Atmospheric Administration.
- Catling, David C. and James F. Kasting (2017). *Atmospheric Evolution on Inhabited and Lifeless Worlds*. Cambridge: Cambridge University Press. ISBN: 978-1107099741. DOI: [10.1017/9781139020558](https://doi.org/10.1017/9781139020558).
- Chamberlain, Joseph W. and Donald M. Hunten (1987). *Theory of Planetary Atmospheres: An Introduction to Their Physics and Chemistry*. 2nd. San Diego: Academic Press. ISBN: 978-0121672500.
- Chandrasekhar, S (1960). *Radiative transfer*. New York: Dover Publications. ISBN: 0-486-60590-6.
- Coulson, Kenneth L. (1988). *Polarization and Intensity of Light in the Atmosphere*. Hampton, Virginia: A. Deepak Publishing. ISBN: 978-0937194150.
- De Pater, Imke and Jack J Lissauer (2015). *Planetary sciences*. Cambridge University Press. ISBN: 978-1-107-09161-0.
- Goody, Richard M. and Yuk L. Yung (1989). *Atmospheric Radiation: Theoretical Basis*. Oxford: Oxford University Press. ISBN: 978-0195051346.
- Houghton, John T. (2002). *The Physics of Atmospheres*. 3rd. Cambridge: Cambridge University Press. ISBN: 978-0521011228.
- Jacob, Daniel J. (1999). *Introduction to Atmospheric Chemistry*. Princeton: Princeton University Press. ISBN: 978-0691001852.

- Kokhanovsky, Alexander A. (2006). *Aerosol Optics: Light Absorption and Scattering by Particles in the Atmosphere*. Dordrecht: Springer. ISBN: 978-1402046153.
- Lammer, Helmut and Siegfried J. Bauer (2003). *Atmospheric Escape and Evolution of Terrestrial Planets and Satellites*. Berlin: Springer. ISBN: 978-3642073978. DOI: [10.1007/978-3-662-09737-0](https://doi.org/10.1007/978-3-662-09737-0).
- Lissauer, J.J. and I. de Pater (2013). *Fundamental Planetary Science: Physics, Chemistry and Habitability*. Cambridge University Press. ISBN: 9781107354616. URL: <https://books.google.co.in/books?id=0iggAwAAQBAJ>.
- Mishchenko, Michael I., Joop W. Hovenier, and Larry D. Travis (2000). *Light Scattering by Nonspherical Particles: Theory, Measurements, and Applications*. San Diego: Academic Press. ISBN: 978-0124986604.
- Pater, Imke de and Jack J. Lissauer (2010). *Planetary Sciences*. 2nd. Cambridge: Cambridge University Press. ISBN: 978-0521853712.
- Peraiah, Annamaneni (2002). *An Introduction to Radiative Transfer: Methods and applications in astrophysics*. Cambridge University Press.
- Perryman, Michael (2011). *The Exoplanet Handbook*. Cambridge University Press.
- (2018). *The exoplanet handbook*. Cambridge university press.
- Pierrehumbert, Raymond T. (2010). *Principles of Planetary Climate*. Cambridge: Cambridge University Press. ISBN: 978-0521865562.
- Scharf, Caleb (2009). *Extrasolar planets and astrobiology*. Sausalito, Calif: University Science Books. ISBN: 978-1-891389-55-9.
- Seager, Sara (2010). *Exoplanet atmospheres : physical processes*. Princeton, N.J: Princeton University Press. ISBN: 9780691146454.
- Walker, James C. G. (1977). *Evolution of the Atmosphere*. New York: Macmillan. ISBN: 978-0028548700.

Paper Sources

- Ackerman, Andrew S. and Mark S. Marley (2001). “Precipitating Condensation Clouds in Substellar Atmospheres”. In: *The Astrophysical Journal* 556.2, pp. 872–884. DOI: [10.1086/321540](https://doi.org/10.1086/321540).
- Ahrer, E.-M. et al. (2023). “Detection of Sulfur Dioxide in the Atmosphere of WASP-39b with JWST”. In: *The Astrophysical Journal Letters*.
- Alonso, Roi (2018). “Characterization of Exoplanets: Secondary Eclipses”. In: *Handbook of Exoplanets*. Cham: Springer International Publishing, pp. 1441–1467. ISBN: 978-

- 3-319-55333-7. DOI: [10.1007/978-3-319-55333-7_40](https://doi.org/10.1007/978-3-319-55333-7_40). URL: https://doi.org/10.1007/978-3-319-55333-7_40.
- Alonso-Floriano, FJ et al. (2015). “CARMENES input catalogue of M dwarfs-I. Low-resolution spectroscopy with CAFOS”. In: *Astronomy & Astrophysics* 577, A128.
- An, Jin H et al. (2004). “The anomaly in the candidate microlensing event PA-99-N2”. In: *The Astrophysical Journal* 601.2, p. 845.
- Anglada-Escudé, Guillem et al. (2016). “A terrestrial planet candidate in a temperate orbit around Proxima Centauri”. In: *Nature* 536.7617, pp. 437–440.
- Armstrong, D. J. et al. (2016). “Variability in the atmosphere of the hot Jupiter HAT-P-7 b”. In: *Nature Astronomy* 1, p. 0004.
- Armstrong, DJ et al. (2016). “The host stars of Kepler’s habitable exoplanets: superflares, rotation and activity”. In: *Monthly Notices of the Royal Astronomical Society* 455.3, pp. 3110–3125.
- Arney, Giada N (2019). “The K Dwarf advantage for biosignatures on directly imaged exoplanets”. In: *The Astrophysical Journal Letters* 873.1, p. L7.
- Arnold, Luc et al. (2002). “Detecting Vegetation on Extrasolar Planets Using Reflectance Spectra”. In: *Astronomy & Astrophysics* 392.1, pp. 231–237. DOI: [10.1051/0004-6361:20020993](https://doi.org/10.1051/0004-6361:20020993).
- Barbato, D et al. (2018). “Revised estimates of the frequency of Earth-like planets in the Kepler field”. In: *arXiv preprint arXiv:1811.08249*.
- Batalha, N et al. (Apr. 2020). *Resampled Opacity Database for PICASO v2*. Version 1.0. DOI: [10.5281/zenodo.3759675](https://doi.org/10.5281/zenodo.3759675). URL: <https://doi.org/10.5281/zenodo.3759675>.
- Batalha, Natalie M et al. (2013). “Planetary Candidates Observed by Kepler. III. Analysis of the First 16 Months of Data”. In: *The Astrophysical Journal Supplement Series* 204.2, p. 24.
- Batalha, Natasha E et al. (2019). “Exoplanet Reflected-light Spectroscopy with PICASO”. In: *The Astrophysical Journal* 878.1, p. 70.
- Bekker, A et al. (2004). “Dating the rise of atmospheric oxygen”. In: *Nature* 427.6970, pp. 117–120.
- Berdyugina, Svetlana V et al. (2018). “The Exo-Life Finder (ELF) telescope: New strategies for direct detection of exoplanet biosignatures and technosignatures”. In: *Ground-based and Airborne Telescopes VII*. Vol. 10700. SPIE, pp. 1453–1466.
- Borucki, William J, Eric Agol, et al. (2013). “Kepler-62: a five-planet system with planets of 1.4 and 1.6 Earth radii in the habitable zone”. In: *Science* 340.6132, pp. 587–590.

- Borucki, William J, David Koch, et al. (2010). “Kepler planet-detection mission: introduction and first results”. In: *Science* 327.5968, pp. 977–980.
- Borucki, William J, David G Koch, et al. (2012). “Kepler-22b: A 2.4 Earth-radius planet in the habitable zone of a Sun-like star”. In: *The Astrophysical Journal* 745.2, p. 120.
- Brocks, Jochen J et al. (1999). “Archean molecular fossils and the early rise of eukaryotes”. In: *Science* 285.5430, pp. 1033–1036.
- Bryson, Steve et al. (2020). “The Occurrence of Rocky Habitable-zone Planets around Solar-like Stars from Kepler Data”. In: *The Astrophysical Journal* 161.1, p. 36.
- Burgasser, Adam J, Sarah E Logsdon, et al. (2015). “The Brown Dwarf Kinematics Project (BDKP). IV. Radial velocities of 85 late-M and L dwarfs with MagE”. In: *The Astrophysical Journal Supplement Series* 220.1, p. 18.
- Burgasser, Adam J and Eric E Mamajek (2017). “On the Age of the TRAPPIST-1 System”. In: *The Astrophysical Journal* 845.2, p. 110.
- Caballero, JA et al. (2022). “A detailed analysis of the Gl 486 planetary system”. In: *Astronomy & Astrophysics* 665, A120.
- Cahoy, Kerri L., Mark S. Marley, and Jonathan J. Fortney (2010). “Exoplanet Albedo Spectra and Colors as a Function of Planet Phase, Separation, and Metallicity”. In: *The Astrophysical Journal* 724.1, pp. 189–214. DOI: [10.1088/0004-637X/724/1/189](https://doi.org/10.1088/0004-637X/724/1/189).
- Chakrabarty, Aritra and Sujana Sengupta (2020). “Effects of thermal emission on the transmission spectra of hot Jupiters”. In: *The Astrophysical Journal* 898.1, p. 89.
- (2021). “Generic models for disk-resolved and disk-integrated phase-dependent linear polarization of light reflected from exoplanets”. In: *The Astrophysical Journal* 917.2, p. 83.
- Charbonneau, David et al. (1999). “Detection of planetary transits across a sun-like star”. In: *The Astrophysical Journal* 529.1, p. L45.
- Claudi, Riccardo and Eleonora Alei (2019). “Biosignatures Search in Habitable Planets”. In: *Galaxies* 7.4, p. 82.
- Coffeen, David L (1969). “Wavelength dependence of polarization. XVI. Atmosphere of Venus”. In: *The Astronomical Journal* 74, p. 446.
- Coffeen, DL and T Gehrels (1969). “Wavelength dependence of polarization. XV. Observations of Venus”. In: *The Astronomical Journal* 74, p. 433.
- Covone, Giovanni et al. (2021). “Efficiency of the oxygenic photosynthesis on Earth-like planets in the habitable zone”. In: *Monthly Notices of the Royal Astronomical Society* 505.3, pp. 3329–3335.

-
- Cowan, N. B. and E. Agol (2011). “The statistics of albedo and heat redistribution on hot exoplanets”. In: *The Astrophysical Journal* 729.1, p. 54.
- Cuntz, M and EF Guinan (2016). “About exobiology: the case for dwarf K stars”. In: *The Astrophysical Journal* 827.1, p. 79.
- Dai, Xinyu and Eduardo Guerras (2018). “Probing extragalactic planets using quasar microlensing”. In: *The Astrophysical Journal Letters* 853.2, p. L27.
- Daylan, Tansu et al. (2021). “TESS discovery of a super-Earth and three sub-Neptunes hosted by the bright, Sun-like star HD 108236”. In: *The Astronomical Journal* 161.2, p. 85.
- De Wit, Julien et al. (2018). “Atmospheric reconnaissance of the habitable-zone Earth-sized planets orbiting TRAPPIST-1”. In: *Nature Astronomy* 2.3, pp. 214–219.
- Demory, B. O. et al. (2013). “Inference of inhomogeneous clouds in an exoplanet atmosphere”. In: *The Astrophysical Journal Letters* 776.2, p. L25.
- Domagal-Goldman, Shawn D et al. (2014). “Abiotic ozone and oxygen in atmospheres similar to prebiotic Earth”. In: *The Astrophysical Journal* 792.2, p. 90.
- Dong, Chuanfei et al. (2017). “Is Proxima Centauri b habitable? A study of atmospheric loss”. In: *The Astrophysical Journal Letters* 837.2, p. L26.
- Ehrenreich, David et al. (2006). “The transmission spectrum of Earth-size transiting planets”. In: *Astronomy and Astrophysics* 448.1, pp. 379–393.
- Esteves, L. J., E. J. W. De Mooij, and R. Jayawardhana (2013). “Changing phases of alien worlds: Probing atmospheres of Kepler planets with high-precision photometry”. In: *The Astrophysical Journal* 772.1, p. 51.
- Faucher, Thomas, Loic Rossi, and Daphne M Stam (2017). “The o₂ a-band in the fluxes and polarization of starlight reflected by earth-like exoplanets”. In: *The Astrophysical Journal* 842.1, p. 41.
- Faucher, Thomas J, Martin Turbet, Geronimo L Villanueva, et al. (2019). “Impact of clouds and hazes on the simulated JWST transmission spectra of habitable zone planets in the TRAPPIST-1 system”. In: *The Astrophysical Journal* 887.2, p. 194.
- Faucher, Thomas J, Martin Turbet, Eric T Wolf, et al. (2020). “TRAPPIST-1 Habitable Atmosphere Intercomparison (THAI): motivations and protocol version 1.0”. In: *Geoscientific Model Development* 13.2, pp. 707–716.
- Fortney, Jonathan J et al. (2007). “A Unified Theory for the Atmospheres of the Hot and Very Hot Jupiters: Two Classes of Irradiated Atmospheres”. In: *The Astrophysical Journal* 678.2, pp. 1419–1435.

- Fowler, David et al. (1999). “The Global Nitrogen Cycle in the Twenty-First Century”. In: *Philosophical Transactions of the Royal Society B: Biological Sciences* 368.1621, p. 20130164. DOI: [10.1098/rstb.2013.0164](https://doi.org/10.1098/rstb.2013.0164).
- Freedman, Richard S, Jacob Lustig-Yaeger, et al. (2014). “Gaseous mean opacities for giant planet and ultracool dwarf atmospheres over a range of metallicities and temperatures”. In: *The Astrophysical Journal Supplement Series* 214.2, p. 25.
- Freedman, Richard S, Mark S Marley, and Katharina Lodders (2008). “Line and mean opacities for ultracool dwarfs and extrasolar planets”. In: *The Astrophysical Journal Supplement Series* 174.2, p. 504.
- Fujii, Yuka et al. (2018). “Exoplanet biosignatures: observational prospects”. In: *Astrobiology* 18.6, pp. 739–778.
- Galuzzo, Daniele et al. (2021). “Three-dimensional climate simulations for the detectability of Proxima Centauri b”. In: *The Astrophysical Journal* 909.2, p. 191.
- Gao, Peter et al. (2021). “Aerosols in the atmospheres of terrestrial exoplanets”. In: *Nature Astronomy* 5, pp. 951–956. DOI: [10.1038/s41550-021-01430-7](https://doi.org/10.1038/s41550-021-01430-7).
- Garraffo, Cecilia, Jeremy J Drake, and Ofer Cohen (2016). “The space weather of Proxima Centauri b”. In: *The Astrophysical Journal Letters* 833.1, p. L4.
- Gaudi, B Scott (2012). “Microlensing Surveys for Exoplanets”. In: *Annual Review of Astronomy and Astrophysics* 50, pp. 411–453.
- Gialluca, Megan T et al. (2021). “Characterizing atmospheres of transiting Earth-like exoplanets orbiting M dwarfs with James Webb Space Telescope”. In: *Publications of the Astronomical Society of the Pacific* 133.1023, p. 054401.
- Gilbert, Emily A et al. (2020). “The First Habitable-zone Earth-sized Planet from TESS. I. Validation of the TOI-700 System”. In: *The Astronomical Journal* 160.3, p. 116.
- Gillon, Michaël, Emmanuël Jehin, et al. (2016). “Temperate Earth-sized planets transiting a nearby ultracool dwarf star”. In: *Nature* 533.7602, pp. 221–224.
- Gillon, Michaël, Amaury HMJ Triaud, et al. (2017). “Seven temperate terrestrial planets around the nearby ultracool dwarf star TRAPPIST-1”. In: *Nature* 542.7642, pp. 456–460.
- Gordon, Kenneth E et al. (2022). “Polarized Signatures of a Habitable World: Comparing Models of an Exoplanet-Earth with VNIR Earthshine Spectra”. In: *Bulletin of the American Astronomical Society* 54.5, pp. 102–408.
- Grenfell, John L et al. (2014). “Sensitivity of biosignatures on Earth-like planets orbiting in the habitable zone of cool M-dwarf Stars to varying stellar UV radiation and surface biomass emissions”. In: *Planetary and Space Science* 98, pp. 66–76.

- Grenfell, John Lee et al. (2007). “The response of atmospheric chemistry on earth-like planets around F, G and K Stars to small variations in orbital distance”. In: *Planetary and Space Science* 55.5, pp. 661–671.
- Groot, A et al. (2020). “Colors of an Earth-like exoplanet-Temporal flux and polarization signals of the Earth”. In: *Astronomy & Astrophysics* 640, A121.
- Guo, Qingjun et al. (2009). “Reconstructing Earth’s surface oxidation across the Archean-Proterozoic transition”. In: *Geology* 37.5, pp. 399–402.
- Gvalani, Siddhant (2022). “A questionnaire-based study to understand knowledge and create awareness on the exoplanet-Kepler 1649c.” In: *The International Journal of Engineering and Science*.
- Hall, JS and LA Riley (1974). “A photometric study of Saturn and its rings”. In: *Icarus* 23.2, pp. 144–156.
- Hansen, James E and Larry D Travis (1974). “Light scattering in planetary atmospheres”. In: *Space science reviews* 16.4, pp. 527–610.
- Hart, Michael H (1979). “Habitable zones about main sequence stars”. In: *ICARUS* 37.1, pp. 351–357.
- Hiatt, Eric E, Peir K Pufahl, and Leandro Guimarães da Silva (2020). “Iron and phosphorus biochemical systems and the Cryogenian-Ediacaran transition, Jacadigo basin, Brazil: Implications for the Neoproterozoic oxygenation event”. In: *Precambrian Research* 337, p. 105533.
- Hill, Michelle L et al. (2022). “A Catalog of Habitable Zone Exoplanets”. In: *arXiv preprint arXiv:2210.02484*.
- Holland, Heinrich D (2002). “Volcanic gases, black smokers, and the Great Oxidation Event”. In: *Geochimica et Cosmochimica acta* 66.21, pp. 3811–3826.
- Hori, Yasunori and Masahiro Ogihara (2020). “Do the TRAPPIST-1 planets have hydrogen-rich atmospheres?” In: *The Astrophysical Journal* 889.2, p. 77.
- Hu, Renyu, Sara Seager, and William Bains (2012). “Photochemistry in terrestrial exoplanet atmospheres. I. Photochemistry model and benchmark cases”. In: *The Astrophysical Journal* 761.2, p. 166.
- Huang, Su-Shu (1959). “Occurrence of life in the universe”. In: *American Scientist* 47.3, pp. 397–402.
- (1960). “Life outside the solar system”. In: *Scientific American* 202.4, pp. 55–63.
- Hunten, Donald M., Robert O. Pepin, and James C. G. Walker (1987). “Mass Fractionation in Hydrodynamic Escape”. In: *Icarus* 69.3, pp. 532–549. DOI: [10.1016/0019-1035\(87\)90022-4](https://doi.org/10.1016/0019-1035(87)90022-4).

- Husser, T-O et al. (2013). “A new extensive library of PHOENIX stellar atmospheres and synthetic spectra”. In: *Astronomy and Astrophysics* 553, A6.
- Ityaksov, D, H Linnartz, and W Ubachs (2008). “Deep-UV absorption and Rayleigh scattering of carbon dioxide”. In: *Chem. Phys. Lett.* 462.1-3, pp. 31–34.
- Joos, F and HM Schmid (2007). “Limb polarization of Uranus and Neptune-II. Spectropolarimetric observations”. In: *Astronomy & Astrophysics* 463.3, pp. 1201–1210.
- Jurgenson, C et al. (2016). “EXPRES: a next generation RV spectrograph in the search for earth-like worlds”. In: *Ground-based and Airborne Instrumentation for Astronomy VI*. Vol. 9908. SPIE, pp. 2051–2070.
- Kaltenegger, L, J Pepper, et al. (2021). “Around Which Stars Can TESS Detect Earth-like Planets? The Revised TESS Habitable Zone Catalog”. In: *The Astronomical Journal* 161.5, p. 233.
- Kaltenegger, L, D Sasselov, and S Rugheimer (2013). “Water-planets in the habitable zone: atmospheric chemistry, observable features, and the case of Kepler-62e and-62f”. In: *The Astrophysical Journal Letters* 775.2, p. L47.
- Kaltenegger, Lisa (2017). “How to characterize habitable worlds and signs of life”. In: *Annu. Rev. Astron. Astrophys.* 55, pp. 433–485.
- Kaltenegger, Lisa, Zifan Lin, and Sarah Rugheimer (2020). “Finding Signs of Life on Transiting Earthlike Planets: High-resolution Transmission Spectra of Earth through Time around FGKM Host Stars”. In: *The Astrophysical Journal* 904.1, p. 10.
- Kaltenegger, Lisa and Wesley A Traub (2009). “Transits of Earth-like planets”. In: *The Astrophysical Journal* 698.1, p. 519.
- Kaltenegger, Lisa, Wesley A Traub, and Kenneth W Jucks (2007). “Spectral evolution of an Earth-like planet”. In: *The Astrophysical Journal* 658.1, p. 598.
- Kane, S. R. et al. (2011). “Phase variations of the thermal emission from the hot Jupiter HD 189733b”. In: *The Astrophysical Journal* 735.2, p. 142.
- Kane, Stephen R, Michelle L Hill, et al. (2016). “A catalog of Kepler habitable zone exoplanet candidates”. In: *The Astrophysical Journal* 830.1, p. 1.
- Kane, Stephen R, Zhexing Li, et al. (2020). “Eccentricity Driven Climate Effects in the Kepler-1649 System”. In: *The Astronomical Journal* 161.1, p. 31.
- Karalidi, T and DM Stam (2012). “Modeled flux and polarization signals of horizontally inhomogeneous exoplanets applied to Earth-like planets”. In: *Astronomy & Astrophysics* 546, A56.
- Karalidi, T, DM Stam, and JW Hovenier (2011). “Flux and polarisation spectra of water clouds on exoplanets”. In: *Astronomy & Astrophysics* 530, A69.

-
- (2012). “Looking for the rainbow on exoplanets covered by liquid and icy water clouds”. In: *Astronomy & Astrophysics* 548, A90.
- Karalidi, T, DM Stam, F Snik, et al. (2012). “Observing the Earth as an exoplanet with LOUPE, the lunar observatory for unresolved polarimetry of Earth”. In: *Planetary and Space Science* 74.1, pp. 202–207.
- Kasting, James F, Daniel P Whitmire, and Ray T Reynolds (1993). “Habitable zones around main sequence stars”. In: *ICARUS* 101.1, pp. 108–128.
- Kasting, James F. and David Catling (2003). “Evolution of a Habitable Planet”. In: *Annual Review of Astronomy and Astrophysics* 41.1, pp. 429–463. DOI: [10.1146/annurev.astro.41.071601.170049](https://doi.org/10.1146/annurev.astro.41.071601.170049).
- Kasting, James F. and Thomas M. Donahue (1980). “The Evolution of Atmospheric Ozone”. In: *Journal of Geophysical Research* 85.C6, pp. 3255–3263. DOI: [10.1029/JC085iC06p03255](https://doi.org/10.1029/JC085iC06p03255).
- Kawashima, Y and S Rugheimer (2019). “Theoretical Reflectance Spectra of Earth-like Planets through Their Evolutions: Impact of Clouds on the Detectability of Oxygen, Water, and Methane with Future Direct Imaging Missions”. In: *The Astronomical Journal* 157.5, p. 213.
- Kedziora-Chudczer, L and J Bailey (2010). “Using Polarization to Detect and Characterize Exoplanets”. In: *Pathways Towards Habitable Planets*. Vol. 430, p. 469.
- Kemmer, J et al. (2022). “Discovery and mass measurement of the hot, transiting, Earth-sized planet, GJ 3929 b”. In: *A&A* 659, A17.
- Kempton, Eliza M-R et al. (2017). “Exo-Transmit: An open-source code for calculating transmission spectra for exoplanet atmospheres of varied composition”. In: *Publications of the Astronomical Society of the Pacific* 129.974, p. 044402.
- Kitzmann, D, ABC Patzer, Philip von Paris, M Godolt, and H Rauer (2011a). “Clouds in the atmospheres of extrasolar planets-II. Thermal emission spectra of Earth-like planets influenced by low and high-level clouds”. In: *Astronomy and Astrophysics* 531, A62.
- (2011b). “Clouds in the atmospheres of extrasolar planets-III. Impact of low and high-level clouds on the reflection spectra of Earth-like planets”. In: *Astronomy and Astrophysics* 534, A63.
- Kitzmann, D, ABC Patzer, Philip von Paris, M Godolt, B Stracke, et al. (2010). “Clouds in the atmospheres of extrasolar planets-I. Climatic effects of multi-layered clouds for Earth-like planets and implications for habitable zones”. In: *Astronomy and Astrophysics* 511, A66.

- Kitzmann, Daniel et al. (2010). “Influence of clouds on the reflection spectra of Earth-like extrasolar planets”. In: *European Planetary Science Congress 2010*, p. 725.
- Klindžić, Dora et al. (2021). “LOUPE: observing Earth from the Moon to prepare for detecting life on Earth-like exoplanets”. In: *Philosophical Transactions of the Royal Society A* 379.2188, p. 20190577.
- Knollenberg, Richard G. and Donald M. Hunten (1980). “The Microphysics of the Clouds of Venus: Results of the Pioneer Venus Particle Size Spectrometer Experiment”. In: *Journal of Geophysical Research: Space Physics* 85.A13, pp. 8039–8058. DOI: [10.1029/JA085iA13p08039](https://doi.org/10.1029/JA085iA13p08039).
- Knutson, H. A. et al. (2007). “A map of the day-night contrast of the extrasolar planet HD 189733b”. In: *Nature* 447.7141, pp. 183–186.
- Kopparapu, Ravi Kumar, Ramses Ramirez, et al. (2013). “Habitable zones around main-sequence stars: new estimates”. In: *The Astrophysical Journal* 765.2, p. 131.
- Kopparapu, Ravi Kumar, Eric T Wolf, and Victoria S Meadows (2020). “Characterizing exoplanet habitability”. In: *Planetary Astrobiology*, p. 449.
- Kreidberg, Laura, Jacob L Bean, et al. (2014). “Clouds in the atmosphere of the super-Earth exoplanet GJ 1214b”. In: *Nature* 505.7481, pp. 69–72.
- Kreidberg, Laura and Abraham Loeb (2016). “Prospects for characterizing the atmosphere of Proxima Centauri b”. In: *The Astrophysical Journal Letters* 832.1, p. L12.
- Krissansen-Totton, Joshua et al. (2018). “Detectability of biosignatures in anoxic atmospheres with the James Webb Space Telescope: A TRAPPIST-1e case study”. In: *The Astronomical Journal* 156.3, p. 114.
- Lin, Zifan and Lisa Kaltenegger (2020). “High-resolution reflection spectra for Proxima b and Trappist-1e models for ELT observations”. In: *Monthly Notices of the Royal Astronomical Society* 491.2, pp. 2845–2854.
- Lin, Zifan, Ryan J MacDonald, et al. (2021). “Differentiating modern and prebiotic Earth scenarios for TRAPPIST-1e: high-resolution transmission spectra and predictions for JWST”. In: *Monthly Notices of the Royal Astronomical Society* 505.3, pp. 3562–3578.
- Lovis, Christophe et al. (2017). “Atmospheric characterization of Proxima b by coupling the SPHERE high-contrast imager to the ESPRESSO spectrograph”. In: *Astronomy & Astrophysics* 599, A16.
- Luger, Rodrigo et al. (2017). “The pale green dot: a method to characterize Proxima Centauri b using Exo-Aurorae”. In: *The Astrophysical Journal* 837.1, p. 63.
- Lupu, RE et al. (2014). “The atmospheres of earthlike planets after giant impact events”. In: *The Astrophysical Journal* 784.1, p. 27.

- Lustig-Yaeger, Jacob, Victoria S Meadows, and Andrew P Lincowski (2019). “The detectability and characterization of the TRAPPIST-1 exoplanet atmospheres with JWST”. In: *The Astronomical Journal* 158.1, p. 27.
- Madden, Jack and Lisa Kaltenegger (2020). “High-resolution Spectra for a Wide Range of Habitable Zone Planets around Sun-like Stars”. In: *The Astrophysical Journal Letters* 898.2, p. L42.
- Madhusudhan, N. et al. (2023). “Carbon-bearing Molecules in the Atmosphere of the Habitable-zone Hycean Exoplanet K2-18b”. In: *The Astrophysical Journal Letters*.
- Mallama, Anthony (2009). “Characterization of terrestrial exoplanets based on the phase curves and albedos of Mercury, Venus and Mars”. In: *Icarus* 204.1, pp. 11–14.
- Marley, Mark S and Sujay Sengupta (2011). “Probing the physical properties of directly imaged gas giant exoplanets through polarization”. In: *Monthly Notices of the Royal Astronomical Society* 417.4, pp. 2874–2881.
- Marois, Christian et al. (2008). “Direct Imaging of Multiple Planets Orbiting the Star HR 8799”. In: *Science* 322.5906, pp. 1348–1352.
- Martinez-Rodriguez, Hector et al. (2019). “Exomoons in the habitable zones of M dwarfs”. In: *The Astrophysical Journal* 887.2, p. 261.
- May, EM et al. (2021). “Water Ice Cloud Variability and Multi-epoch Transmission Spectra of TRAPPIST-1e”. In: *The Astrophysical Journal Letters* 911.2, p. L30.
- Mayor, Michel and Didier Queloz (1995). “A Jupiter-mass companion to a solar-type star”. In: *Nature* 378.6555, pp. 355–359.
- Meadows, Victoria et al. (Aug. 2016). “The Habitability of Proxima Centauri b: II: Environmental States and Observational Discriminants”. In: *Astrobiology* 18. DOI: [10.1089/ast.2016.1589](https://doi.org/10.1089/ast.2016.1589).
- Meadows, Victoria S et al. (2018). “The habitability of Proxima Centauri b: environmental states and observational discriminants”. In: *Astrobiology* 18.2, pp. 133–189.
- Meadows, Victoria S. (2017). “Reflections on O as a Biosignature in Exoplanetary Atmospheres”. In: *Astrobiology* 17.10, pp. 1022–1052. DOI: [10.1089/ast.2016.1578](https://doi.org/10.1089/ast.2016.1578).
- Meadows, Victoria S. and David Crisp (1996). “Ground-Based Near-Infrared Observations of the Venus Night Side: The Thermal Structure and Water Abundance Near the Surface”. In: *Journal of Geophysical Research: Planets* 101.E2, pp. 4595–4622. DOI: [10.1029/95JE03567](https://doi.org/10.1029/95JE03567).
- Michael F. Sterzik Stefano Bagnulo, Claudia Emde and Mihail Manev (2020). “The cloudbow of planet Earth observed in polarisation”. In: *Astronomy and Astrophysics*. DOI: <https://doi.org/10.1051/0004-6361/202038270>.

- Michalsky, JJ and RA Stokes (1977). “Whole-disk polarization measurements of Uranus at visible wavelengths”. In: *The Astrophysical Journal* 213, pp. L135–L137.
- Molina, J Berzosa, Loic Rossi, and Daphne M Stam (2018). “Traces of exomoons in computed flux and polarization phase curves of starlight reflected by exoplanets”. In: *Astronomy & Astrophysics* 618, A162.
- Molina, Javier, DM Stam, and L Rossi (2017). “Traces of exomoons in flux and polarization signals of starlight reflected by exoplanets”. In: *European Planetary Science Congress 2017*.
- Mollière, P et al. (2019). “petitRADTRANS-A Python radiative transfer package for exoplanet characterization and retrieval”. In: *Astronomy and Astrophysics* 627, A67.
- Moran, Sarah E et al. (2018). “Limits on Clouds and Hazes for the TRAPPIST-1 Planets”. In: *The Astronomical Journal* 156.6, p. 252.
- Morley, Caroline V et al. (2015). “Thermal emission and reflected light spectra of super Earths with flat transmission spectra”. In: *The Astrophysical Journal* 815.2, p. 110.
- Muñoz, A Garcia (2018). “On mapping exoplanet atmospheres with high-dispersion spectro-polarimetry: Some model predictions”. In: *The Astrophysical Journal* 854.2, p. 108.
- Neubauer, David et al. (2012). “The life supporting zone of Kepler-22b and the Kepler planetary candidates: KOI268. 01, KOI701. 03, KOI854. 01 and KOI1026. 01”. In: *Planetary and Space Science* 73.1, pp. 397–406.
- O’Malley-James, Jack T and Lisa Kaltenegger (2019). “Lessons from early Earth: UV surface radiation should not limit the habitability of active M star systems”. In: *Monthly Notices of the Royal Astronomical Society* 485.4, pp. 5598–5603.
- Och, Lawrence M and Graham A Shields-Zhou (2012). “The Neoproterozoic oxygenation event: Environmental perturbations and biogeochemical cycling”. In: *Earth-Science Reviews* 110.1-4, pp. 26–57.
- Owen, Tobias (1980). “The search for early forms of life in other planetary systems: future possibilities afforded by spectroscopic techniques”. In: *Strategies for the Search for Life in the Universe*. Springer, pp. 177–185.
- Pallé, E et al. (2010). “Observations and modelling of earth’s transmission spectrum through lunar eclipses: A window to transiting exoplanet characterization”. In: *Proc Int Astron Union* 6.S276, pp. 385–388.
- Pallé, Enric et al. (2009). “Earth’s transmission spectrum from lunar eclipse observations”. In: *Nature* 459.7248, pp. 814–816.
- Patty, CH Lucas et al. (2021). “Biosignatures of the Earth-I. Airborne spectropolarimetric detection of photosynthetic life”. In: *Astronomy & Astrophysics* 651, A68.

- Pepin, Robert O. (1991). “On the Origin and Early Evolution of Terrestrial Planet Atmospheres and Meteoritic Volatiles”. In: *Icarus* 92.1, pp. 2–79. DOI: [10.1016/0019-1035\(91\)90036-S](https://doi.org/10.1016/0019-1035(91)90036-S).
- Peraiah, A (2001). “An Introduction to Radiative Transfer, by Annamaneni Peraiah”. In: Cambridge, UK: Cambridge University Press.
- Peraiah, A and IP Grant (1973). “Numerical solution of the radiative transfer equation in spherical shells”. In: *J. Int. Math. Appl* 12.1, pp. 75–90.
- Pickles, AJ (1998). “A stellar spectral flux library: 1150–25000 Å”. In: *Publications of the Astronomical Society of the Pacific* 110.749, p. 863.
- Pidhorodetska, Daria et al. (2020). “Detectability of Molecular Signatures on TRAPPIST-1e through Transmission Spectroscopy Simulated for Future Space-based Observatories”. In: *The Astrophysical Journal Letters* 898.2, p. L33.
- Quanz, Sascha P et al. (2021). “Atmospheric characterization of terrestrial exoplanets in the mid-infrared: biosignatures, habitability, and diversity”. In: *Experimental Astronomy*, pp. 1–25. DOI: <https://doi.org/10.1007/s10686-021-09791-z>.
- Ribas, Ignasi et al. (2017). “The full spectral radiative properties of Proxima Centauri”. In: *Astronomy and Astrophysics* 603, A58.
- Rice, Ken (2014). “The detection and characterization of extrasolar planets”. In: *Challenges* 5.2, pp. 296–323.
- Robinson, Tyler D. and David C. Catling (2014). “Common 0.1 Bar Tropopause in Thick Atmospheres Set by Pressure-Dependent Infrared Transparency”. In: *Nature Geoscience* 7.1, pp. 12–15. DOI: [10.1038/ngeo2020](https://doi.org/10.1038/ngeo2020).
- Rodriguez, Joseph E et al. (2020). “The first habitable-zone Earth-sized planet from TESS. II. Spitzer confirms TOI-700 d”. In: *The Astronomical Journal* 160.3, p. 117.
- Rodriguez-Mozos, JM and A Moya (2017). “Statistical-likelihood Exo-Planetary Habitability Index (SEPHI)”. In: *Monthly Notices of the Royal Astronomical Society* 471.4, pp. 4628–4636.
- Rogers, Leslie A (2015). “Most 1.6 Earth-radius planets are not rocky”. In: *The Astrophysical Journal* 801.1, p. 41.
- Rossi, Loic, DM Stam, and M Turbet (2017). “Retrieving the cloud coverage on Earth-like exoplanets using polarimetry”. In: *European Planetary Science Congress 2017*.
- Rossi, Loic, Javier Berzosa-Molina, and Daphne M Stam (2018). “PyMieDAP: a Python–Fortran tool for computing fluxes and polarization signals of (exo) planets”. In: *Astronomy & Astrophysics* 616, A147.
- Rossi, Loic and Daphne M Stam (2018). “Circular polarization signals of cloudy (exo) planets”. In: *Astronomy & Astrophysics* 616, A117.

- Rugheimer, S et al. (2015). “UV surface environment of Earth-like planets orbiting FGKM stars through geological evolution”. In: *The Astrophysical Journal* 806.1, p. 137.
- Rugheimer, Sarah and Lisa Kaltenegger (2018). “Spectra of Earth-like planets through geological evolution around FGKM stars”. In: *The Astrophysical Journal* 854.1, p. 19.
- Rugheimer, Sarah, Lisa Kaltenegger, et al. (2013). “Spectral fingerprints of Earth-like planets around FGK stars”. In: *Astrobiology* 13.3, pp. 251–269.
- Rustamkulov, Z. et al. (2023). “Early Release Science of the exoplanet WASP-39b with JWST NIRSpec PRISM”. In: *Nature*.
- Sabotta, S et al. (2021). “The CARMENES search for exoplanets around M dwarfs— Planet occurrence rates from a subsample of 71 stars”. In: *arXiv preprint arXiv:2107.03802*.
- Sagan, Carl et al. (1993). “A search for life on Earth from the Galileo spacecraft”. In: *Nature* 365.6448, pp. 715–721.
- Sánchez-López, A et al. (2020). “Discriminating between hazy and clear hot-Jupiter atmospheres with CARMENES”. In: *Astronomy & Astrophysics* 643, A24.
- Sanz-Forcada, Jorge et al. (2011). “Estimation of the XUV radiation onto close planets and their evaporation”. In: *Astronomy & Astrophysics* 532, A6.
- Scheucher, Markus et al. (2020). “Proxima Centauri b: A Strong Case for Including Cosmic-Ray-induced Chemistry in Atmospheric Biosignature Studies”. In: *The Astrophysical Journal* 893.1, p. 12.
- Seager, S (2008). “Exoplanet transit spectroscopy and photometry”. In: *Space Science Reviews* 135.1, pp. 345–354.
- Seager, Sara (2014). “The Next Steps in Exploring Habitable Planets”. In: *Proceedings of the National Academy of Sciences* 111.35, pp. 12634–12640. DOI: [10.1073/pnas.1304213111](https://doi.org/10.1073/pnas.1304213111).
- Seager, Sara et al. (2005). “Vegetation’s Red Edge: A Possible Spectroscopic Biosignature of Extraterrestrial Plants”. In: *Astrobiology* 5.3, pp. 372–390. DOI: [10.1089/ast.2005.5.372](https://doi.org/10.1089/ast.2005.5.372).
- Segura, A et al. (2007). “Abiotic formation of O₂ and O₃ in high-CO₂ terrestrial atmospheres”. In: *Astronomy & Astrophysics* 472.2, pp. 665–679.
- Segura, Antígona, James F Kasting, et al. (2005). “Biosignatures from Earth-like planets around M dwarfs”. In: *Astrobiology* 5.6, pp. 706–725.
- Segura, Antígona, Kara Krelove, et al. (2003). “Ozone concentrations and ultraviolet fluxes on Earth-like planets around other stars”. In: *Astrobiology* 3.4, pp. 689–708.

-
- Selsis, F (2000). “Physics of planets I: Darwin and the atmospheres of terrestrial planets”. In: *Darwin and Astronomy: the Infrared Space Interferometer*. Vol. 451, p. 133.
- (2004). “Atmospheric biomarkers on terrestrial Exoplanets”. In: *Boletin SEA* 12, pp. 27–38.
- Selsis, F, D Despois, and J-P Parisot (2002). “Signature of life on exoplanets: Can Darwin produce false positive detections?” In: *Astronomy & Astrophysics* 388.3, pp. 985–1003.
- Selsis, F. (Dec. 2004). “The Atmosphere of Terrestrial Exoplanets: Detection and Characterization”. In: *Extrasolar Planets: Today and Tomorrow*. Ed. by J. Beaulieu, A. Lecavelier Des Etangs, and C. Terquem. Vol. 321. Astronomical Society of the Pacific Conference Series, p. 170.
- Selsis, Franck, Lisa Kaltenegger, and Jimmy Paillet (2008). “Terrestrial exoplanets: diversity, habitability and characterization”. In: *Physica Scripta* 2008.T130, p. 014032.
- Sengupta, Sujan (2008). “Cloudy atmosphere of the extrasolar planet HD 189733b: a possible explanation of the detected B-band polarization”. In: *The Astrophysical Journal* 683.2, p. L195.
- (2016a). “An upper limit on the ratio between the Extreme Ultraviolet and the bolometric luminosities of stars hosting habitable planets”. In: *Journal of Astrophysics and Astronomy* 37.2, pp. 1–11.
- (2016b). “Polarimetric detection of exoplanets transiting T and L brown dwarfs”. In: *The Astronomical Journal* 152.4, p. 98.
- (2018). “Polarization of Trappist-1 by the Transit of its Planets”. In: *The Astrophysical Journal* 861.1, p. 41.
- Sengupta, Sujan, Aritra Chakrabarty, and Giovanna Tinetti (2020). “Optical transmission spectra of hot jupiters: effects of scattering”. In: *The Astrophysical Journal* 889.2, p. 181.
- Sengupta, Sujan and Vinod Krishan (2001). “Probing dust in the atmosphere of brown dwarfs through polarization”. In: *The Astrophysical Journal* 561.1, p. L123.
- Sengupta, Sujan and Malay Maiti (2006). “Polarization of starlight by an unresolved and oblate extrasolar planet in an elliptical orbit”. In: *The Astrophysical Journal* 639.2, p. 1147.
- Sengupta, Sujan and Mark S Marley (2009). “Multiple scattering polarization of substellar-mass objects: T dwarfs”. In: *The Astrophysical Journal* 707.1, p. 716.
- (2010). “Observed polarization of brown dwarfs suggests low surface gravity”. In: *The Astrophysical Journal Letters* 722.2, p. L142.

- Sengupta, Sujan and Mark S Marley (2011). “Multiple scattering polarization—Application of Chandrasekhar’s formalisms to the atmosphere of brown dwarfs and extrasolar planets”. In: *Pramana* 77.1, pp. 157–168.
- (2016). “Detecting exomoons around self-luminous giant exoplanets through polarization”. In: *The Astrophysical Journal* 824.2, p. 76.
- Shields, Aomawa L, Sarah Ballard, and John Asher Johnson (2016). “The habitability of planets orbiting M-dwarf stars”. In: *Phys. Rep.* 663, pp. 1–38.
- Shields-Zhou, Graham and Lawrence Och (2011). “The case for a Neoproterozoic oxygenation event: geochemical evidence and biological consequences”. In: *GSA Today* 21.3, pp. 4–11.
- Sing, David K et al. (2016). “A continuum from clear to cloudy hot-Jupiter exoplanets without primordial water depletion”. In: *Nature* 529.7584, pp. 59–62.
- Stam, Daphne M (2003). “Polarization spectra of extrasolar planets”. In: *Earths: DARWIN/TPF and the Search for Extrasolar Terrestrial Planets*. Vol. 539, pp. 615–619.
- Stam, Daphne M, Joop Hovenier, and Rens Waters (2003). “Polarization of extrasolar planets: sample simulations”. In: *Scientific Frontiers in Research on Extrasolar Planets*. Vol. 294, pp. 535–538.
- Stam, Daphne M. (2008). “Spectropolarimetric Signatures of Earth-like Extrasolar Planets”. In: *Astronomy & Astrophysics* 482.3, pp. 989–1007. DOI: [10.1051/0004-6361:20078358](https://doi.org/10.1051/0004-6361:20078358).
- Stam, DM (2008). “Spectropolarimetric signatures of Earth-like extrasolar planets”. In: *Astronomy & Astrophysics* 482.3, pp. 989–1007.
- Stam, DM, WA De Rooij, et al. (2006). “Integrating polarized light over a planetary disk applied to starlight reflected by extrasolar planets”. In: *Astronomy & Astrophysics* 452.2, pp. 669–683.
- Stam, DM and JW Hovenier (2005). “Errors in calculated planetary phase functions and albedos due to neglecting polarization”. In: *Astronomy & Astrophysics* 444.1, pp. 275–286.
- Sterzik, Michael F et al. (2019). “Spectral and temporal variability of Earth observed in polarization”. In: *Astronomy & Astrophysics* 622, A41.
- Struve, Otto (1952). “Proposal for a project of high-precision stellar radial velocity work”. In: *The Observatory* 72, pp. 199–200.
- Sudarsky, David, Adam Burrows, and Philip Pinto (2000). “Albedo and Reflection Spectra of Extrasolar Giant Planets”. In: *The Astrophysical Journal* 538.2, pp. 885–903. DOI: [10.1086/309228](https://doi.org/10.1086/309228).

- Suissa, Gabrielle et al. (2020). “The First Habitable-zone Earth-sized Planet from TESS. III. Climate States and Characterization Prospects for TOI-700 d”. In: *The Astrophysical Journal* 160.3, p. 118.
- Teegarden, BJ et al. (2003). “Discovery of a new nearby star”. In: *The Astrophysical Journal* 589.1, p. L51.
- Tinetti, Giovanna (2006). “Characterizing extrasolar terrestrial planets with reflected, emitted and transmitted spectra”. In: *Origins of life and evolution of biospheres* 36.5, pp. 541–547.
- Tinetti, Giovanna, Pierre Drossart, et al. (2018). “A chemical survey of exoplanets with ARIEL”. In: *Experimental astronomy* 46, pp. 135–209.
- Tinetti, Giovanna, Thérèse Encrenaz, and Athena Coustenis (2013a). “Spectroscopy of planetary atmospheres in our Galaxy”. In: *The Astronomy and Astrophysics Review* 21.1, p. 63. DOI: [10.1007/s00159-013-0063-6](https://doi.org/10.1007/s00159-013-0063-6).
- (2013b). “Spectroscopy of planetary atmospheres in our Galaxy”. In: *The Astronomy and Astrophysics Review* 21.1, pp. 1–65.
- Tinetti, Giovanna, Sky Rashby, and Yuk L. Yung (2006). “Detectability of Planetary Characteristics in Disk-Averaged Spectra. II: Synthetic Spectra and Light-Curves of Earth”. In: *Astrobiology* 6.6, pp. 881–900. DOI: [10.1089/ast.2006.6.881](https://doi.org/10.1089/ast.2006.6.881).
- Torres, Guillermo et al. (2015). “Validation of 12 small Kepler transiting planets in the habitable zone”. In: *The Astrophysical Journal* 800.2, p. 99.
- Turbet, Martin, Emeline Bolmont, et al. (2020). “A review of possible planetary atmospheres in the TRAPPIST-1 system”. In: *Space science reviews* 216.5, pp. 1–48.
- Turbet, Martin, Jérémy Leconte, et al. (2016). “The habitability of Proxima Centauri b. II. Possible climates and observability”. In: *Astronomy and Astrophysics* 596, A112.
- Vanderburg, Andrew et al. (2020). “A habitable-zone Earth-sized planet rescued from false positive status”. In: *The Astrophysical Journal Letters* 893.1, p. L27.
- Waldmann, Ingo P et al. (2015). “Tau-REx I: A next generation retrieval code for exoplanetary atmospheres”. In: *The Astrophysical Journal* 802.2, p. 107.
- Wandel, Amri and Lev Tal-Or (2019). “On the habitability of Teegarden’s Star planets”. In: *The Astrophysical Journal Letters* 880.2, p. L21.
- Wang, Shuang, Zhong-Quan Qu, and Hao Li (2019). “The diurnal variation of polarization characteristics of the Earth treated as an exoplanet”. In: *Research in Astronomy and Astrophysics* 19.8, p. 117.
- Wei, Song and Qu Zhong-quan (2017). “Polarimetric study of an Earth-like Planet”. In: *Chinese Astronomy and Astrophysics* 41.2, pp. 235–253.

- West, RA et al. (1983). “Photometry and polarimetry of Saturn at 2640 and 7500 Å”. In: *Journal of Geophysical Research: Space Physics* 88.A11, pp. 8679–8697.
- Whitmire, DP, RT Reynolds, and JF Kasting (1991). “Habitable zones for Earth-like planets around main sequence stars”. In: *Bioastronomy*. Springer, pp. 173–178.
- Wildi, F et al. (2017). “NIRPS: an adaptive-optics assisted radial velocity spectrograph to chase exoplanets around M-stars”. In: *Techniques and Instrumentation for Detection of Exoplanets VIII*. Vol. 10400. SPIE, pp. 321–335.
- Wolf, Eric T (2017). “Assessing the habitability of the TRAPPIST-1 system using a 3D climate model”. In: *The Astrophysical Journal Letters* 839.1, p. L1.
- (2018). “Erratum: “Assessing the Habitability of the TRAPPIST-1 System Using a 3D Climate Model”(2017, ApJL, 839, L1)”. In: *The Astrophysical Journal Letters* 855.
- Wolszczan, Aleksander and Dale A Frail (1992). “A planetary system around the millisecond pulsar PSR1257+12”. In: *Nature* 355.6356, pp. 145–147.
- Wunderlich, Fabian, Mareike Godolt, et al. (2019). “Detectability of atmospheric features of Earth-like planets in the habitable zone around M dwarfs”. In: *Astronomy and Astrophysics* 624, A49.
- Wunderlich, Fabian, Markus Scheucher, et al. (2020). “Distinguishing between Wet and Dry Atmospheres of TRAPPIST-1 e and f”. In: *The Astrophysical Journal* 901.2, p. 126.
- Yan, Fei et al. (2015). “High-resolution transmission spectrum of the Earth’s atmosphere-seeing Earth as an exoplanet using a lunar eclipse”. In: *Int. J. Astrobiology* 14.2, pp. 255–266.
- Zechmeister, M et al. (2019). “The CARMENES search for exoplanets around M dwarfs- Two temperate Earth-mass planet candidates around Teegarden’s Star”. In: *Astronomy & Astrophysics* 627, A49.
- Zhang, M. and A. P. Showman (2017). “Global three-dimensional atmospheric circulation and climate of eccentric hot Jupiter HAT-P-7b”. In: *The Astrophysical Journal* 836.1, p. 73.
- Zhang, Zhanbo et al. (2018). “The Near-infrared Transmission Spectra of TRAPPIST-1 Planets b, c, d, e, f, and g and Stellar Contamination in Multi-epoch Transit Spectra”. In: *The Astronomical Journal* 156.4, p. 178.
- Zubko, N, N Baba, and N Murakami (2008). “Polarization analysis as a means of detecting exoplanets and measuring their objective spectra”. In: *Space Telescopes and Instrumentation 2008: Optical, Infrared, and Millimeter*. Vol. 7010. SPIE, pp. 503–507.

Zugger, ME et al. (2011). “Searching for water earths in the near-infrared”. In: *The Astrophysical Journal* 739.1, p. 12.

Zugger, Michael E et al. (2010). “Light scattering from exoplanet oceans and atmospheres”. In: *The Astrophysical Journal* 723.2, p. 1168.